Mechanismen des CO_2 - und HCO_3^- - Transports an Zellmembranen

Von der Naturwissenschaftlichen Fakultät
der Gottfried Wilhelm Leibniz Universität Hannover
zur Erlangung des Grades
Doktor der Naturwissenschaften
Dr. rer. nat.

genehmigte Dissertation
von
Dipl.-Biol. Samer Al-Samir

geboren am 10.06.1981 in Hannover

2012

Referent: Prof. Dr. Gerolf Gros

Korreferent: Prof. Dr. Anaclet Ngezahayo

Tag der Promotion: 17.09.2012

Mechanismen des CO_2 - und HCO_3^- - Transports an Zellmembranen

Diese Arbeit umfasst zwei Teile, von denen der erste sich zunächst mit dem Mechanismus der CO_2-Permeation durch künstliche und biologische Lipidmembranen beschäftigt. Neuere Befunde, dass einige Membranproteine Funktionen als Gaskanäle zeigen, stehen im Widerspruch mit der klassischen Ansicht, dass Zellmembranen generell hoch-permeabel sind für Gase. Diese Ansicht beruht auf der Beobachtung, dass künstliche planare Phospholipid-Doppelschichten eine sehr hohe Permeabilität für CO_2 (P_{CO2}) von ~ 1cm/s haben. Im Rahmen dieser Arbeit wird gezeigt, dass Membranen mit normalem Cholesteringehalt (30-50 mol% der Gesamtheit der Membran-Lipide), sowie MDCK Zellmembranen, in Wahrheit eine unerwartet niedrige P_{CO2} von nur ~ 0,01 cm/s haben. Phospholipidvesikel, angereichert mit identischen Cholesteringehalt, zeigen ebenfalls eine P_{CO2} von ~ 0,01 cm/s. MDCK-Zellmembranen, welche mit Cholesterin angereichert oder deren Cholesteringehalt reduziert wurde, zeigen eine signifikante Erniedrigung bzw. eine drastische Erhöhung der P_{CO2}. Der Einbau von humanen Aquaporin 1 in solche cholesterinhaltigen Vesikel, sowie die Expression von Aquaporin 1 in MDCK Zellen, führen zu signifikanten Anstiegen der P_{CO2}. Dies zeigt, dass Gaskanäle eine hohe funktionelle Bedeutung für den Transport von CO_2 über Zellmembranen haben.
Ein zweiter Aspekt dieser Arbeit ist die Untersuchung der Frage, ob eine physikalische Assoziation und eine direkte funktionelle Interaktion zwischen Carboanhydrase II (CAII) und dem Anionenaustauscher 1 (AE1) besteht ("Metabolon"), wie dies von einigen Gruppen in zahlreichen Publikationen veröffentlicht wurde. In der vorliegenden Arbeit werden tsA201 Zellen transfiziert mit den Fusionsproteinen CyPet-CAII und YPet-AE1. Zum einen wurde an diesen Zellen die HCO_3^- Permeabilität (P_{HCO3-}) für eine Reihe von Kotransfektionen mit unterschiedlichen Konstrukten von YPet-AE1 und CyPet-CAII gemessen, wobei auch zwei mutierte CAII-Formen untersucht wurden. Konfokale Mikroskopie der doppelt transfizierten tsA201 Zellen zeigt, dass YPet-AE1 eindeutig mit der Zellmembran assoziiert, CyPet-CAII dagegen homogen im Zytoplasma verteilt ist. FRET Messungen zeigen ebenfalls keine enge räumliche Nähe von YPet-AE1 und CyPet-CAII. Beide diese Fusionsproteine sind in tsA201 Zellen voll funktionell, sowohl was die Carboanhydrase-Aktivität als auch was die zelluläre P_{HCO3-} betrifft. P_{HCO3-} zeigt in allen Fällen die erwartete Hemmbarkeit durch DIDS. Die Expression der akatalytischen CAII-Mutante V143Y führt zu einer signifikanten Reduktion der endogenen CAII und einer Reduktion der intrazellulären Carboanhydrase-Aktivität, die mit einer geringen Abnahme der Bikarbonatpermeabilität einhergeht. Überexpression einer CAII mit gekürztem N-Terminus (wobei die Kürzung die Entfernung der postulierten Bindungssequenz der CAII an den C-terminalen zytoplasmatischen Teil von AE1 bedeutet) führt genau wie die Expression der Wildtyp-CAII zu einem Anstieg der intrazellulären Carboanhydrase-Aktivität und in Verbindung damit auch zu einem Anstieg der HCO_3^- - Permeabilität. Die unterschiedlichen doppelt transfizierten tsA201-Zellen zeigen eine einfache positive Korrelation zwischen zellulärer P_{HCO3-} und intrazellulärer Carboanhydrase-Aktivität, wie sie auch theoretisch zu erwarten ist. Diese Korrelation ist bedingt durch Änderungen des HCO_3^- Transportes von AE1 infolge einer durch die intrazelluläre Carboanhydrase-Aktivität vermittelten Modulation der Anlieferung von HCO_3^- am AE1-Transporter oder des Abtransports von HCO_3^- vom Transporter, wobei eine hohe intrazelluläre Carboanhydrase-Aktivität diese Vorgänge beschleunigt und verbessert. Alle Ergebnisse der Arbeit deuten darauf hin, dass ein AE1-CAII Metabolon weder auf funktioneller Ebene noch auf der Ebene einer physikalischen Interaktion besteht.

Stichwörter: CO_2- Permeabilität, Bikarbonat-Permeabilität, Cholesterin, Carboanhydrase

Mechanisms of CO_2 and HCO_3^- Transport in Cell Membranes

Abstract

The first part of this dissertation studies the mechanism of CO_2 transport across artificial and biological membranes. Recent observations that some membrane proteins can act as gas channels seem to be in contrast to the classical view that membranes generally are highly permeable to gases. This view has also been based on the finding that pure planar phospholipid bilayers exhibit a very high permeability for CO_2 (P_{CO_2}) of ~ 1 cm/s. In this work it is shown that biological membranes containing normal amounts of cholesterol (30–50 mol % of total lipid), e.g. MDCK cells, in fact possess an unexpectedly low P_{CO_2} of ~ 0.01 cm/s. Phospholipid vesicles enriched with similar cholesterol concentrations also exhibit $P_{CO2} \approx 0.01$ cm/s. MDCK cells depleted of or enriched with membrane cholesterol show dramatic increases or decreases in P_{CO_2}, respectively. Incorporation of the gas channel human aquaporin-1 into cholesterol-containing vesicles, as well as its expression in MDCK cells, lead to drastic increases in P_{CO_2}, showing that gas channels are of high functional significance for membrane CO_2 transfer.
The second part of this work concerns the investigation of the evidence for physical association of and direct functional interaction between carbonic anhydrase II (CAII) and the anion exchanger 1 (AE1) in tsA201 cells co-expressing heterologous fluorescent fusion proteins CyPet-CAII and YPet-AE1, and the effect on HCO_3^- permeability (P_{HCO3-}). In these doubly transfected tsA201 cells, YPet-AE1 is clearly associated with the cell membrane, whereas CyPet-CAII is homogeneously distributed throughout the cell in a cytoplasmic pattern. FRET measurements fail to detect close proximity of YPet-AE1 and CyPet-CAII. Both the CAII and AE1 fusion proteins are fully functional in tsA201 cells as judged by CA activity and by cellular P_{HCO3-} including the latter's sensitivity to inhibition by DIDS. Expression of the non-catalytic CAII mutant V143Y leads to a drastic reduction of endogenous CAII and to a corresponding reduction of intracellular CA activity. Overexpression of an N-terminally truncated CAII lacking the proposed site of interaction with the C-terminal cytoplasmic tail of AE1 substantially increases intracellular CA activity, as does overexpression of wildtype CAII. All these variously co-transfected tsA201 cells exhibit a simple positive relationship between cellular P_{HCO3-} and intracellular CA activity, consistent with changes in HCO_3^- transport that reflect either substrate supply to or removal from AE1 via altered intracellular CA activity, without requirement for a hypothesized CAII-AE1 metabolon involving physical interaction.

Keywords: CO_2 permeability, bicarbonate permeability, cholesterol, carbonic anhydrase

Inhaltsverzeichnis

Erklärung zur Dissertation

gemäß §6(1) der Promotionsordnung der Naturwissenschaftlichen Fakultät der Gottfried-Wilhelm-Leibniz-Universität Hannover

für die Promotion zum Dr. rer. nat.

Hierdurch erkläre ich, dass ich meine Dissertation mit dem Titel

Mechanismen des CO_2 – und HCO_3^- - Transportes an Zellmembranen

selbständig verfasst und die benutzen Hilfsmittel und Quellen sowie gegebenenfalls die zu Hilfeleistung herangezogenen Institutionen vollständig angegeben habe.

Die Dissertation wurde nicht schon als Masterarbeit, Diplomarbeit oder andere Prüfungsarbeit verwendet.

Abkürzungsverzeichnis

AE1: HCO_3^- / Cl^- - Austauscher, Anionenaustauscher 1

AQP1: Aquaporin 1

AQPz: Bakterielles Aquaporin z

CAII: Carboanhydrase 2

chol: Cholesterin

CyPet: FRET Optimiertes blaues Fluoreszenzprotein

DIDS: 4,4'-Diisothiocyanatostilbene-2,2'-disulfonate

FRET: Förster Resonanz Energie Transfer

hAE1: Humaner Anionenaustauscher 1

hAQP1: Humanes Aquaporin 1

LPR: Lipid Protein Ratio

mAE1: Muriner Anionenaustauscher 1

PC: L-α-Phosphatidylcholin

P_{CO2}: CO_2 - Permeabilität

P_{HCO3-}: Bikarbonatpermeabilität

PS: L-α-Phopsphatidylserin

RhAG: Rhesus-assoziiertes Glykoprotein

truncCAII: N-terminal um 24 Aminosäuren gekürzte Carboanhydrase II

YPet: FRET Optimiertes gelbes Fluoreszenzprotein

Einleitung

Im Rahmen dieser Arbeit wurden die Permeabilitäten und Transportmechanismen von HCO_3^- und CO_2 an Zellmembranen untersucht.

Der **erste Teil der Arbeit** beschäftigt sich mit der niedrigen intrinsischen Permeabilität von Zellmembranen für das Gas CO_2. Kleine Gase wie O_2, CO_2 und NO passieren künstliche Phospholipid-Doppelschichten ohne jede Behinderung (Overton, 1901). Es wurde seit vielen Jahrzehnten angenommen, dass dieser Befund auch für Zellmembranen gilt.

Unser Labor hat nun kürzlich nachgewiesen, dass einige Zellmembranen eine wesentlich niedrigere Permeabilität für CO_2 aufweisen, als künstliche Phospholipid-Doppelschichten (Endeward and Gros 2005). Diese Befunde widersprechen der bisherigen Annahme, dass CO_2 die Zellmembran ohne Behinderung passieren kann.

Ein weiterer Befund weicht von dieser bisherigen Annahme ab: Die Wasserpore Aquaporin 1 des Menschen (Endeward et al., 2006), sowie einige andere Isoformen und pflanzliches Aquaporin, können den Transport von CO_2 über die Zellmembran anscheinend fördern und dienen somit als CO_2- Kanäle. Dies führte zu einer anhaltenden Diskussion, ob eine solche Funktion überhaupt notwendig sei, wenn Zellmembranen eine ebenso hohe Permeabilität für Gase aufweisen wie künstliche Lipid-Doppelschichten.

Ein wesentlicher Unterschied zwischen den künstlichen Phospholipid-Doppelschichten und Zellmembranen ist aber die Zusammensetzung. Zellmembranen besitzen einen nennenswerten Cholesteringehalt zwischen 30 und 45 mol%, sowie natürlich eine große Zahl von Proteinen. Cholesterin ist bekannt dafür, die Barriereeigenschaften der Zellmembran für wasserlösliche Stoffe zu verstärken. Aufgrund dieser Vorkenntnisse wurde im Laufe dieser Arbeit die Fragestellung untersucht, ob das Cholesterin innerhalb der Zellmembran evtl. für eine wesentlich niedrigere CO_2-Permeabilität verantwortlich ist als man sie in Lipid-Doppelschichten beobachtet. Außerdem wurde mit neuen Ansätzen die Hypothese überprüft, dass Aquaporin 1 als CO_2-Kanal fungiert.

Zu diesem Zweck wurde die CO_2-Permeabilität von Zellmembranen und Vesikeln gemessen, die unterschiedliche Mengen an Cholesterin enthielten. Zudem wurde untersucht, ob der Einbau von Aquaporin 1 in die Membran sowohl von Vesikeln wie von Zellmembranen die Permeabilität für CO_2 maßgeblich beeinflussen kann.

Der **zweite Teil der Arbeit** beschäftigt sich mit der Permeabilität der Zellmembran für HCO_3^-. Dies ist physiologisch in sofern relevant, als das CO_2 innerhalb des Blutkreislaufes primär in der Form von HCO_3^- transportiert wird, nachdem es als molekulares CO_2 in den Erythrocyten eingetreten und dort in Bikarbonat umgewandelt worden ist. Dem HCO_3^--Transport liegt die Reaktion von $CO_2 + H_2O$ zu $HCO_3^- + H^+$ in wässriger Lösung zugrunde. Diese Reaktion ist ohne Katalyse viel zu langsam für den Gasaustausch und wird deshalb innerhalb des Organismus durch Carboanhydrasen beschleunigt. Von hohem Interesse ist dabei die katalytisch hochaktive Carboanhydrase II, welche in großen Mengen im Cytoplasma des Erythrozyten und vieler anderer Zelltypen zu finden ist.
Beim Transport von CO_2/HCO_3^- im Blut wird ein Großteil des HCO_3^- aber nicht im Cytoplasma der Erythrocyten transportiert, sondern im Blutplasma. Dafür muss das HCO_3^- die Zellmembran des Erythrozyten in beide Richtungen passieren. Dabei wird HCO_3^- durch den HCO_3^- -Cl^- Antiporter, den Anionenaustauscher 1 (AE1), über die Zellmembran transportiert. Somit wird die Permeabilität der Zellmembran für HCO_3^- von der Aktivität von AE1 bestimmt.
Es wurde in der Literatur vorgeschlagen, dass die Transportaktivität von AE1 durch eine direkte Interaktion mit der Carboanhydrase II (CAII) beschleunigt wird. Diese sog. "Metabolon" - Hypothese geht davon aus, dass der N-Terminus der CAII an den C-Terminus von AE1 bindet. Dadurch soll die Reaktion von CO_2 zu HCO_3^- (Bereitstellung von HCO_3^- beim Auswärtstransport von HCO_3^-) oder die Rückreaktion (beim Einstrom von HCO_3^- in die Zelle) direkt an der Membran bzw. direkt an der Transportregion des AE1 stattfinden. Das soll die Transportaktivität des AE1 erheblich steigern, da unmittelbar an der Transportregion von AE1 ein großer transmembranaler HCO_3^- - Konzentrationsgradient aufrechterhalten werden kann.
Dieses Existenz dieses "Metabolon" betreffend gibt es unterschiedliche Befunde, die zum einen eine Bindung von CAII and AE1 in vitro nachweisen (Vince and Reithmeier, 1998, 2000), zum anderen aber solche, die diese Bindungsstudien widerlegen (Piermarini et al., 2007). Einen Nachweis einer engen räumlichen Nähe von AE1 und CAII in Zellen in vivo gibt es nicht.

In Rahmen dieser Arbeit soll daher diese Frage zum ersten Mal innerhalb einer intakten Zelle mithilfe farbmarkierter Proteine untersucht werden. Dabei wurde die fragliche direkte räumliche Aneinanderlagerung von AE1 und CAII mittels konfokaler Mikroskopie betrachtet, und zugleich wurde die mögliche funktionelle Interaktion der beiden Proteine mithilfe von Messungen der Bikarbonat-Permeabilität mittels der O^{18} –Austausch-Methode untersucht (Endeward and Gros, 2005).

I. CO_2-Permeabilität von Membranen

Ergebnisse CO_2 Messungen

Betrachtet man die CO_2 Permeabilität von ausgewählten Zellmembranen, wie in Tab. 1 gezeigt, ist eine signifikant niedrigere Permeabilität für CO_2 zu beobachten, als sie in artifiziellen Lipid-Doppelschichten vorliegt. Die Permeabilitäten liegen bis zu drei Zehnerpotenzen unter der durchschnittlichen CO_2- Permeabilität synthetischer Lipid-Doppelschichten von ~ 1 cm/s. Zellen können also nach diesen Ergebnissen in der Tat eine erheblich niedrigere "intrinsische" CO_2-Permeabilität aufweisen als Lipid-Doppelschichten.

Permeabilitätsmessungen an Phospholipid-Vesikeln mit unterschiedlichem Gehalt von Cholesterin in der Membran zeigen, dass die Permeabilität von CO_2 mit steigendem Cholesteringehalt drastisch abnimmt. In Abb. 1 wird die CO_2 Permeabilität von Vesikeln in Abhängigkeit vom Cholesteringehalt dargestellt. Dabei ist die CO_2-Permeabilität logarithmisch gegen den Cholesteringehalt in mol% (mol Cholesterin in % von mol Gesamt-Membranlipide) aufgetragen. Für die P_{CO2}-Werte zwischen 0 und 20 mol% Cholesterin kann aus methodischen Gründen nur ein oberer Grenzwert von 0,16 cm/s angegeben werden. Möglicherweise liegt der P_{CO2} in Abwesenheit von Cholesterin deutlich höher und gleicht dem in Tab. 1 genannten Wert für planare Lipid-Doppelschichten von ~ 1 cm/s. Die hier verwendete massenspektrometrische Messung der CO_2-Permeabilität ist vom Produkt P_{CO2} x a abhängig, wobei a das Oberflächen-Volumenverhältnis der Vesikel darstellt, das bei diesen Vesikeln – z.B. im Vergleich zu Zellen – besonders groß ist. Daher liegt der maximal erfassbare Wert der Permeabilität relativ niedrig (Endeward and Gros, 2005).

Bei einem Cholesteringehalt von 30 mol% ist jedoch ein eindeutiger Wert für P_{CO2} bestimmbar. Dieser Wert liegt bei ~ 0,015 cm/s, was eine Zehnerpotenz unter dem Grenzwert von 0,16 cm/s und zwei Zehnerpotenzen unter dem Wert für planare Lipd-Doppelschichten von ~ 1,0 cm/s liegt. Eine Steigerung des Cholesterins von 30 mol% auf 70 mol% führt zu einer Abnahme der Permeabilität um eine weitere Zehnerpotenz auf ~ 0,0015 cm/s.
Die Abhängigkeit des P_{CO2} vom Cholesteringehalt der Membranen wurde auch an intakten Zellen nachgewiesen. Die Permeabilität von MDCK-Zellmembranen (s. Abb. 2) weist ebenfalls eine Abhängigkeit vom Cholesteringehalt auf. Dargestellt ist die CO_2-Permeabiltität von unterschiedlich manipulierten MDCK Zellen. Mittig sind unbehandelte MDCK Zellen als Kontrolle mit einer Permeabilität von 0,017 cm/s abgebildet. Wird der Cholesteringehalt der Zellmembran durch Inkubation mit Methyl-ß-Cyclodextrin verringert, so steigt die Permeabilität von 0,017 cm/s auf über 0,75 cm/s an, also mehr als 40-fach, wie anhand des linken Balkens zu sehen ist. Hier ist anzumerken, dass der Wert 0,75 ebenfalls einen oberen Grenzwert darstellt, der aber wegen der Größe dieser Zellen erheblich höher liegt als im Fall der Vesikel. Der rechte Balken zeigt den Effekt des Beladens der Zellmembran mit Cholesterin, was durch Inkubation der isolierten Zellen mit Methyl-ß-Cyclodextrin erfolgt, welches mit Cholesterin vorbeladen ist. Dies führt zu einer Reduktion von P_{CO2} auf 1/3 des Kontrollwertes.
Wenn die Kurve in Abb. 1 zugrunde gelegt wird, kann man eine mögliche Permeabilität einer Zellmembran für CO_2 aufgrund ihres Cholesteringehaltes vorhersagen. Die Tab. 2 zeigt eine Gegenüberstellung der gemessenen CO_2-Permeabilitäten verschiedener Zellen im Vergleich mit den aus den Messungen an Vesikeln identischen Cholesteringehaltes erhaltenen CO_2-Permeabilitäten. MDCK Zellen zeigen eine Permeabilität von 0,17 cm/s bei einen Cholesteringehalt von 37 mol%. Vesikel mit identischem Cholesteringehalt zeigen eine sehr ähnliche Permeabilität von 0,15 cm/s. Als extremes Beispiel kann die apikale Membran des proximalen Colon-Epithels betrachtet werden. Bei einem Cholesteringehalt von 77 mol% weist die Membran, genau wie die korrespondierenden Vesikel, eine Permeabilität von 0,0015 cm/s auf, also ca. 10 mal niedriger als die übrigen in Tab. 2 aufgelisteten Zellmembran-Permeabilitäten. Insgesamt ist eine erstaunliche Überseinstimmung zwischen den Permeabilitäten der Zellmembranen und den aus Vesikelmessungen vorhergesagten Permeabilitäten festzuhalten.

	PCO2 (cm/s) ± S.D.
Synthetische Lipid- Doppelschicht	0,35 bis 3,2
MDCK-Zellen	0,017 ± 0004
tsA201-Zellen	0,007 ± 0,003
Basolaterale Membran des proximalen Colon-Epithels	0,022
Apikale Membran des proximalen Colon-Epithels	0,0015 ± 0,0006

Tabelle 1: Aufstellung der gemessenen CO_2-Permeabilitäten (P_{CO2}) verschiedener Zellmembranen im Vergleich zu Literaturwerten für synthetische Lipid-Doppelschichten. Diese letzteren Werte liegen im Mittel bei ~ 1cm/s.

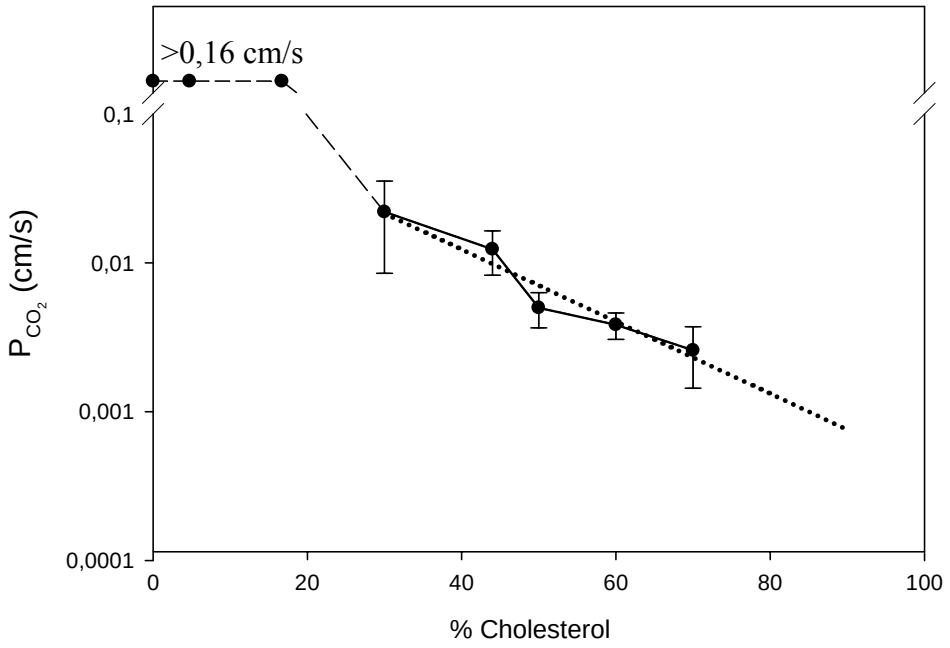

Abbildung 1: Effekt von Cholesterin auf die CO_2-Permeabilität (P_{CO2}) von Vesikeln mit PC:PS in einem molaren Verhältnis von 8:2. Der Cholesteringehalt der Vesikelmembran variierte zwischen 0 und 70 mol% Cholesterin pro Gesamtlipidmenge. Durchmesser der Vesikel aller Arten war ca. 150 nm. Alle Vesikel hatten einen intravesikuläre Carboanhydrase-Aktivität von ~ 10,000 (=Faktor, um den die Kinetik der CO_2-Hydratationsreaktion beschleunigt ist). Die massenspektrometrische Messung der P_{CO2} wurde bei 37°C durchgeführt. Die ersten drei Datenpunkte von 0, 5 und 17 mol% Cholesterin liegen höher als das obere Detektionslimit der massenspektrometrischen Methode. In diesen Fall 0,16 cm/s. Zwischen 17 und 30 mol% Cholesterin fällt P_{CO2} um eine Zehnerpotenz, zwischen 30 und 70 mol% Cholesterin um eine weitere Zehnerpotenz. Die gerade Linie repräsentiert eine Regressionsgrade zwischen den Messpunkten 30 bis 70 mol%. Balken repräsentieren die Standardabweichung. n=7-18.

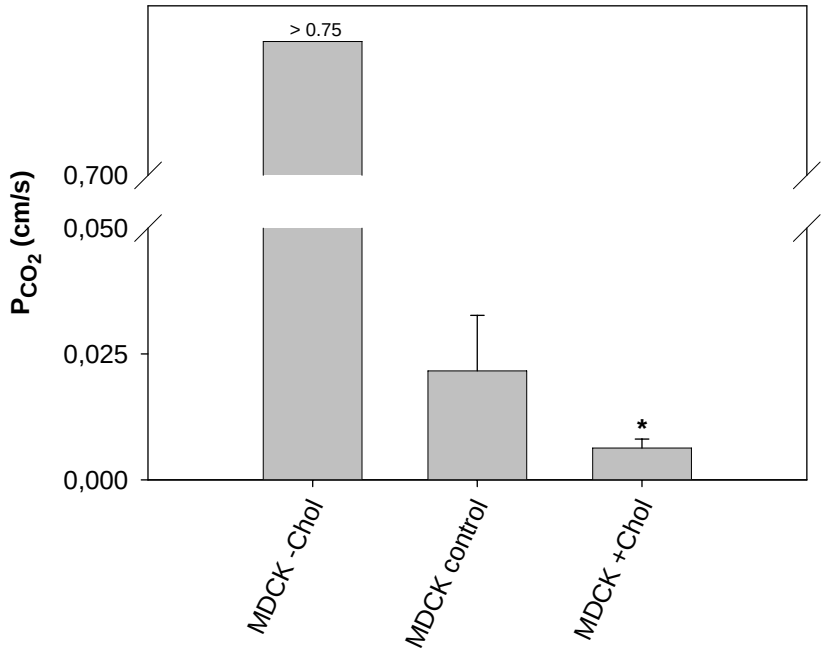

Abbildung 2: Effekt von Cholesterin auf die CO_2 Permeabilität (P_{CO2}) von MDCK-Zellmembranen. Vergleich zwischen MDCK-Kontrollzellen (Säule in der Mitte), MDCK-Zellen mit reduziertem Cholesteringehalt, die nach Behandlung mit Methyl-ß-Cyclodextrin einen drastischen Anstieg im P_{CO2} (>0,75 cm/s; linke Säule) zeigen, und MDCK-Zellen mit erhöhtem Cholesteringehalt (rechte Säule), die eine Senkung von P_{CO2} einen Faktor von 3 zeigen. n=12-20. Sterne zeigen signifikante Unterschiede zur Kontrolle mit $P<0,05$.

	P_{CO2} (cm/s) ± S.D	Cholesterin-gehalt (Mol%)	P_{CO2} erwartet auf-grund der Vesikel-permeabilitäten (cm/s)
Lipid-Doppelschicht	**0,35** bis **3,2**	0	**-**
MDCK-Zellen	**0,017** ± 0,004	37	**0,015**
tsA201-Zellen	**0,007** ± 0,003	-	**-**
Basolaterale Membran des proximalen Colon-Epithels	**0022**	42	**0,011**
Apikale Membran des proximalen Colon-Epithels	**0,0015** ± 0,0006	77	**0,0016**

Tabelle 2: Gegenüberstellung der gemessenen CO_2-Permeabilitäten (P_{CO2}) von Zellmembranen mit der Permeabilität von Vesikeln mit identischem Cholesteringehalt. Die CO_2-Permeabilität der Vesikel wurde aus der Kurve der Abb. 1 abgelesen. Werte für Lipid-Doppelschichten sind aus der Literatur.

In den nun folgenden beiden Abbn. wird dargestellt, dass die Membranpermeabilität für CO_2, die bei normalem Cholesteringehalt recht niedrig liegt, durch den Einbau von Aquaporin 1 erheblich gesteigert werden kann. In Abb. 3 ist der Effekt der Rekonstitution von humanem Aquaporin 1 (hAQP1) in Vesikelmembranen zu sehen. Die CO_2 Permeabilität von Vesikeln mit 50 mol% Cholesterin und unterschiedlichen „Lipid Protein Ratios“ (LPR) wurden gemessen. Mit sinkenden LPR von links nach rechts (von LPR 400 bis LPR 140) nimmt die Konzentration von hAQP1 in der Vesikelmembran zu. Dies konnten wir mittels Gefrierbruch-Elektronenmikroskopie bestätigen (s. Manuskript 1 CO2 permeability of cell membranes is regulated by membrane cholesterol and protein gas channels).

Mit zunehmender Konzentration von hAQP1 in der Membran steigt die Permeabilität für CO_2. Ein LPR von 400, ganz links auf der Abb. 3, führt zu einer Steigerung von P_{CO2} um ~ 0,0025 cm/s gegenüber Protein-freien Vesikeln. Hierzu ist anzumerken, dass die CO_2-Permeabilität der AQP1-freien Vesikel 0,005 cm/s beträgt (s. Manuskript 1). Ein LPR von 140, zweite Säule von rechts, bewirkt eine 10-fach größere Steigerung um 0,024 cm/s im Vergleich zu Protein-freien Vesikeln.

Der Einbau von einer bakteriellen Isoform des Aquaporins (AQPz), s. die rechte Säule in der Abb. 3, bewirkt keine Steigerung der Permeabilität für CO_2. AQPz scheint also kein CO_2-Kanal zu sein; das Experiment belegt zugleich, dass der bloße Einbau eines Membranproteins keine Steigerung von P_{CO2} bewirkt.

Die Abb. 4 zeigt die Permeabilitäten von MDCK Zellen, welche permanent mit hAQP1 transfiziert wurden, im Vergleich zu P_{CO2} der Kontrollzellen. Die Kontrollzellen zeigen eine CO_2-Permabilität von ~ 0,017 cm/s. Eine Inkubation mit dem Inhibitor DIDS zeigt hier keinen signifikanten Effekt. Transfizierte Zellen zeigen eine signifikant höhere Permeabilität als Kontrollzellen. Die Permeabilität steigt durch die Expression von hAQP1 um über 50% auf ~ 0,027 cm/s an. Inkubation mit dem als Hemmer des AQP1-CO_2-Kanals bekannten Inhibitor DIDS senkt die Permeabilität auf ~ 0,018 cm/s, ein Wert der von den Kontrollzellen nicht signifikant verschieden ist.

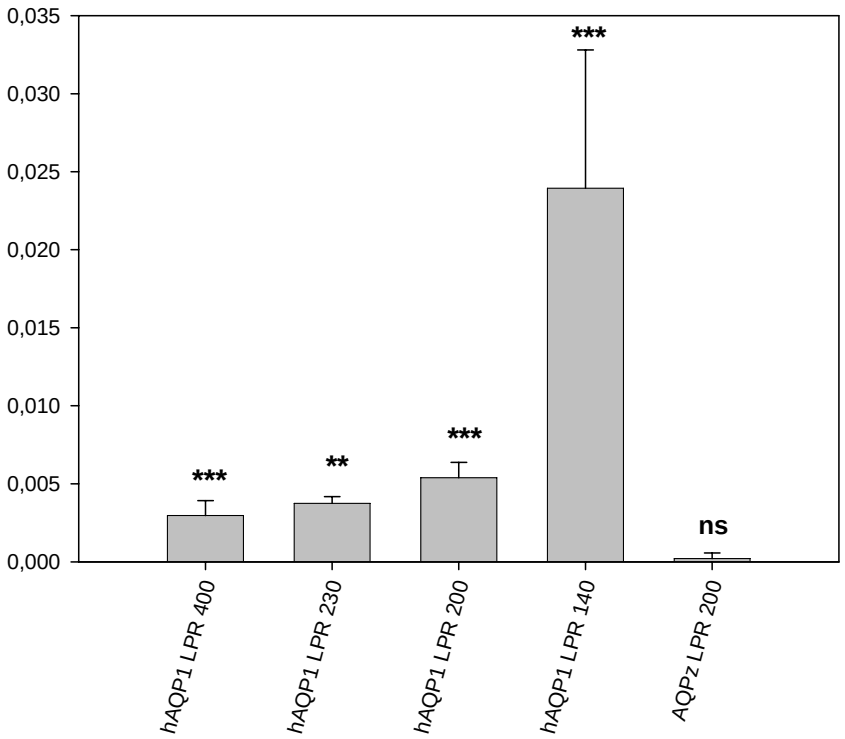

Abildung 3: Effekt von hAQP1 und AQPz Rekonstitution in Phospholipid-Vesikeln mit 50 mol% Cholesterin auf P_{CO2}. Gezeigt wird der Anstieg der CO_2-Permeabilität über den Kontrollwert als ΔP_{CO2} bei unterschiedlichen Lipid-Protein-Verhältnissen (LPR), die in Mol Lipid pro Mol Protein ausgedrückt sind. Für hAQP1 ist ein Anstieg von ΔP_{CO2} mit ansteigender AQP1- Konzentration zu sehen. Alle ΔP_{CO2} Werte zwischen LPR 400 und LPR 140 sind signifikant unterschiedlich zu null (** P<0,02; *** P<0,01; Balken repräsentieren Standardabweichung; n= 9,6,8,7,12 in der Reihenfolge von links nach rechts). AQPz mit LPR200 ist nicht signifikant unterschiedlich zu Null. Für alle gezeigten Vesikelpräparationen wurde mittels Freeze fracture Elektronenmikroskopie nachgewiesen, dass die Anzahl der Aquaporin-Tetramere pro Vesikelmembranfläche etwa proportional zu 1/LPR zunahm.

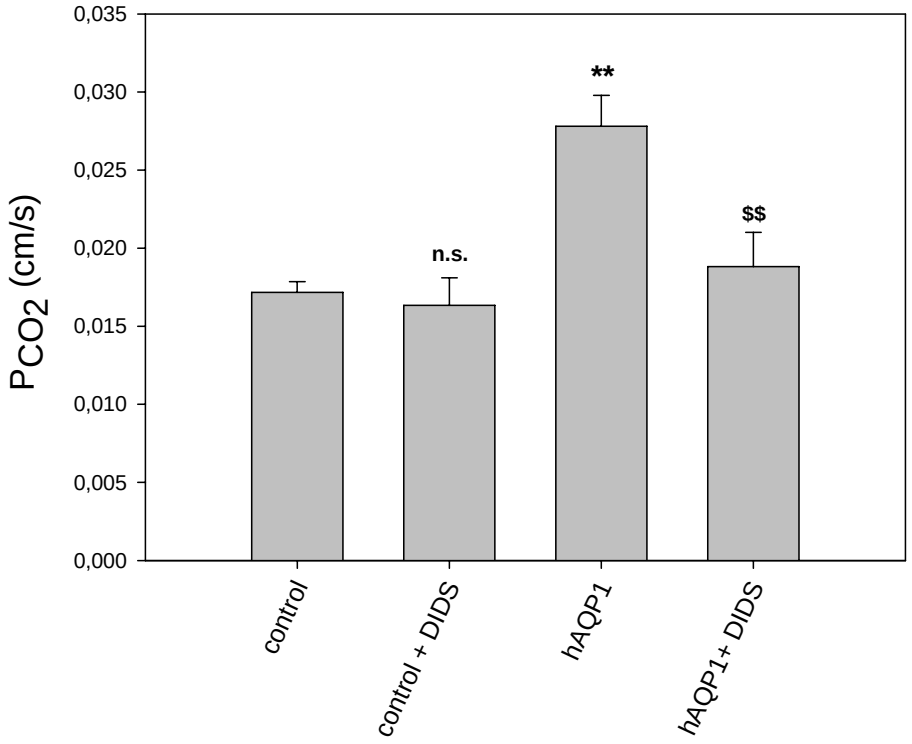

Abbildung 4: Effekt von hAQP1 Expression in MDCK Zellen unter permanenter Transfektion. MDCK Zellen, welche hAQP1 exprimieren, zeigen einen signifikanten Anstieg in P_{CO2} (3. Säule von links vs. 1. Säule von links, ** P<0,02) DIDS zeigt keinen Effekt auf Kontroll-MDCK Zellen, senkt aber signifikant P_{CO2} bei hAQP1-exprimierenden MDCK Zellen (4. Säule von links vs. 3. Säule von links, P<0,02). Balken stellen die Standardabweichung dar. n≥7.

Die Tab. 3 soll dazu dienen, zu demonstrieren, wie eine mit hohem Cholesteringehalt ausgestattete Zelle mit dementsprechend niedriger intrinsischer CO_2-Permeabilität, ihre Gaspermeabilität erhöhen kann, wenn die physiologische Funktion dies erfordert. Die Tab. 3 zeigt einen Vergleich zwischen normalen humanen Erythrozyten (obere Zeile) und Typ Colton Null Erythrozyten, welche kein AQP1 in ihrer Zellmembran aufweisen und deren zweiter CO_2-Kanal, das Rhesusprotein, mit DIDS inhibiert wurde (zweite Zeile). Diesen Werten gegenübergestellt ist die anhand des Cholesteringehaltes vorhergesagte CO_2-Permeabilität, wie sie aus Abb. 1 abgeleitet werden kann. Normale Erythrozyten weisen eine Permeabilität von 0,15 cm/s auf, was fünfzehn mal höher ist als die für 45 mol% Cholesterin vorhergesagte Permeabilität von 0,010 cm/s. Die Colton Null Erythrozyten, nach Inkubation mit DIDS, zeigen dagegen eine Permeabilität für CO_2 von ~ 0,015 cm/s, was der vorhergesagten Permeabilität von 0,01 cm/s recht nahe kommt.

	P_{CO2} (cm/s)	Cholesterin-gehalt (mol%)	Erwartete P_{CO2} (cm/s)
Erythrozyt	**0,15** ± 0,08	45	0,010
Erythrozyt ∅ AQP1, ∅ funktionelles Rh-Protein	**0,015** ± 0,003	45	0,010

Tabelle 3: Gegenüberstellung gemessener CO_2-Permeabilitäten (P_{CO2}) von humanen Erythrozytenmembranen und der Permeabilität von Vesikeln mit identischem Cholesteringehalt. Die CO_2-Permeabilität der Vesikel wurde aus der Kurve der Abb. 1 abgeleitet. Bei den Erythrozyten ohne AQP1 und ohne funktionellen Rhesuskomplex handelt es sich Erythrozyten von Patienten, die kein AQP1 haben (Colton null). Der CO_2-Kanal des Rhesuskomplexes wird mittels DIDS inhibiert.

Diskussion CO_2 Messungen

Cholesterin orientiert sich innerhalb der Lipid-Doppelschicht mit seiner Hydroxylgruppe nahe an den polaren Kopfregionen der Phospholipide. In dieser Position immobilisiert die steife Steroidringsruktur des Cholesterins die Kohlenstoffkette nahe der polaren Kopfregion der Phospholipide. Dadurch wird die Doppelschicht in diesen Bereich weniger verformbar und somit weniger durchlässig für kleine wasserlösliche Stoffe (Alberts et al., Molecular Biology of the Cell, 4th Edition). Dieser Effekt ist in Abb. 1 eindeutig für die CO_2 Permeabilität von Vesikelmembranen zu sehen. Mit steigendem Cholesteringehalt nimmt die Permeabilität der Vesikelmembran für CO_2 ab und es lässt sich eine Korrelation zwischen dem Cholesteringehalt und der Permeabilität für CO_2 ableiten.
Die Permeabilität von Vesikeln mit unter 17 mol% Cholesterin konnte, wie oben bereits erwähnt, nicht korrekt bestimmt werden, da deren Permeabilität über der methodisch bedingten oberen Messgrenze für die CO_2-Permeabilität von Vesikeln von 0,16 cm/s lag. Dieser Befund steht im Einklang mit Corvera et al. (1992) und Trandum et al. (2000), die bei einem Cholesteringehalt bis ca. 20 mol% zunächst eine Erhöhung – statt einer Verminderung – der Permeabilität für kleine lösliche Substanzen gefunden haben. In ihren Untersuchungen nahm die Permeabilität dann erst oberhalb von 20 mol% mit steigen der Cholesterinkonzentration wieder ab. Ein solcher Effekt würde natürlich in unseren Messungen nicht sichtbar werden, da bereits die CO_2-Permeabilität in Abwesenheit von Cholesterin die obere Messgrenze unserer Methode überschreitet.
Jedoch könnte dies den abrupt erscheinenden Abfall der CO_2-Permeabilität zwischen dem dritten (17 mol%) und vierten (30 mol%) Messpunkt der Abb. 1 erklären. Bei einem Vesikel-

Cholesteringehalt von 30 mol% liegt die CO_2-Permeabilität bei ~ 0,015 cm/s und damit eine Zehnerpotenz unter dem gemessenen oberen Grenzwert und fast zwei Zehnerpotenzen unter dem Wert für planare cholesterinfreie Lipid-Doppelschichten, der in der Literatur mit ~ 1 cm/s angegeben wird. Ein Cholesteringehalt der Vesikel von 70 mol% führt zu einer Permeabilität von ~ 0,0017 cm/s, ein Wert, der dann nahezu drei Zehnerpotenzen unter der Permeabilität von ~ 1 cm/s liegt.

Die Schlussfolgerung, dass Cholesterin die CO_2-Permeabilität der Zellmembranen massiv beeinflusst, wird durch die Ergebnisse der Abb. 2 unterstützt. Der Effekt von Cholesterin welcher sich in Abb. 1 in Vesikeln zeigt, ist hier in intakten Zellen wiederzufinden. Sowohl Cholesterin-Anreicherung wie auch Cholesterin-Depletion in den Membranen von MDCK-Zellen zeigt einen drastischen Effekt auf deren CO_2-Permeabilität. Es ist anzumerken, dass das Beladen der Zellen mit Cholesterin keinen negativen Einfluss auf die Zellvitalität zeigte. Das Entfernen von Cholesterin aus der Zellemembran führte zu einer Reduktion der Vitalität um maximal 11%. Der Durchmesser der Zellen wurde durch die Behandlung mit Methyl-ß-Cyclodextrin nicht beeinflusst, weder beim Beladen noch beim Herauslösen von Cholesterin. Es wird angemerkt, dass tote Zellen keinen Beitrag zum Messsignal leisten und somit keinen Einfluss auf die gemessene CO_2 Permeabilität haben.

Die für Cholesterin-verarmte MDCK-Zellen angegebene Permeabilität von > 0,75 cm/s stellt das obere Limit für die Messbarkeit der Permeabilität von MDCK Zellen dar, welches aufgrund des kleineren Oberflächen-Volumenverhältnisses von MDCK-Zellen höher liegt als im Fall der Vesikel. Es zeigt sich jedenfalls klar, dass das Verringern des Cholesteringehaltes der MDCK-Zellmembran zu einer > 40-fachen Steigerung der CO_2-Permeabilität führt. Das Beladen der Zellmembranen mit Cholesterin führt dagegen zur einer Reduktion der Permeabilität von 0,017 cm/s auf 0,0065 cm/s, also auf ca. 1/3. Diese beiden Ergebnisse zeigen einen markanten Effekt von Cholesterin auf die CO_2-Permeabilität der Zellmembran. Eine Beeinflussung dieser Ergebnisse durch Cholesterin-bedingte Veränderungen der Permeabilität durch veränderte Oberflächen-Volumen-Verhältnisse oder möglicher „Löcher“ in den Zellmembranen, also Membranen nicht-vitaler Zellen, konnte ausgeschlossen werden.

Die Daten in der Tab. 2 zeigen, dass die CO_2-Permeabilitäten der Membranen verschiedener Zellen der Permeabilität entsprechen, die man für die jeweilige Cholesterinkonzentration anhand der Kurve aus Abb. 1 erwarten würde. Die Werte zeigen eine Übereinstimmung

innerhalb von etwa ± 50%. Dies belegt die Hypothese, dass Cholesterin der Hauptfaktor für die Höhe der CO_2-Permeabilität von Zellmembranen und hauptverantwortlich für die niedrige intrinsische Permeabilität offenbar vieler Zellmembranen ist. Ein Cholesteringehalt von 40 bis 50 mol%, wie er in vielen Zellen gefunden werden kann, führt zu einer Permeabilität von ~ 0,01 cm/s. Dies ist zwei Zehnerpotenzen niedriger, als früher anhand der Ergebnisse an künstlichen Lipid-Doppelschichten angenommen wurde. Ein Cholesteringehalt von 77 mol% führt nach den Daten der Tab. 2 zu einer zehnfach niedrigeren Permeabilität von ~ 0,001 cm/s (und somit drei Zehnerpotenzen niedriger als cholesterinfreie Lipid-Doppelschichten). Dies wurde bisher noch nicht nachgewiesen und verändert erheblich die Ansichten über die CO_2-Permeabilität von Zellmembranen.

Einige Zellen, wie z.B. Erythrozyten, weisen wie in der Tab. 3 zu sehen aber eine höhere Permeabilität auf, als aufgrund ihres Cholesteringehalts zu erwarten wäre. Eine mögliche Ursache für diese höhere CO_2 Permeabilität ist der Gaskanal Aquaporin 1. Endeward et al. (2006) haben gezeigt, dass Colton-Null-Erythrocyten, denen das Aquaporin 1 vollständig fehlt, eine Reduktion ihres P_{CO2} um etwa 50% aufweisen (s. Tab. 3, die jedoch zusätzlich den Effekt der Hemmung des zweiten erythrocytären Gaskanals RhAG, Rhesus-assoziertes Glykoprotein, zeigt). Somit war Aquaporin 1 als möglicher Gaskanal bereits identifiziert. Die jetzigen Untersuchungen sollten die Frage beantworten, ob sich das Experiment auch in dem Sinne umkehren lässt, dass Aquaporin 1-Proteinmoleküle in eine Aquaporin-freie Membran eingebaut werden und sich dann ein Anstieg der CO_2-Permeabilität nachweisen lässt. Dies geschah in dieser Arbeit mit künstlichen Lipidvesikeln und mit Membranen intakter Zellen.

Die Abb. 4 zeigt, dass Aquaporin 1 in der Tat auch in Vesikeln mit 50 mol% Cholesteringehalt einen steigernden Effekt auf die Permeabilität für CO_2 hat. Dieser Effekt ist direkt von der Menge der bei der Herstellung der Vesikel eingesetzten Aquaporin 1-Menge abhängig. Je mehr Apuarporin 1 sich in der Membran befindet, desto höher ist die Permeabilität für CO_2.
Das bakterielle Aquaporin Z zeigt dabei, dass der positive Effekt von Aquaporin 1 auf die Permeabilität von CO_2 kein allgemeines Artefakt der Rekonstitution der Membran mit einem Membran-Protein ist. Da Aquaporin Z keinen Effekt auf die Permeabilität zeigt, kann ausgeschlossen werden, dass das alleinige Einbringen von Protein in die Membran ausreicht die Permeabilität zu erhöhen. Zudem liefert das Experiment mit AQPz die neue Information, dass AQPz – im Gegensatz zu AQP1 – kein CO_2-Kanal ist.

Die Expression von Aquaporin 1 in MDCK Zellen untermauert diesen Befund. In MDCK Zellen zeigt Aquaporin 1 einen steigernden Effekt auf die Permeabilität für CO_2. Die Steigerung beträgt in dem konkreten Fall in MDCK Zellen ca 50% im Vergleich zu Kontroll-MDCK-Zellen, die kein Aquaporin 1 exprimieren.
Dieser Effekt von Aquaporin 1 ist durch Anwendung des Inhibitors DIDS reversibel, wie in der Abb. 4 ersichtlich ist. Die Inkubation mit DIDS führt in Kontrollzellen dagegen zu keinem Effekt auf die CO_2-Permeabilität. Ein ähnliches Ergebnis wurde, wie im beiliegenden Manuskript 1 ersichtlich, völlig analog auch an Vesikeln erhoben. DIDS bringt den Anstieg der Vesikelpermeabilität durch eingebautes Aquaporin 1 praktisch zum Verschwinden, während es an Aquaporin-freien Vesikeln keinen Effekt auf die CO_2-Permeabilität hat. Die beiden Ergebnisse bestätigen somit klar, dass Aquaporin 1 als CO_2 Kanal dient.

Schlussfolgerung CO_2

Cholesterin kann die Permeabilität für CO_2 in Membranen von Phospolipidvesikeln und Zellen um zwei Zehnerpotenzen senken, im Vergleich mit künstlichen planaren Lipid-Doppelschichten um drei Zehnerpotenzen. Zellmembranen mit normalen Cholesteringehalten von 30 bis 50 mol% zeigen relativ geringe Permeabilitäten von ~ 0,01 cm/s. Noch geringere Permeabilitäten von ~ 0,001 cm/s sind das Resultat von einem Cholesteringehalt von über 70 mol%, wie er z.B. in den apikalen Membranen von Colonepithelien vorkommt. Hohe Permeabilitäten für CO_2 werden durch den Einbau von Gaskanälen, wie Aquaporin 1, oder durch sehr geringe Cholesteringehalte der Membran erzielt. Höhere Cholesteringehalte sind aus ganz anderen Gründen für viele Zellmembranen erforderlich, z.B. zur Aufrechterhaltung der allgemeinen Barrierefunktion und der mechanischen Membranstabilität. Daher bleibt bei solchen Zellen dann nur die Ausstattung mit Gaskanälen, wenn eine hohe Gaspermeabilität aus Gründen der notwendigen Transportraten für CO_2 (und O_2) erforderlich ist.

Somit können auf diese Weise sehr unterschiedliche CO_2-Permeabilitäten erreicht werden. Zum einen können sehr hohe CO_2 Permeabilitäten etabliert werden, wie sie in Erythrozyten und Lungenepithelien benötigt werden.
Zum anderen können auch sehr niedrige Permeabilitäten erreicht werden, wie sie bei der apikalen Membran des Colons und der Magenepithelien funktionell sinnvoll sind. Dies ermöglicht es, hohe luminale CO_2- und NH_3-Drucke vom Cytoplasma der Epithelzellen

fernzuhalten und damit dessen Säurebelastung durch hohe CO_2-Drucke, wie sie in beiden Lumina vorkommen, zu vermeiden, und ebenso das Cytoplasma dieser Zellen vor der toxischen Wirkung von NH_3 zu schützen. Wenn solche Eigenschaften auch für O_2 vorlägen, was bisher nicht gezeigt worden ist, wäre auch zu verstehen, wie die Epithelzelle sich davor schützen kann, ihre von der Kapillarseite her erfolgende O_2-Versorgung durch den im Colonlumen herrschenden O_2-Partialdruck von nahezu Null zu gefährden. Wenn Zellmembranen die gleichen Permeabilitäten wie cholesterinfreie künstliche Lipid-Doppelschichten aufweisen würden, wäre dies nicht möglich.
Eine analoge Situation könnte, wie soeben angedeutet, auch für andere wichtige Gase wie O_2, N_2, NO und CO bestehen. Dies soll auch noch weiter untersucht werden. Es könnte sich das Bild ergeben, dass die Permeabilität für CO_2 und für andere Gase über eine breite Spanne durch die beiden Parameter Cholesterin und den Einbau von Gaskanälen reguliert ist.

II. Anionaustauscher 1 vermittelte Bikarbonat-Permeation an Zellmembranen

Ergebnisse HCO_3^- Messungen

Abb. 5a zeigt die Expression von N-terminal mit dem Fluoreszensprotein YPet Gelb markierten murinen AE1 (YPet-mAE1) und der C-terminal mit dem Fluoreszenzprotein CyPet Cyan markierten CAII (CAII-CyPet) innerhalb einer tsA201 Zelle. Es ist klar zu erkennen, dass YPet-mAE1 in der Zellmembran lokalisiert ist, während CAII-CyPet homogen intrazellular verteilt ist. Die Grafik in der Abb. 5b zeigt das Intensitätsprofil der beiden Farbstoffe entlang der roten Linie in Abb. 5a. Der Farbstoff YPet zeigt eine nahezu exklusive Lokalisation an der Zellmembran, während CyPet sich homogen in der Zelle verteilt und keinerlei Anreicherung an der Zellmembran aufweist. Es sind keine übereinstimmenden Intensitätsspitzen von YPet und CyPet zu sehen.

Die gleichen Befunde konnten für die Coexpression von CAII ohne N-Terminus (truncCAII) und von katalytisch inaktiver CAII (CAII-V143Y) gefunden werden (Daten befinden sich im beigefügten Manuskript 2 Activity and distribution of intracellular carbonic anhydrase II and their effects on the transport activity of anion exchanger AE1/SLC4A1). Um eine geringe, eventuell in Abb. 5 nicht sichtbare, Interaktion zwischen AE1 und CAII auszuschließen, wurde eine FRET Messung durchgeführt (Förster Resonanz Energie Transfer). Weder für murines AE1 noch für humanes AE1 konnte bei einer Coexpression von AE1 mit CAII ein FRET Effekt gemessen werden (s. ebenfalls beiliegendes Manuskript 2).

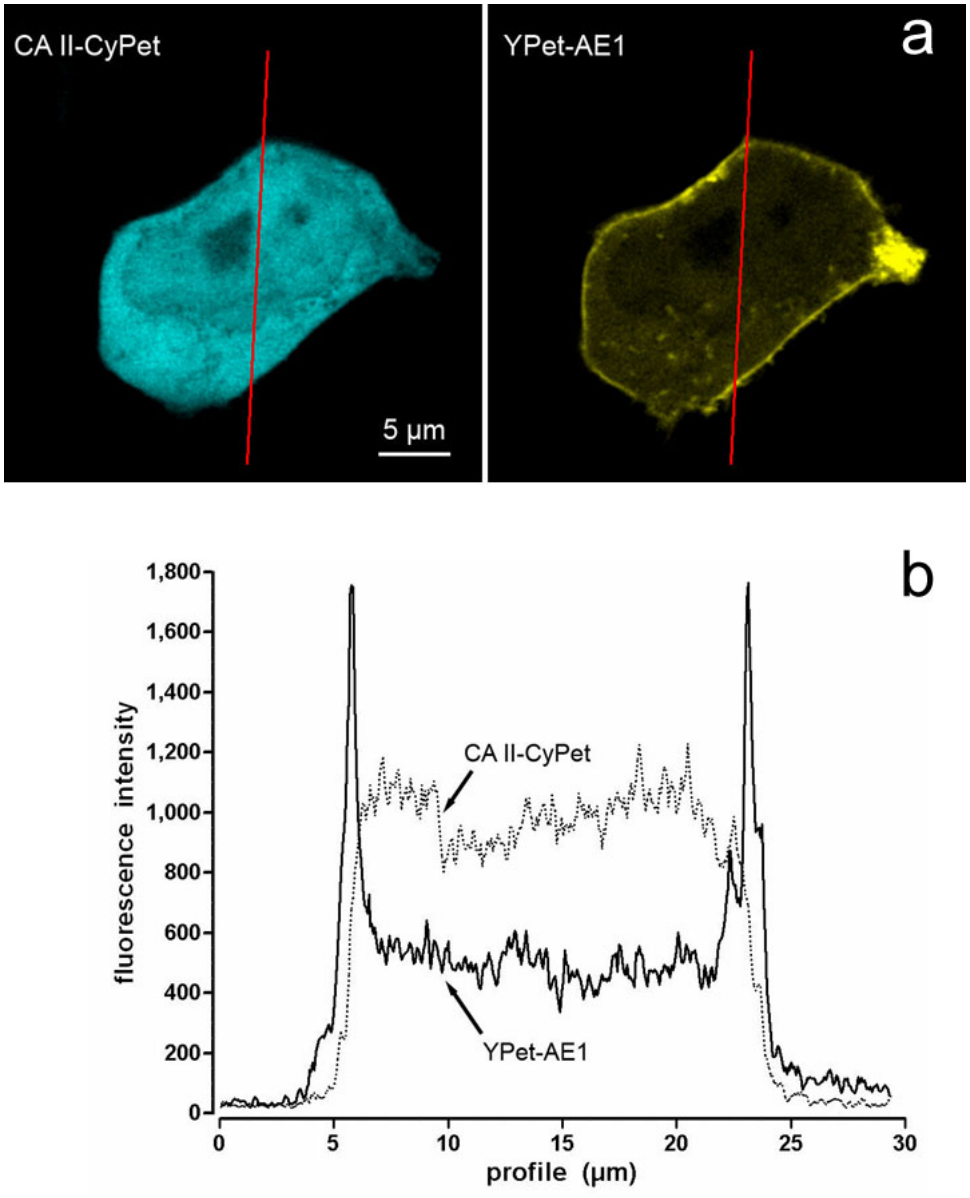

Abbildung 5: Doppelexpression von YPet-mAE1 und CAII-CyPet in einer tsA201 Zelle. **a)** YPet wurde N-terminal an murines AE1 gebunden. CyPet wurde C-terminal an humane CAII gebunden. Entlang der roten Linie wurden die Intensitäten der einzelnen Farbstoffe gemessen. **b)** Intensitätsprofile entlang der roten Linie aus a).

Abb. 6 zeigt den Effekt verschiedener CAII-Konstrukte auf die Permeabilität von HCO_3^- an der tsA201 Zellmembran. Die HCO_3^- Permeabilität ist gegen die intrazelluläre Carboanhydrase-Aktivität (A_i) aufgetragen. Der zweite Punkt von links (▼) zeigt die Permeabilität von Zellen, die nur mit dem Konstrukt YPet-mAE1 transfiziert wurden, und ansonsten lediglich die endogene CAII-Aktivität aufweisen. Diese Zellen können in der Abb. 6 als Kontrollzellen angesehen werden, welche eine HCO_3^- -Permeabilität von $3{,}8x10^{-4}$ cm/s aufweisen. Der Datenpunkt ganz links auf der Abb. 7 (▲) zeigt die HCO_3^- -Permeabilität bei einer Koexpression der akatalytischen CAII-Mutante CAII-V143Y mit dem mAE1-Konstrukt. Dieser Punkt zeigt etwas geringere Permeabilität von $3{,}6x10^{-4}$ cm/s. Diese Zellen zeigen allerdings eine stark von ca. 800 auf ca. 500 erniedrigte intrazelluläre Carboanhydrase-Aktivität. Der dritte Punkt von links (♦) repräsentiert tsA201 Zellen, welche zusätzlich zu YPet-mAE1 noch funktionelle CAII vom Wildtyp exprimieren. Diese Koexpression führt zu einer Steigerung der intrazellulären Carboanhydraseaktivität und in Verbindung damit auch zu einer Erhöhung der HCO_3^- Permeabilität auf $5{,}6x10^{-4}$ cm/s. Ganz rechts auf der Abb. 7 ist der Datenpunkt (●) der Zellen zu sehen, die mit der Carboanhydrase II ohne N-Terminus, "truncCAII", koexpremiert wurden. Die Deletion des N-Terminus verhindert ein mögliches Binden der Carboanhydrase an den C-Terminus von AE1, da nach vorangegangenen Literaturergebnissen die Histidine der hier deletierten N-terminalen Sequenz die Bindung an AE1 vermitteln (Vince et al., 2000). Diese Zellen zeigen eine weitere Erhöhung der intrazellulären Carboanhydrase-Aktivität, um den Faktor 2 gegenüber den Kontrollzellen, und in Verbindung damit auch eine weitere Steigerung der HCO_3^- Permeabilität auf $6x10^{-4}$ cm/s. Alle Messpunkte fallen auf eine Regressionsgerade, welche eine Abhängigkeit der HCO_3^- -Permeabilität von der intrazellulären Carboanhydrase-Aktivität zeigt.

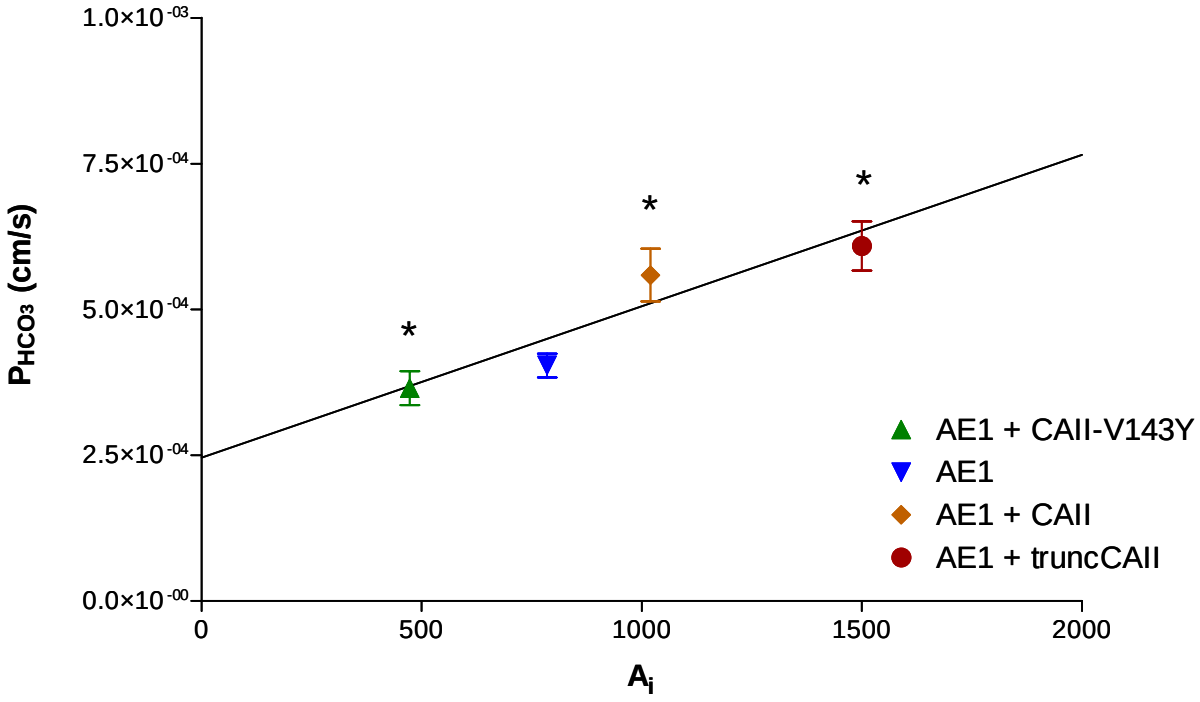

Abbildung 6: HCO_3^- -Permeabilitäten (P_{HCO3-}) von tsA201 Zellen, aufgetragen gegen die intrazelluläre Carboanhydrase-Aktivität (Ai):

▲ zeigt tsA201 Zellen die doppelt-transfiziert mit CAII-V143Y-CyPet und YPet-mAE1 sind.

▼ repräsentiert "Kontrollzellen" welche in diesem Fall nur YPet-mAE1 transfiziert sind.

♦ repräsentiert tsA201 Zellen, doppelt transfiziert mit CAII-CyPet und YPet-mAE1.

● tsA201 Zellen, die doppelt mit N-terminal gekürzter CAII-CyPet (truncCAII-CyPet) und YPet-mAE1 transfiziert wurden.

* weist auf statistisch signifikante Unterschiede zwischen dem jeweiligen Mittelwert der Bikarbonatpermeabilität und dem Mittelwert der Bikarbonatpermeabilität der "Kontrollzellen" hin.

Zusammenfassend ergibt sich, dass die verschiedenen Transfektionen zu unterschiedlichen Ai führten und die Unterschiede in den Bikarbonatpermeabilitäten (P_{HCO3-}) einer etwa linearen Abhängigkeit zwischen P_{HCO3-} und Ai folgen. Es liegt kein Hinweis auf Metabolon-vermittelte Änderungen der Bikarbonatpermeabilität vor.

Diskussion HCO_3^- Messung

Bisher wurden weder konfokale Ko-Lokalisationsuntersuchungen noch FRET-Messungen an intakten Zellen für AE1 und CAII durchgeführt. Die Abb. 5a und 5b sowie weitere Untersuchungen, hier nicht mit Bildern belegt, mit CAII ohne N-Terminus und funktionell inaktive CAII (CAII - V143Y) zeigen die Carboanhydrase II immer homogen verteilt im Cytoplasma. Es ist keine Anreicherung an der Zellmembran zu erkennen, unabhängig von der exprimierten Variante der Carboanhydrase II. AE1 dagegen ist stets, wie zu erwarten, immer klar mit der Zellmembran assoziiert. Die kleineren Spuren von AE1 im Cytoplasma sind mit vesikulären Strukturen assoziiert und reflektieren den noch ablaufenden Transport des Membranproteins zur Zellmembran. Der Befund, dass sich CAII nicht an der Zellmembran anreichert, wurde durch das Fehlen eines FRET-Signals bestätigt. Somit gibt es anhand dieser Daten keinen Beweis, dass sich AE1 und CAII innerhalb der Zelle auf bis zu 8-10 nm (der kritischen Grenze für das Zustandekommen eines FRET-Signals) einander annähern. Mit diesen Befunden kann die Existenz des postulierten "Metablonkomplexes" ausgeschlossen werden.

Die Daten der Abb. 6 lassen mehrere weitere Schlussfolgerungen zu:

1) Zwischen der Bikarbonat-Permeabilität von tsA201-Zellen, in denen mAE1 exprimiert wird, und der intrazellulären Carboanhydrase-Aktivität besteht eine positive Korrelation. Dass dies theoretisch zu erwarten ist, wird im zugehörigen beigelegten Manuskript 2 ausführlich dargestellt. Dieses Verhalten kommt dadurch zustande, dass z.B. bei der zellulären Aufnahme von Bikarbonat Carboanhydrase benötigt wird, um eine schnelle Umwandlung von HCO_3^- in CO_2 zu ermöglichen, welches dann die Zelle verlassen kann und somit eine schnelle Fortsetzung des Bikarbonat-Aufnahmeprozesses ermöglicht. Die intrazelluläre Carboanhydrase ermöglicht also die Aufrechterhaltung eines großen transmembranalen HCO_3^- - Konzentrationsgradienten und bewirkt damit eine Beschleunigung des HCO_3^- - Influxes. Diese Abhängigkeit des Bikarbonateinstroms von der Carboanhydrase-Aktivität besteht im Wesentlichen im Aktivitätsbereich zwischen 0 und 5000, also im Bereich der in Abb. 6 vorkommenden Aktivitäten. In diesem Bereich führt – nach einem Rechenmodell wie auch nach den Ergebnissen der Abb. 6 – eine Zunahme der intrazellulären Carboanhydrase-Aktivität zu einer Zunahme der Bikarbonat-Permeabilität.

2) Die Expression von CAII-CyPet führt zu einer Steigerung der intrazellulären Carboanhydrase-Aktivität und damit auch zu einen Anstieg der HCO_3^- Permeabilität. Dieser Befund ist nach dem unter 1) Ausgeführten zu erwarten und stellt keinerlei Hinweis auf die Anwesenheit eines sog. Metabolons dar, also auf durch physikalische Assoziation bedingte Aktivierung des AE1-Transporters. Der Befund für sich allein bedeutet natürlich auch noch keine Widerlegung des Metabolon-Konzeptes.

3) Die Expression der katalytisch inaktiven Carboanhydrase CAII - V143Y führt zu einer erheblichen Reduktion der intrazellulären Carboanhydrase-Aktivität von ca 800 auf ca 480. Bei vielen Expressionsversuchen wurde eine leichte Reduktion der endogenen Carboanhydrase-Aktivität gegenüber den unbehandelten Zellen gemessen, wenn Carboanhydrase-Mutanten transient exprimiert wurden. Bei der Expression der inaktiven Carboanhydrase jedoch ist dieser Effekt drastisch, und führt zu einer moderaten, aber der allgemeinen Abhängigkeit zwischen P_{HCO3-} und Ai folgenden, Reduktion der HCO_3^- -Permeabilität. Experimente von Sterling et al. (2001) mit dieser Mutante führten zu einer 60%igen Reduktion der Bikarbonat-Permeabilität. Das experimentelle Vorgehen von Sterling et al. (2001) legt nahe, dass bei deren Experimenten die Expression der Mutante weitaus stärker war als in den hier gezeigten Versuchen. Daher beobachteten diese Autoren auch eine stärkere Absenkung der Bikarbonat-Permeation. Wir interpretieren daher die von Sterling et al. (2001) berichteten Ergebnisse wie folgt: Die dort noch drastischer als hier erfolgte Absenkung der intrazellularen Carboanhydrase-Aktivität führte zu einer stärkeren Absenkung der Bikarbonat-Permeabilität als hier beobachtet. Damit zeigt der Befund dieser Autoren die auch hier beobachtete Abhängigkeit der Bikarbonat-Permeabilität von der intrazellulären Carboanhydrase-Aktivität, er muss jedoch nicht durch die Verdrängung der endogenen CAII durch die inaktive Mutante CAII-V143Y von einem Metabolon erklärt werden. Weder der von uns gezeigte Befund noch der von Sterling et al. (2001) liefert somit einen schlüssigen Hinweis auf die Existenz eines Metabolons.

4) Ein weiterer wichtiger Befund der Abb. 6 ist die Expression der Carboanhydrase II, deren N-Terminus gekürzt ist (truncCAII). Nach der Metabolonhypothese dürfte diese Carboanhydrase zu keiner Steigerung der HCO_3^- Permeabilität führen, da diese CAII-Form wegen ihrer fehlenden Bindungssequenz sich nicht an den C-Terminus von AE1 anlagern und so die Transportrate von AE1 beeinflussen kann. Im Gegensatz dazu führt hier die Expression der truncCAII zu einer signifikanten Steigerung der Bikarbonat-Permeabilität von $3{,}8 \times 10^{-4}$ cm/s auf 6×10^{-4} cm/s. Dieser Effekt wird allein durch die erhebliche Steigerung der intrazellulären Aktivität von 800 auf 1500 erzielt, da die truncCAII eine normale katalytische Aktivität aufweist.

Schlussfolgerung HCO_3^- Messungen

Ein mögliches Metabolon von AE1 und CAII wurde hier auf unterschiedliche Weisen untersucht. Anhand von mathematischen Simulationen aus dem beiliegenden Manuskript 2, welche hier nicht genauer aufgezeigt wurden, wurde die Carboanhydrase-Aktivität bestimmt, bei der keine Limitierung des HCO_3^- Transportes durch intrazelluläre Aktivität mehr vorliegt. Diese Aktivität liegt zwischen 3000 und 5000. Da die typische intrazelluläre Carboanhydrase-Aktivität vieler Zelllinien unter 1000 liegt, ist eine Limitierung dieser HCO_3^- -Transportrate im Bereich dieser Aktivität zu erwarten. Dies konnte auch in der vorliegenden Arbeit nachgewiesen werden. Es konnte ein moderater Anstieg der HCO_3^- -Transportrate in tsA201 Zellen nachgewiesen werden, wenn die intrazelluläre Aktivität von 500 auf 1500 ansteigt. Es wurde nachgewiesen, dass die Expression der akatalytischen CAII Mutante V143Y zwar moderat die HCO_3^- Transportrate absenkte, dies jedoch durch die stark abgesenkte intrazelluläre Aktivität bedingt war. Die Expression der Wildtyp-CAII und der CAII ohne N-Terminus führten zu einer signifikanten Steigerung der HCO_3^- Transportrate, obwohl die N-terminal gekürzte CAII an ein postuliertes Metabolon nicht binden könnte. Alle beobachteten Änderungen der HCO_3^- Transportrate folgen in konsistenter Weise den jeweiligen Änderungen der intrazellulären Carboanhydrase-Aktivität. Somit unterstützen keine dieser vorliegenden funktionellen Befunde eine Metabolontheorie.
Weiter wurde dies durch die Befunde an menschlichen Erythrozyten mit fehlender Carboanhydrase II unterstützt (s. beigefügte Manuskript 2). Diese Erythrozyten weisen trotz fehlender CAII keine geringere HCO_3^- Transportrate auf als normale Erythrozyten. Das zeigt, dass die CAII nicht wesentlich für die Aktivität des AE1 ist.

Infolge des Vorhandenseins der Carboanhydrase I in diesen Erythrocyten, welche nicht an AE1 binden kann, verfügen diese Zellen noch über genügende Carboanhydrase-Aktivität, sodass eine Limitierung der Bikarbonat-Transportrate durch die intrazelluläre Aktivität vermieden wird.
Auch die Untersuchungen mit dem konfokalen Mikroskop zeigte keine Kolokalisation des Cl^- - HCO_3^- -Antiporters AE1 und der Carboanhydrase II. Dieser Befund wurde durch das nicht Vorhandensein eines FRET-Signals noch weiter gefestigt. Es konnte somit ausgeschlossen werden, dass sich die beiden Proteine auf weniger als 8-10 nm aneinander annähern und einen Komplex bilden. In der Summe zeigen morphologische und funktionelle Befunde, dass AE1 und CAII kein Metabolon bilden.

Literaturverzeichnis

Alberts, B. (2002) Molecular Biology of the Cell 4th Edition, *Garland Science*

Corvera, E., Mouritsen, O.G., Singer, M.A., Zuckermann, M.J. (1992) The permeability and the effect of acyl-chain length for phospholipid bilayers containing cholesterol: theory and experiment. *Biochim. Biophys. Act*a. **1107,** 261-70.

Endeward, V., Gros, G. (2005) Low carbon dioxide permeability of the apical epithelial membrane of guinea-pig colon. *J. Physiol.* **567**, 253-265.

Endeward, V., Musa-Aziz, R., Cooper, G.J., Chen, L.M., Pelletier, M.F. (2006) Evidence that aquaporin 1 is a major pathway for CO2 transport across the human erythrocyte membrane. *FASEB J* **20**, 1974-1981.

Overton, E. (1901) Studien über die Narkose. Jena: *Gustav Fischer Verlag*.

Piermarini, P.M., Kim, E.Y., Boron, W.F. (2007) Evidence against a direct interaction between intracellular carbonic anhydrase II and pure C-terminal domains of SLC4 bicarbonate transporters. *J. Biol. Chem.* **282**, 1409-1421

Sterling, D., Reithmeier, R.A., Casey, J.R. (2001) Carbonic anhydrase: in the driver's seat for bicarbonate transport. *J. Pancreas.* **2**, 165-170

Trandum, C., Westh, P., Jorgensen, K., Mouritsen, O.G. (2000) A thermodynamic study of the effects of cholesterol on the interaction between liposomes and ethanol. *Biophys J.* **78,** 2486-92.

Vince, J.W., Reithmeier R.A. (1998) Carbonic anhydrase II binds to the carboxyl terminus of human band 3, the erythrocyte C1-/HCO3- exchanger. *J. Biol. Chem.* **273**, 28430-28437

Vince, J.W., Reithmeier, R.A. (2000) Identification of the carbonic anhydrase II binding site in the Cl(-)/HCO(3)(-) anion exchanger AE1. *Biochemistry*. **39**, 5527-5533.

Vince, J.W., Carlsson, U., Reithmeier, R.A. (2000) Localization of the Cl-/HCO3- anion exchanger binding site to the amino-terminal region of carbonic anhydrase II. *Biochemistry*. **39**, 13344-13349

Manuskript 1

CO_2 permeability of cell membranes is regulated by membrane cholesterol and protein gas channels

Fabian Itel*, Samer Al-Samir*, Fredrik Öberg, Mohamed Chami, Manish Kumar, Claudiu T. Supuran, Peter M.T. Deen, Wolfgang Meier, Kristina Hedfalk, Gerolf Gros, Volker Endeward

* Gleichberechtigte Erstautoren

Veröffentlicht in „The FASEB Journal“
Published online September 10, 2012, doi: 10.1096/fj.12-209916 ***fj.12-209916***

Beitrag zu der Wissenschaftlichen Publikation „**CO_2 permeability of cell membranes is regulated by membrane cholesterol and protein gas channels**” von Samer Al-Samir.

An dieser Publikation bin ich als gleichberechtigter Erstautor zusammen mit Fabian Itel beteiligt. Die von mir durchgeführten Experimente sind folgende: Die MDCK-Zellkultur mit der stabilen Expression von humanem Aquaporin 1 und deren Kontrolle mittels Western Blot. Des Weiteren habe ich die Manipulation des Cholesteringehaltes von MDCK Zellen mit Methyl-ß-Cyclodextrin durchgeführt. Sodann habe ich die CO_2 - Permeabilitätsmessungen dieser Zellen und von HEK293 und tsA201 Zellen sowie die dazugehörige Auswertung durchgeführt. An der CO_2-Permeabilitätsmessung der Vesikel war ich beteiligt. Ich habe weiterhin eine erste Version der Publikation verfasst und mich an der Weiterverbesserung des Manuskripts beteiligt. Des Weiteren bin ich für die Erstellung der Mehrzahl der Abbildungen verantwortlich.

CO_2 permeability of cell membranes is regulated by membrane cholesterol and protein gas channels

Fabian Itel*[2], Samer Al-Samir*[1], Fredrik Öberg[3], Mohamed Chami[4], Manish Kumar[5], Claudiu T. Supuran[6], Peter M.T. Deen[7], Wolfgang Meier[2], Kristina Hedfalk[3], Gerolf Gros[§1], Volker Endeward[1]

From the

[1]Zentrum Physiologie, Vegetative Physiologie 4420, Medizinische Hochschule Hannover, 30625 Hannover, Germany; [2]Departement Chemie, Universität Basel, CH-4056 Basel, Switzerland; [3]Dept. Chemistry/Biochemistry, University of Gothenburg, SE-405 30 Göteborg, Sweden; [4]C-CINA Center For Cellular Imaging and Nano Analytics, Biozentrum, Universität Basel, CH 4058 Basel, Switzerland; [5]Dept. Chem. Engineering, Pennsylvania State University, PA 16802-4400, USA; [6]Dipartimento di Chimica, Lab. di Chim. Bioinorg., Università di Firenze, Florence, Italy; [7]Dept. Physiology, Radboud University Nijmegen Medical Centre, 6500 HB Nijmegen, The Netherlands

*These authors have contributed equally to this work

§ Corresponding author: Zentrum Physiologie
Vegetative Physiologie -4220-
Medizinische Hochschule Hannover
30625 Hannover
Germany
e-mail: Gros.Gerolf@MH-Hannover.de
Fax: +49-511-5322938; Tel.: +49-511-5322735

Abstract

Recent observations that some membrane proteins can act as gas channels seem to be in contrast to the classical view that membranes generally are highly permeable to gases. This view has also been based on the finding that pure planar phospholipid bilayers exhibit a very high permeability for CO_2 (P_{CO_2}) of ~1 cm/s. Here, we show that biological membranes containing normal amounts of cholesterol (30–50 mol % of total lipid), e.g. MDCK cells, in fact possess an unexpectedly low P_{CO_2} of ~ 0.01 cm/s. Phospholipid vesicles enriched with similar cholesterol concentrations also exhibit P_{CO2}≈0.01 cm/s. MDCK cells depleted of or enriched with membrane cholesterol show dramatic increases or decreases in P_{CO_2}, respectively. Incorporation of the gas channel human aquaporin-1 into cholesterol-containing vesicles, as well as its expression in MDCK cells, lead to drastic increases in P_{CO_2}, showing that gas channels are of high functional significance for membrane CO_2 transfer.

Introduction

It has been a long-standing paradigm in biology that cell membranes are highly permeable to all gases (1). This seemed to be supported by the observation that artificial phospholipid bilayers show extremely high gas permeabilities (2-5). In the case of the respiratory gases CO_2 and O_2, the major resistances to the release of CO_2 from the sites of cellular production to the blood, and vice versa for O_2 uptake, are well established for most tissues. These resistances are constituted by a) the speed of the chemical reactions in red blood cells and the chemical binding capacity of the blood for the two gases, and b) the CO_2 or O_2 diffusivities and the diffusion distances to be overcome during the process of CO_2 release from mitochondria into capillary red blood cells, or of O_2 uptake in the reverse direction (6). Processes a and b are so fast that neither in the tissue nor in the normal lung a difference is expected between tissue or alveolar CO_2 or O_2 partial pressure (pCO_2 / pO_2) and endcapillary pCO_2 / pO_2. Never, until recently, have indications been observed that cell membranes constitute a significant barrier to CO_2 transfer, and neither has such a barrier been reported for O_2 transfer. Just two exceptions from this apparent general principle have been reported for CO_2. After an early observation of the apical membrane in the medullary thick ascending limb of Henle being virtually impermeable to NH_3 (7), it was reported that the apical membrane of gastric gland epithelium is poorly permeable to CO_2 (8) and that this holds also for the apical membrane of colonic gland (9) and colonic surface epithelium (10). These observations suggested that there are at least a few exceptions to the rule that biological membranes exhibit CO_2 permeabilities as high as those of artificial phospholipid bilayers.

Another departure from the general view that cell membranes through their lipid phases possess extremely high gas permeabilities comes from recent reports indicating that the membrane proteins human aquaporin-1 (AQP-1), a few other AQP isoforms and plant aquaporin (11-15) can increase CO_2 transfer across membranes. Endeward et al. (16) were the first to show that in addition to aquaporin the Rhesus protein can constitute a channel for CO_2. These studies were confined to only a small number of experimental models, essentially human red blood cells and the Xenopus oocyte expression system. It has remained an open question, however, how gas channels can be of functional significance, when most cell membranes have similarly high intrinsic CO_2 permeabilities (P_{CO2}) as phospholipid bilayers. This apparent discrepancy has led and continues to lead to an extensive discussion

fundamentally questioning the physiological significance of gas channels (4, 5, 17-22). The present paper, therefore, addresses the hitherto unanswered question what the CO_2 permeability of a variety of gas channel-free mammalian cells actually is. We show here that biological membranes containing normal amounts of cholesterol (30-50 mol % of total lipid) in fact possess a P_{CO2} of ~ 0.01 cm/s, two orders of magnitude lower than that of pure phospholipid bilayers (~ 1 cm/s). Using the experimental models phospholipid vesicles and MDCK cells, we demonstrate that the low P_{CO2} value of biological membranes is essentially due to their cholesterol content. With the same two models, we go on to show that the gas channel AQP-1, when inserted into a cholesterol-containing membrane of low background P_{CO2}, does cause a physiologically highly significant increase in membrane CO_2 permeability. We conclude that the permeability of biological membranes for CO_2 – and possibly for other gases as well – is regulated by two parameters: a) cholesterol, which imparts mechanical stability to the membrane but causes low gas permeability, and b) protein gas channels, which can markedly raise the gas permeability in membranes possessing a high content of cholesterol.

Results and Discussion

Intrinsic P_{CO2} of different types of cell membranes.- CO_2 permeabilities of phospholipid bilayers have been determined to have values of 0.35 cm/s (3), 3.2 cm/s (4) and > 0.16 cm/s (present study). Here, we report the P_{CO2} values of the membranes of different types of mammalian cells, which are all devoid of functional gas channels (Table I). As determined by Western Blotting (present study, Fig. 6, and ref. 4) and shown in Table I, MDCK and the tsA201 cell line do not express AQP-1. The human red cells also included in Table I were AQP-1 deficient while the Rhesus CO_2 channel was present but largely inhibited by DIDS (16). These three cell types were studied at 37°C in suspensions of the isolated cells by the mass spectrometric ^{18}O exchange technique reported earlier (10). Their P_{CO2} values are all of the order of ~ 0.01 cm/s, i.e. they are more than one to two orders of magnitude lower than P_{CO2} of artificial phospholipid membranes. The 4th type of membrane given in Table I, the basolateral membrane measured in intact proximal colon epithelium layers, exhibits a P_{CO2} similar to that of these three cell types, ~ 0.02 cm/s (10). The 5th cell membrane in Table I, the

apical membrane, again determined in intact epithelial layers of the proximal colon, also lacks gas channels and represents a special case by exhibiting a P_{CO2} of 0.001 cm/s (10), one further order of magnitude below the P_{CO2} of the first four membranes. Such a difference in P_{CO2} between the apical and basolateral membranes in the colon is qualitatively in agreement with previous evidence reported by Hasselblatt et al. (9). We conclude that all cell membranes considered here have – in the absence of gas channels – P_{CO2} values that are >> one order of magnitude lower than P_{CO2} of phospholipid bilayers.

Which component of the biological membranes is responsible for this property? Two possibilities have recently been discussed in a state-of-the-field letter (5): a) a special component of the lipid phase of cell membranes that would increase substantially its resistance to CO_2, or b) the proteins of the membranes that would have to render > 90% of the membrane area inaccessible to CO_2. Even with a membrane protein content of 50%, this would require that the ectodomains of membrane proteins interact tightly with the majority of the surface lipids of the membrane (23); such a situation would, however, hinder access of all other solutes to the membrane lipid phase as well.

Drastic effect of cholesterol enrichment on P_{CO2} of artificial lipid vesicles. - Since it is well known that cholesterol not only enhances the mechanical stability of membranes and increases their microviscosity (24) but can also significantly reduce membrane permeability to uncharged solutes such as water (25-27) and NH_3 (26, 28), we investigated the effect of incorporation of cholesterol into phospholipid vesicles. The phospholipid composition in all measurements was L-α-phosphatidylcholine (POPC, chicken egg) and L-α-phopsphatidylserine (POPS, porcine brain) at a molar ratio of 8:2. In many cell membranes, PC is a major component of the membrane lipids (29, 30), especially in the outer membrane leaflet, and is important for membrane structure and permeability barrier, while PS is typically present in the inner leaflet (26). To these phospholipids increasing amounts of cholesterol were added, accounting for from 5 to 70 mol % of total membrane lipids. Vesicles were produced in the presence of bovine carbonic anhydrase II, attaining an intravesicular CA activity of ~ 10,000 (i.e. 10,000-fold acceleration of the CO_2 hydration reaction), as necessary for the ^{18}O exchange measurement (10). Vesicle diameter by electron microscopy was 150 nm.

Mass spectrometric determinations of P_{CO2} in suspensions of the vesicles at 37°C yielded the results shown in Fig. 1. The central message from this figure is i) a drastic fall in P_{CO2}, by at

least one order of magnitude, between 0 and 30% cholesterol (dashed line), and ii) the continuation of this fall between 30 and 70% cholesterol (solid lines and regression line), resulting in a decrease in P_{CO2} by one further order of magnitude. Thus, 70% cholesterol causes a decrease in P_{CO2} by ≥ two orders of magnitude.

A second aspect of Fig. 1 is the finding that we cannot determine the correct P_{CO2} of the pure phospholipid vesicles, but can only give a lower limit indicating that P_{CO2} in the absence of cholesterol is > 0.16 cm/s. The mass spectrometric method is sensitive to changes in P_{CO2} only up to an upper limit, whose value depends on the surface-to-volume ratio of the vesicles or cells (see eqs. in Endeward and Gros (10)). This upper limit value per se indicates that the unstirred layer around the vesicles must be ≤ 1 μm ($D_{CO2} / P_{CO2} \leq 1.7 \cdot 10^{-5}$ $cm^2 s^{-1} / 0.16$ cm s^{-1} = $1 \cdot 10^{-4}$ cm, an estimate based on the consideration that the diffusion resistance due to the unstirred layer is ≤ the observed total diffusion resistance of the vesicle). However, previous studies suggest the unstirred layer is in fact not greater than 0.1 μm (31).

Thirdly, it may be noted in Fig. 1 that cholesterol concentrations of 5 and 17% have no detectable effect on P_{CO2}, whose values also exceed the upper limit of detection. This result is compatible with findings that lipid bilayer permeability for small solutes may actually increase with increasing cholesterol content up to ~20 mol %, and begins to decrease in a concentration-dependent manner at cholesterol concentrations above 20% (32, 33). Such increases would then of course also exceed the present detection limit, become therefore not visible in Fig. 1, and could explain the apparent sharp bend at 17 % cholesterol in the curve of Fig. 1.

We note that most previous investigators have not studied the effect of cholesterol on vesicle P_{CO2}, with the exception of Missner at al. (4), who in contrast to the present results report that presence vs. absence of cholesterol did not affect P_{CO2} of planar lipid bilayers. It should be considered here that planar lipid bilayers, produced by using decane as a solvent, may retain considerable amounts of decane in the final bilayer (34), which is expected to raise the P_{CO2} of the bilayer due to the high solubility of CO_2 in decane (35) and its likely effect of increasing membrane fluidity (3). It should also be mentioned that previous studies using rapid reaction stopped-flow spectrophotometry (36, 37) have reported P_{CO2} of phospholipid vesicles to be extremely low, ~ 10^{-3} cm/s, i.e. three orders of magnitude lower than the above-mentioned values for planar phospholipid bilayers. As discussed previously (31), the enormous

discrepancy between these two groups of measurements is, besides an overestimation in the case of decane-containing planar lipid bilayers, likely to be due to an underestimation in the stopped-flow apparatus experiments caused by severe unstirred layers and poor mixing in the face of the extremely fast process of CO_2 uptake by phospholipid vesicles.

We conclude that the present study with $P_{CO2} \geq 0.16$ cm/s tends to support the high estimates of P_{CO2} derived from pure planar phospholipid bilayers. However, the membrane lipid composition representative of a cell membrane, containing 40-50 mol% cholesterol, by virtue of the drastic effect of cholesterol results in a P_{CO2} that is 1-2 orders of magnitude below these figures.

Effect of cholesterol depletion and enrichment on P_{CO2} of MDCK cells. – Non-polarized MDCK cells in suspension were treated with 20 mM methyl-β-cyclodextrin largely as described by Francis et al. (38) to reduce membrane cholesterol, or were treated with methyl-β-cyclodextrin preloaded with cholesterol at a molar ratio 1:8 (39) to increase membrane cholesterol. These treatments did not alter cell diameter, and cholesterol enrichment had no effect on cell vitality, while cholesterol depletion decreased vitality moderately by between 0 and 11%. It should be noted that non-vital cells do not contribute to the mass spectrometric signal and thus do not affect P_{CO2}. Fig. 2 shows the results of P_{CO2} determinations at 37°C. Control MDCK cells, whose membrane lipids have a cholesterol content of ~ 37% (29), exhibit a P_{CO2} of 0.017 cm/s at 37°C (Fig. 2, Table I). Cholesterol depletion increases P_{CO2} dramatically to > 0.75 cm/s, which is the upper detection limit in the case of the MDCK cells. Cholesterol enrichment, on the other hand, decreases P_{CO2} to 0.0065 cm/s, i.e. ~ 1/3 of control. The data clearly show that cholesterol content controls cell membrane P_{CO2} in a massive way. This is qualitatively in line with the vesicle results of Fig. 1.

Cholesterol content quantitatively determines P_{CO2} of cell membranes. – The cholesterol content of the membrane lipids of four of the five cell membranes of Table I is known and given in the 4th column. We have used these figures to predict P_{CO2} on the basis of the regression line of Fig. 1, which describes the vesicle data between 30 and 70 mol % cholesterol. The predicted P_{CO2} values are given in the 5th column of Table 1. Comparison with the measured P_{CO2} values (2nd column) shows a marked agreement within ≤50% (factor of two in the case of the basolateral colon membrane) between what has been measured in a biological membrane and what has been observed in vesicles with an identical cholesterol

content. We conclude that in the range of cholesterol concentrations as they occur in cell membranes, and in the absence of gas channels, cholesterol is the major determinant of the membrane permeability for CO_2. This leads to intrinsic P_{CO2} values of cell membranes with a "normal" cholesterol content of 40-50 mol % of ~ 0.01 cm/s, and to a 10x lower P_{CO2} of ~ 0.001 cm/s when cholesterol amounts to as much as 77 mol %. This has not been recognized before and revises drastically the view that the P_{CO2} of cell membranes – a view also held for other gases such as O_2, CO and NO – is similar to that of pure phospholipid membranes (4, 5).

Effect of AQP-1 reconstitution on P_{CO2} of lipid vesicles. **–** The data presented so far show that mammalian cell membranes exhibit a rather low "intrinsic" CO_2 permeability. We have already reported previously that P_{CO2} of the red cell membrane increases 10-fold, to 0.15 cm/s, when functional AQP-1 and Rh protein are present (14, 16). Here, we demonstrate in lipid vesicles containing 50 mol % cholesterol that P_{CO2} of this relatively gastight membrane can be raised 3.5-fold from 0.007 cm/s to 0.032 cm/s by incorporating human AQP-1 into the vesicle membrane. Vesicles were prepared in the presence of lipid-to-protein ratios (LPR) of 400, 230, 200 and 140 (an example of AQP-1 incorporation into the membrane is shown in Fig. 3c), giving graded increases in P_{CO2} as seen in Fig. 3a. With LPR 400, vesicles exhibited 54 aquaporin monomers per μm^2 membrane area, determined by freeze-fracture electron microscopy, while with LPR 230 and 140 these numbers were 63 and 80/μm^2, respectively. The ratio of these AQP-1 densities corresponds roughly to the ratio of increases in P_{CO_2} (Figure 3a). Bacterial AqpZ, reconstituted at an LPR of 200 (70 AqpZ/μm^2), did not increase P_{CO2}, seeming to conduct no or little CO_2. Figure 3b shows that DIDS, while having no significant effect on P_{CO_2} of vesicles without AQP-1, markedly inhibits the increase in P_{CO_2} caused by AQP-1. A strong inhibiting effect of DIDS on CO_2 conductivity of AQP-1 is consistent with previous observations (14-16) and, together with the lack of effect of AqpZ, confirms the specificity of the AQP-1 effect on P_{CO_2}.

Effect of AQP-1 expression on P_{CO2} of MDCK cells. – Since the intrinsic membrane CO_2 permeabilities of vesicles with 40% cholesterol and of MDCK cell membranes are in a similar order of magnitude, it should be possible to discern the CO_2 conduction by AQP-1 in MDCK cells as well as in vesicles. We stably transfected non-polarized MDCK cells with the human AQP-1 expression construct pCB6-hAQP-1. Fig. 4b confirms that this resulted in a significant expression of AQP-1. Mass spectrometric measurements with MDCK cells in suspension

(Fig. 4a) show that expression of AQP-1 results in an ~ 50% increase of P_{CO2}. AQP-1-mediated CO_2 conduction is, as in the case of reconstituted vesicles, inhibited by DIDS. These measurements clearly confirm that AQP-1 is significant in CO_2-channeling across cell membranes with an average content of cholesterol.

This effect of AQP-1 in MDCK cells has not been observed by Missner et al. (4). We have previously presented evidence that the setup used by these authors, due to thick water layers associated with their layer of MDCK cells, does not allow detection of an increase in membrane CO_2 permeability of the size seen in Fig. 4a (31). In contrast, the isolated MDCK cells used in the present mass spectrometric setup are expected to have an unstirred layer of < 1μm (31).

Conclusion. - Cholesterol can decrease membrane CO_2 permeability by >2 orders of magnitude in phospholipid vesicles and intact cells. While cell membranes with normal cholesterol contents of 30–50 mol% exhibit relatively low P_{CO_2} of ~0.01 cm/s, very low P_{CO_2} values of 0.001 cm/s result from cholesterol contents >70%. By diffusion calculations, we have previously illustrated that a P_{CO2} of 0.01 cm/s implies a significant impairment of CO_2 exchange of red cells, especially under conditions of exercise (14). Likewise, we have demonstrated that across the apical membrane of colon epithelium the P_{CO2} of 0.001 cm/s is associated with a large gradient of pCO_2 across this membrane (10). Higher CO_2 permeabilities than both these low values appear to be achieved by inserting membrane protein gas channels, as shown here with hAQP-1, but may also result from extremely low cholesterol contents, as they are found in mitochondrial membranes. With these two variables, depending on functional requirements, either highly gas-permeable (red cells, lung epithelium) or nearly gas-tight membranes (apical membranes of colon, stomach and kidney epithelia) can be established. The latter property is functionally important when epithelial cells are to be protected against a severe acid load by the extremely high CO_2 pressure as it can occur, for example, in the colonic lumen (10). The conclusions of this work may hold similarly for physiologically important gases other than CO_2, such as O_2, N_2, NO and CO, which have membrane lipid-water partition coefficients just slightly higher than CO_2 (40-42). It should be clear that the behaviour of these diatomic gases remains speculative as long as it has not been possible to measure the effect of cholesterol on their membrane transfer. It may be noted, nevertheless, that a gas permeability of 0.01 cm/s would be expected to constitute a much greater problem for O_2 than for CO_2, due to the 24 times lower O_2 solubility in water

compared to that of CO_2. Then channels such as AQP1, which has been shown by molecular dynamics simulations to posses a conductance for O_2 similar to that for CO_2 (43), would be even more crucial for gas exchange across membranes. Permeabilities of cell membranes for CO_2 – and possibly for other gases as well – thus appear to be regulated over a wide range spanning about two to three orders of magnitude by means of the two parameters membrane cholesterol content and incorporation of protein gas channels into the membrane.

Methods

P_{CO_2} from mass spectrometric measurement of ^{18}O exchange. With this method, the CO_2 permeability of isolated cells in suspension or of layers of intact, stripped colon mucosa epithelium is determined (10). The principle is to expose the cells to a solution containing 25 mM bicarbonate (1% ^{18}O-labelled) in 125 mM NaCl. The approach to isotopic equilibrium takes much longer than establishment of the chemical equilibrium (complete after ~ 1 min) and requires ~ 2 h when carbonic anhydrase-containing cells at a cytocrit of ~ 0.5% are present. During this latter process most of the labelled CO_2 and HCO_3^- of the extracellular space moves to the intracellular space where they are fed into the carbonic anhydrase-catalysed CO_2/HCO_3^- hydration-dehydration reaction that continuously runs back and forth. In each dehydration step, there is a chance of 1/3 that the ^{18}O label leaves the CO_2-HCO_3^- pool (~25 mM) and enters into the much larger water pool (55 M), from where it can virtually not come back into the CO_2-HCO_3^- pool. This causes a relatively slow decay of the extracellular $C^{18}O^{16}O$ concentration, whose time course we measure by mass spectrometry via a special inlet system (48). The kinetics of the decay in $C^{18}O^{16}O$ is determined by the cell permeabilities for CO_2 and HCO_3^- and by the intracellular carbonic anhydrase activity. The latter quantity is determined separately from lysed cells and the two former parameters are calculated from the recorded time courses of $C^{18}O^{16}O$ decay as described previously (10). The experiments with intact cells were performed in the presence of a 5×10^{-5} M concentration of the extracellular carbonic anhydrase inhibitor 2,4,6-trimethyl-1-[(4-sulfamoylphenyl)ethyl]-pyridinium perchlorate (C14H17ClN2O6S) (49). Theory and further experimental details of the method have been described (10,14,16).

Cell culture and cell manipulations. MDCK cells (Madin-Darby canine kidney) and tsA201 cells (transformed human embryonic kidney 293 cells) were obtained from the European Collection of Cell Cultures (ECACC). MDCK cells were kept in EMEM (Eagle's minimal essential medium) with 1% NEAA (non-essential amino acids, both from Sigma Aldrich), 10% FBS (fetal bovine serum "Gold", PAA), 2 mM L-glutamine and penicillin-streptomycin (both from Gibco Invitrogen) at 37°C and 5% CO_2. Cells were grown until no more than 80% confluency was reached, i.e. it was avoided that along with full confluency polarization of the MDCK cells developed (50). tsA201 cells were grown in DMEM (Dulbecco's modified Eagle medium, Sigma Aldrich) with 2 mM L-glutamine (Invitrogen), penicillin-streptomycin and 10% FBS. Cells were harvested by enzymatic detachment using Accutase (PAA), then centrifuged at 2000 g for 10 min and washed twice in PBS.

Stable transfection of MDCK cells was achieved with a pCB6-hAQP-1 vector. To generate pCB6-hAQP-1, a PCR was performed on the pXβgev1hAQP-1 vector (kindly gifted by Peter Agre (51)) using the following primers: sense: gctctagagccagcatggccagcgag and antisense: gctctagactatttgggcttcatctcc, the fragment was cut with XbaI and ligated into the XbaI site of the pCB6 vector (52). Orientation and proper sequence were checked using DNA sequence analysis. For the control plasmid, the hAQP-1 sequence was deleted. Cells were transfected using the calcium phosphate method (53). Positive clones were selected during two weeks incubation in EMEM containing 0.6 mg G418/ml (Carl Roth, Karlsruhe, Germany). Expression of hAQP-1 in MDCK cells was verified by Western Blotting using AQP-1 antibody (affinity-purified polyclonal antibody against the AQP-1 C-terminal region, RA3391/2353AP; Nejsum et al.(54)) and, as secondary antibody, anti-rabbit-IgG IRDye800CW (Li Cor Biosciences). A Trans-Blott SD semi-dry transfer cell (Biorad) was used with a nitrocellulose membrane. The Odyssey Infrared Imaging System (Li-Cor Biosciences) was used for visualization of the antibody-labelled protein bands. SDS PAGE was performed on a 1 mm thick 9% acrylamide gel in a Mini-Protean 3 SDS Page Chamber (Biorad). Samples were mixed 1:2 with sample buffer (130 mM Tris-HCl, 20% glycerol, 4.6% SDS, 0.02% bromophenol blue, 2% DTT) and heated to 95°C for 5 min. 15 µl of this mixture was loaded per lane onto the gel.

Membrane cholesterol of isolated MDCK cells was reduced by resuspending the cells from 8 culture dishes of 10 cm diameter, after washing them once, in 40 ml EMEM containing 20 mM MβCD (methyl-β-cyclodextrin, Sigma Aldrich) without FBS, and then incubating them

under mild stirring at 37°C and 5% CO_2 for 1 h. The protocol essentially follows the procedure described by Francis *et al* (38). After incubation, cells were centrifuged for 10 min at 2000 g and washed once with PBS. The cell pellet was resuspended in 4 vols. of PBS and the cell number and vitality determined with an automatic cell counter (Countess, Invitrogen). Controls were subjected to the identical protocol but in the absence of MβCD in EMEM. Vitality of controls was 90%, that of MβCD-treated cells 85%. We note that leaky cells do not contribute to the $C^{18}O^{16}O$ mass spectrometric signal because any carbonic anhydrase activity of these cells is inhibited by the extracellular carbonic anhydrase inhibitor that is present during the experiment (10, 14).

Membrane cholesterol of MDCK cell membranes was increased by suspending them in 80 ml EMEM with 5 mM cholesterol-loaded MβCD (39), after cells had been washed once. This suspension was incubated under mild stirring overnight at 37°C and 5% CO_2. Then, cells were centrifuged at 2000 g and washed once with PBS. The cell pellet was resuspended in 4 vols. PBS and cell number and vitality were determined. Control cells were treated identically except for MβCD being absent. Vitality was 80% in both control and MβCD-treated cells. The cholesterol content of untreated MDCK cells (29) is compared in Table I with that of human red blood cells (43-45).

Liposomes. Control liposomes and proteoliposomes were prepared by standard methods (55, 56). Briefly, phospholipids L-α-phosphatidylcholine (PC) (Egg, Chicken), L-α-phosphatidylserine (PS) (Brain, Porcine; sodium salt) (Avanti Polar Lipids) and cholesterol (Sigma Grade, ≥99%, Sigma) dissolved in chloroform were mixed at the desired molar ratios (PC:PS 8:2 and variable amounts of cholesterol). The lipid mixture was dried under a gentle nitrogen stream forming a smooth lipid film on the inside of a small glass vial followed by high vacuum drying for at least 6 h. The lipid film was hydrated to a concentration of 3 mg/ml in a Hepes buffer (20 mM Hepes, 100 mM NaCl) containing 1.25 mg/ml CAII (Sigma) and the detergent β-OG (n-octyl-β-D-glucopyranoside, Affymetrix) was added to a concentration of 4% (w/v). For proteoliposomes, a certain volume of AQP stock solution was added to give the desired lipid-protein-ratios (LPR). The resulting mixture was incubated with intermittent agitation for 1 h at room temperature, loaded into dialysis tubings (Spectra/Por®, Spectrum®Labs) with a molecular cut-off of 3500 Da and dialysed against 5.0 L of Hepes buffer for 24-48 hours at room temperature. The resulting suspension was extruded 15 times through a 0.2 μm track-etched filter (Nucleopore, Whatman). Extravesicular material was

removed on a Superdex^{TM} 200 column (GE Healthcare). Liposomes and proteoliposomes were stored at 4°C and permeability measurements were performed within 3-4 days. Average vesicle size was determined by transmission electron microscopy on a Philips FEI Morgagni 268D instrument and found to be 150 nm, independent of cholesterol concentration.

In order to count the number of aquaporin molecules of the proteoliposomes, freeze fracture preparations were performed as described previously (57). Proteoliposomes were centrifuged at 300,000 g in a TL100 ultracentrifuge (Beckman) for 30 min at 4°C. The resulting pellet was cryoprotected with glycerol (30% v/v). A small droplet of the sample was placed on the copper holder and quenched in liquid propane (58). The frozen sample was fractured at -125 °C in high vacuum of about 10^{-5} pascals with a liquid nitrogen-cooled knife in a Balzers 400 freeze-etching unit (Balzers AG, Liechtenstein). The fractured sample was replicated with a 1-1.5 nm deposit of platinum-carbon, and coated with 20 nm carbon film. The Pt/C replica was cleaned with 2% SDS, washed with pure water, transferred onto copper EM grid and observed with a Philips CM10 electron microscope. Particle densities were determined by counting the total number of visible particles (AQP tetramers) divided by the total vesicle area calculated from the diameter of each vesicle visible on the freeze fracture images.

Aquaporins. Human AQP-1 was produced in *Pichia pastoris* and characterized as described previously (59) with some fine tuning of the growth and purification protocols. Mainly, X-33/pPICZB-hAQP-1-Myc-His_6 was cultivated in 1 L BMMY (Invitrogen) shake flask cultures and expression was induced for 48 h with additional methanol (0.5%) added after 24 h. Cells were collected and resuspended in Breaking Buffer (50 mM KPi, 5% glycerol, pH 7.5) and broken using X-press. Urea and NaOH washed membranes were solubilised (20 mM Tris-HCl, 100 mM NaCl, 10% glycerol, 5% β-OG (Anatrace), 2 mM β-mercaptoethanol (β-MeOH), protease inhibitor cocktail (Complete EDTA-free, Roche Diagnostics), pH 8.0) at a concentration of 2 mg total protein/ml for 1 h at RT. Imidazole, 10 mM, was added to the solubilised material (140,000 g, 30 min, 4°C) which was incubated with equilibriated (20 mM Tris-HCl, 300 mM NaCl, 10% glycerol, 2 mM β-MeOH, 1% β-OG, 10 mM imidazole, pH 8.0) Ni-NTA agarose for 16 h at 4°C. The matrix was washed in 30 mM, and eluted in 300 mM imidazole, respectively, using the same buffer. The protein containing samples were concentrated using a 30,000 MWCO filter (VivaSpinn) and protein buffer was exchanged (20 mM Tris-HCl, 100 mM NaCl, 10% glycerol, 1% β-OG, pH 8.0) on a Superdex^{TM}200 column (GE Healthcare). Purity and concentration of hAQP-1 after concentration (12 mg/ml) were

ascertained by SDS PAGE electrophoresis and by UV spectrophotometry (Nanodrop, ThermoScientific), respectively.

AqpZ was purified as described by Borgnia *et al.* (54) with slight adjustments. Briefly, the plasmid for overexpression of histidine-tagged AqpZ (pTrc10HisAqpZ) was transfected into the E. coli strain JM109 by electroporation (60). Luria Broth cultures (10 ml, 50 µg/ml ampicillin) were incubated for 17 h, diluted into 1 L of fresh LB media and propagated to an A_{600} of about 2.5. 10-His-AqpZ production was induced by addition of 1 mM isopropyl-β-D-thiogalactoside (IPTG) for 3 h and centrifuged (10,000 g, 20 min. 4°C). Harvested cells were resuspended in 10 ml of ice cold lysis buffer (100 mM K_2HPO_4, 1 mM $MgSO_4$, 1 mM phenylmethylsulfonylfluoride (PMSF), 0.1 mg/ml deoxyribonuclease I (DNAse I), 10 mM imidazole, pH 7.0). Cells were lysed by ultrasonication on ice for 30 – 40 min with intermittent cooling steps. Unbroken cells were separated by a 20 min centrifugation at 10,000 g at 4 °C, subsequently the supernatant was centrifuged at 140,000 g at 4°C for 60 min. The resulting pellet was solubilized in 10 ml of solubilisation buffer (5% β-OG, 100 mM K_2HPO_4, 10% glycerol, 200 mM NaCl, 15 mM imidazole, pH 8.0) and incubated with agitation on ice overnight. The suspension was then filtered through a 0.45 µm pore size filter (Whatman) and 1 ml of freshly washed Ni-NTA agarose beads (Qiagen) was added to the filtrate and incubated on ice for 2 h. The resin was then packed on a column, washed with 10 ml of wash buffer (1% β-OG, 100 mM K_2HPO_4, 10% glycerol, 200 mM NaCl, 100 mM imidazole, pH 7.0). Bound material was first incubated for 15 min with 1ml of elution buffer (1% β-OG, 100 mM K_2HPO_4, 10% glycerol, 200 mM NaCl, 400mM imidazole, pH 7.0) at room temperature and collected in Eppendorf tubes. For more protein recovery, repeated 1 ml elution steps were performed. After AqpZ purification, protein buffer was exchanged (1% β-OG, 20mM Hepes, 100mM NaCl, pH 7.4) by size exclusion chromatography through two coupled HiTrap™ desalting columns (Sephadex™ G-25 Superfine, GE Healthcare). Protein purity and concentrations (typically 3-10 mg/l of culture) were determined by gel electrophoresis and UV/VIS spectroscopy (NanoDrop™ 2000c, ThermoScientific).

Statistics.- Statistical significance was tested by Student's T-test where applicable, or by ANOVA followed by a suitable post-test (Bonferoni, comparing selected pairs of data groups, or Tukey, multiple comparisons).

References

1. Overton E (1901) Studien über die Narkose. Jena: Gustav Fischer Verlag.

2. Forster RE (1969) The rate of CO_2 equilibration between red cells and plasma. In: Forster RE, Edsall JT, Otis AB, Roughton FJW, editors. CO_2: Chemical, Biochemical, and Physiological Aspects. Washington DC: National Technical Information Service, NASA SP-188. pp. 275–284

3. Gutknecht J, Bisson MA, Tosteson FC (1977) Diffusion of carbon dioxide through lipid bilayer membranes: effects of carbonic anhydrase, bicarbonate, and unstirred layers. J. Gen. Physiol. 69: 779-794.

4. Missner A, Kügler P, Saparov SM, Sommer K, Mathai JC et al. (2008) Carbon dioxide transport through membranes. J Biol Chem 283: 25340-25347.

5. Boron WF, Endeward V, Gros G, Musa-Aziz R, Pohl P (2011) Intrinsic CO_2 permeability of cell membranes and potential biological relevance of CO_2 channels. Chemphyschem 12: 1017-1019.

6. Geers C, Gros G (2000) Carbon dioxide transport and carbonic anhydrase in blood and muscle. Physiol Rev 80: 681-715.

7. Kikeri D, Sun A, Zeidel ML, Hebert SC. (1989) Cell membranes impermeable to NH_3. Nature 339: 478-480.

8. Waisbren SJ, Geibel JP, Modlin IM, Boron WF (1994) Unusual permeability properties of gastric gland cells. Nature 368: 332-335.

9. Hasselblatt P, Warth R, Schulz-Baldes A, Greger R, Bleich M (2000) pH regulation in isolated in vitro perfused rat colonic crypts. Pflügers Arch 441: 118-124.

10. Endeward V, Gros G (2005) Low carbon dioxide permeability of the apical epithelial membrane of guinea-pig colon. J Physiol 567: 253-265.

11. Nakhoul NL, Davis BA, Romero MF, Boron WF (1998) Effect of expressing the water channel aquaporin-1 on the CO_2 permeability of Xenopus oocytes. Am. J. Physiol. 274: C543-548.

12. Uehlein N, Lovisolo C, Siefritz F, Kaldenhoff R (2003) The tobacco aquaporin NtAQP-1 is a membrane CO_2 pore with physiological functions. Nature 425: 734-737.

13. Blank ME, Ehmke H (2003) Aquaporin-1 and HCO_3^--Cl^- transporter-mediated transport of CO_2 across the human erythrocyte membrane. J Physiol 550: 419-429.

14. Endeward V, Musa-Aziz R, Cooper GJ, Chen LM, Pelletier MF et al. (2006) Evidence that aquaporin 1 is a major pathway for CO_2 transport across the human erythrocyte membrane. FASEB J 20: 1974-1981.

15. Musa-Aziz R, Chen LM, Pelletier MF, Boron WF (2009) Relative CO_2/NH_3 selectivities of AQP-1, AQP4, AQP5, AmtB, and RhAG. Proc. Natl. Acad. Sci. U S A 106: 5406-5411.

16. Endeward V, Cartron JP, Ripoche P, Gros G (2008) RhAG protein of the Rhesus complex is a CO_2 channel in the human red cell membrane. FASEB J 22: 64-73.

17. Verkman AS (2002) Does aquaporin-1 pass gas? An opposing view. J Physiol 542:31.

18. Hub JS, de Groot BL (2006) Does CO_2 permeate through aquaporin-1? Biophys J 91: 842-848.

19. Missner A, Pohl P (2009) 110 years of the Meyer-Overton rule: predicting membrane permeability of gases and other small compounds. Chemphyschem 10: 1405-1414.

20. Mathai JC, Missner A, Kügler P, Saparov SM, Zeidel ML et al. (2009) No facilitator required for membrane transport of hydrogen sulfide. Proc Natl Acad Sci U S A 106: 16633-16638.

21. Verkman AS (2011) Aquaporins at a glance. J Cell Sci 124: 2107-2112.

22. de Groot BL, Hub JS (2011) A decade of debate: significance of CO_2 permeation through membrane channels still controversial. Chemphyschem 12:1021-1022.

23. Engel DM (2005) Membranes are more mosaic than fluid. Nature 438: 578-580.

24. Shinitzky M, Inbar M (1976) Microviscosity parameters and protein mobility in biological membranes. Biochim Biophys Acta. 433: 133-149.

25. Lande MB, Donovan JM, Zeidel ML (1995) The relationship between membrane fluidity and permeabilities to water, solutes, ammonia, and protons. J Gen Physiol 106: 67-84.

26. Hill WG, Zeidel ML (2000) Reconstituting the barrier properties of a water-tight epithelial membrane by design of leaflet-specific liposomes. J Biol Chem 275: 30176-30185.

27. Finkelstein A (1976) Water and nonelectrolyte permeability of lipid bilayer membranes. J Gen Physiol 68: 127-135.

28. Antonenko YN, Pohl P, Denisov GA (1997) Permeation of ammonia across bilayer lipid membranes studied by ammonium ion selective microelectrodes. Biophys J 72: 2187-2195.

29. Hansson GC, Simons K, van Meer G (1986) Two strains of the Madin-Darby canine kidney (MDCK) cell line have distinct glycosphingolipid compositions. EMBO J 5: 483-489.

30. Hsiao LL, Howard RJ, Aikawa M, Taraschi TF (1991) Modification of host cell membrane lipid composition by the intra-erythrocytic human malaria parasite Plasmodium falciparum. Biochem J 274**:** 121-132.

31. Endeward V, Gros G (2009) Extra- and intracellular unstirred layer effects in measurements of CO_2 diffusion across membranes - a novel approach applied to the mass spectrometric ^{18}O technique for red blood cells. J Physiol. 587: 1153-1167.

32. Corvera E, Mouritsen OG, Singer MA, Zuckermann MJ (1992) The permeability and the effect of acyl-chain length for phospholipid bilayers containing cholesterol: theory and experiment. Biochim Biophys Acta 1107: 261-70.

33. Trandum C, Westh P, Jorgensen K, Mouritsen OG (2000) A thermodynamic study of the effects of cholesterol on the interaction between liposomes and ethanol. Biophys J. 78: 2486-92.

34. Bunce AS, Hider RC (1974) The composition of black lipid membranes formed from egg-yolk lecithin, cholesterol and n-decane. Biochim Biophys Acta 363: 423-427.

35. Wilcock RJ, Battino R, Danforth WF, Wilhelm E (1978) Solubilities of gases in liquids II. The solubilities of He, Ne, Ar, Kr, O_2, N_2, CO, CO_2, CH_4, CF_4, and SF_6 in n-octane, 1-octanol, n-decane, and 1-decanol. J Chem Thermodynamics 10: 817-822.

36. Prasad GV, Coury LA, Finn F, Zeidel ML (1998) Reconstituted aquaporin 1 water channels transport CO_2 across membranes. J Biol Chem 273: 33123-33126.

37. Yang B, Fukuda N, van Hoek A, Matthay MA, Ma T et al. (2000) Carbon dioxide permeability of aquaporin-1 measured in erythrocytes and lung of aquaporin-1 null mice and in reconstituted proteoliposomes. J Biol Chem 275: 2686-2692.

38. Francis SA, Kelly JM, McCormack J, Rogers RA, Lai J et al. (1999) Rapid reduction of MDCK cell cholesterol by methyl-beta-cyclodextrin alters steady state transepithelial electrical resistance. Eur J Cell Biol 78**:** 473-84.

39. Christian AE, Haynes MP, Phillips MC, Rothblat GH (1997) Use of cyclodextrins for manipulating cellular cholesterol content. J. Lipid Res. 38: 2264-2272.

40. Simon SA, Gutknecht J (1980) Solubility of carbon dioxide in lipid bilayer membranes and organic solvents. Biochim Biophys Acta 596: 352-358.

41. Möller M, Botti H, Batthyany C, Rubbo H, Radi R et al. (2005) Direct measurement of nitric oxide and oxygen partitioning into liposomes and low density lipoprotein. J Biol Chem 280: 8850-8854.

42. Battino R, Rettich TR, Tominaga T (1984) The solubility of nitrogen and air in liquids. J. Phys. Chem. Ref. Data 13: 563-600.

43. Wang Y, Cohen J, Boron WF, Schulten K, Tajkhorshid E (2007) Exploring gas permeability of cellular membranes and membrane channels with molecular dynamics. J Struct Biol 157: 534-544.

44. Musa-Aziz R, Geyer RR, Boron WF (2011) Relative CO2/NH3 permeabilities of several members of the mammalian aquaporin familiy: bAQP0, hAQP1, hAQP3, rAQP4-M1, rAQP4-M23, and hAQP8. FASEB J 25: 1040.5.

45. O'Brien JS (1967) Cell membranes - composition: structure: function. J. Theor. Biol. 15: 307-324.

46. Korn ED (1969) Cell membranes: structure and synthesis. Annu. Rev. Biochem.38: 263-288.

47. Meyer zu Düttingdorf H, Sallmann H, Glockenthör U, von Engelhardt W, Busche R (1999) Isolation and lipid composition of apical and basolateral membranes of colonic segments of guinea pig. Anal. Biochem. 269: 45-53.

48. Itada N, Forster RE (1977) Carbonic anhydrase activity in intact red blood cells measured with ^{18}O exchange. J Biol Chem 252: 3881-90.

49. Supuran CT (2008) Carbonic anhydrases: novel therapeutic applications for inhibitors and activators. Nature Rev Drug Discov 7: 168-181.

50. van Beek M, Robben JH, Savelkoul PJM, Hendriks G, Devonald MAJ, Konings IBM, Lagendijk AK, Karet F, Deen PMT (2006) Polarization, key to good localization. Biochim Biophys Acta 1758: 1126-1133.

51. Jung JS, Preston GM, Smith BL, Guggino WB, Agre P (1994) Molecular structure of the water channel through aquaporin CHIP. The hourglass model. J Biol Chem 269: 14648–14654.

52. Brewer CB (1994) Cytomegalovirus plasmid vectors for permanent lines of polarized epithelial cells. Methods Cell Biol 43: 233–245.

53. Wigler M, Pellicer A, Silverstein S, Axel R, Urlaub G et al. (1979) DNA-mediated transfer of the adenine phosphoribosyltransferase locus into mammalian cells. Proc. Natl. Acad. Sci. U S A 76: 1373-1376.

54. Nejsum LN, Kwon T-H, Jensen UB, Fumagalli O, Frøkiaer J, et al. (2002) Functional requirement of aquaporin-5 in plasma membranes of sweat glands. Proc Natl Acad Sci USA 99: 511-516

55. Smith SA, Morrissey JH (2004) Rapid and efficient incorporation of tissue factor into liposomes. J Thromb Haemost 2: 1155–1162.

56. Borgnia MJ, Kozono D, Calamita G, Maloney PC, Agre P (1999) Functional reconstitution and characterization of AqpZ, the E. coli water channel protein. J Mol Biol 291: 1169-1179.

57. Plançon L, Chami M, Letellier L (1997) Reconstitution of FhuA, an Escheria coli outer membrane protein, into liposomes. J Biol Chem 272: 16868-16872.

58. Aggerbeck LP, Gulik-Krzywicki T (1986) Studies of lipoproteins by freeze-fracture and etching electron microscopy. Methods Enzymol 128: 457-472.

59. Nyblom M, Oberg F, Lindkvist-Petersson K, Hallgren K, Findlay H et al. (2007) Exceptional overproduction of a functional human membrane protein. Protein Expr Purif 56: 110-120.

60. Kumar M, Grzelakowski M, Zilles J, Clark M, Meier W (2007) Highly permeable polymeric membranes based on the incorporation of the functional water channel protein Aquaporin Z. Proc Natl Acad Sci U S A 104: 20719-20724.

Acknowledgments.- The authors thank Prof. Ernst Ungewickell (Medizinische Hochschule Hannover) and Dawid Krenc (Universität Kiel) for helpful discussions, and Mr. Mark Inglin of the University of Basel for language-editing the manuscript. We are indebted to Dr. Aleksandra Rojek (University of Aarhus) for a kind gift of the AQP-1 antibody RA3391/2353AP. This work was supported through grant EN 908/1-1 to V.E., S.A.-S. and G.G. by the Deutsche Forschungsgemeinschaft. F.I., W.M. and M.C. gratefully acknowledge the National Center of Competence in Nanoscale Science for financial support and Prof. Henning Stahlberg (University of Basel) for access to the electron microscopy facility. P.M.T.D. is a recipient of a VICI grant of the Netherlands Organization for Scientific research (NWO) and acknowledges VICI grant 865.07.002.

Author Contributions.- V.E. and G.G. conceived the study. V.E. designed the research and performed all mass spectrometric ^{18}O exchange experiments. F.I. and W.M. prepared liposomes and proteoliposomes as well as AqpZ; S.A.-S. performed all experiments with MDCK and tsA201 cells; F.Ö. and K.H. contributed hAQP-1 protein; M.C. performed the freeze-fracture studies; P.T.M.D. contributed the pCB6-hAQP-1 expression construct; C.T.S.

contributed the extracellular carbonic anhydrase inhibitor; M.K. contributed to lipo- and proteoliposome preparation. G.G. and V.E. wrote the paper. All authors critically commented the manuscript.

Author information.- The authors declare no conflicts of interest. Correspondence and requests for materials should be addressed to G.G. (Gros.Gerolf@MH-Hannover.de).

Table I. P_{CO2} of cell membranes vs. cholesterol content

	P_{CO2} (cm/s) ± S.D.	**AQP1**	**mol% cholesterol in membrane lipids**	**P_{CO2} predicted from cholesterol content**
MDCK	**0.017** ± 0.004	— §	37 % a)	**0.015**
tsA201	**0.007** ± 0.003	— *		
Red cell: ∅ AQP1, ∅ functional Rh	**0.015** ± 0.003 #	— #	45 % b)	**0.010**
Basolateral membrane prox colon epithelium	**~ 0.022** $	— $	42 % c)	**0.011**
Apical membrane of prox colon epithelium	**0.0015** ± .0006$	— $	77 % c)	**0.0016**

The P_{CO2} values of the above cell membranes may be compared with the P_{CO2} values reported for planar lipid bilayers as 0.35 cm/s and 3.2 cm/s (refs.3, 4). # from Endeward *et al*. (14, 16). $ from Endeward and Gros (10). While both apical and basolateral membranes of the proximal colon possess no AQP-1, the basolateral membrane expresses AQP3, which is has a very low CO_2 conductance although it conducts water very well (44). Thus both membranes are presumably free of major protein CO_2 channels. § see Fig. 4b of this work and Missner *et al.* (4). * present work, not shown. a) ref. 29, b) refs. 45-46, c) ref. 47.

Legends

Fig. 1. Effects of cholesterol on CO_2 permeability of artificial phospholipid vesicles with PC:PS at a molar ratio of 8:2. Cholesterol content of the vesicle membranes varied between 0 and 70 mol% cholesterol per total lipids. Vesicle diameter for all concentrations of cholesterol was 150 nm. All vesicles had an intravesicular carbonic anhydrase activity of ~ 10.000 (=acceleration factor of the kinetics of CO_2 hydration). The mass spectrometric measurement was conducted at 37°C. The first three data points at 0, 5 and 17 mol% cholesterol are ≥ than the upper limit of detectability of P_{CO_2} by the mass spectrometric method, in this case 0.16 cm/s. It is possible that the P_{CO2} values at 5 and 17 mol% cholesterol are actually higher than the value at 0 % cholesterol as it has been reported that lipid bilayer permeability for small molecules may increase with increasing cholesterol up to ~20 mol %, before it decreases with further increasing cholesterol content (32, 33). Between 17 and 30 mol% cholesterol P_{CO2} is seen to fall by ≥ one order of magnitude, and between 30 and 70 mol% it decreases by a further order of magnitude. The straight line represents the linear regression of the data points between 30 and 70 mol% cholesterol. Bars represent S.D., n=7-18.

Fig. 2 Effects of cholesterol on CO_2 permeability of MDCK cell membranes. Compared to the P_{CO_2} of control MDCK cells (column in the center), MDCK cells depleted of cholesterol by exposure to methyl-β-cyclodextrin exhibit a drastically increased P_{CO_2} (>0.75 cm/s; left-hand column) and MDCK cells loaded with cholesterol (right-hand column) show a P_{CO2} about three times lower than controls. Bars represent S.E., n=12-20. The star indicates that this P_{CO_2} is significantly different from the control P_{CO_2} with $P<0.05$.

Fig. 3. Effects on P_{CO_2} of hAQP-1 and AqpZ reconstitution in phospholipid vesicles containing 50 mol% cholesterol, and effect of DIDS. a) Increase in CO_2 permeability over control, ΔP_{CO_2}, at various lipid-protein ratios, LPR, i.e. moles of lipid per mole of aquaporin. For hAQP-1 a graded increase in ΔP_{CO_2} with increasing AQP concentration is seen. All ΔP_{CO_2} values between LPR 400 and 140 are significantly different from zero (** $P<0.02$; *** $P<0.01$; bars represent S.E.; n=9,6,8,7,12 in the order as seen in Fig. 2a). AqpZ at an LPR of 200 is not significantly different from zero. Number of vesicles analysed per condition was 600-900. b) Effect of DIDS on P_{CO_2} of liposomes and proteoliposomes. While DIDS has no effect on control PLV, it significantly inhibits the CO_2 permeability of hAQP-1 (* $P<0.05$; n=6-9; bars represent S.E.). c) Visualization of reconstituted aquaporins in proteoliposomes by freeze fracture electron microscopy. hAQP-1 at LPR 140 (A, upper panel) and AqpZ at LPR 200 (B, lower panel). Arrows indicate aquaporin tetramers; scale bar represents 100 nm.

Fig. 4. Expression of hAQP-1 in MDCK cells increases P_{CO_2}. a) MDCK cells expressing hAQP-1 show an increased P_{CO_2} (3rd vs. 1st column, ** $P<0.02$). DIDS has no effect on control MDCK cell P_{CO_2}, but significantly decreases P_{CO_2} in AQP-1-expressing MDCK cells (4th column vs. 3rd column, $^{\$\$}$ $P<0.02$). Bars indicate S.E., n ≥7. b) Western Blot showing that MDCK cells transfected with pCB6-hAQP-1 express hAQP-1 protein (arrow). 1: Lysed suspension of control cells transfected with empty vector pCB6, applied at a final dilution of cell pellet of 1:16. 2: Same sample at a dilution of 1:8. 3: MDCK cells transfected with pCB6-hAQP-1, diluted 1:32. 4: Same sample diluted 1:16. 5: Same sample diluted 1:8 6: Lysed human red blood cells, diluted 1:800, also showing hAQP-1. Right hand side: molecular weight scale (kDa).

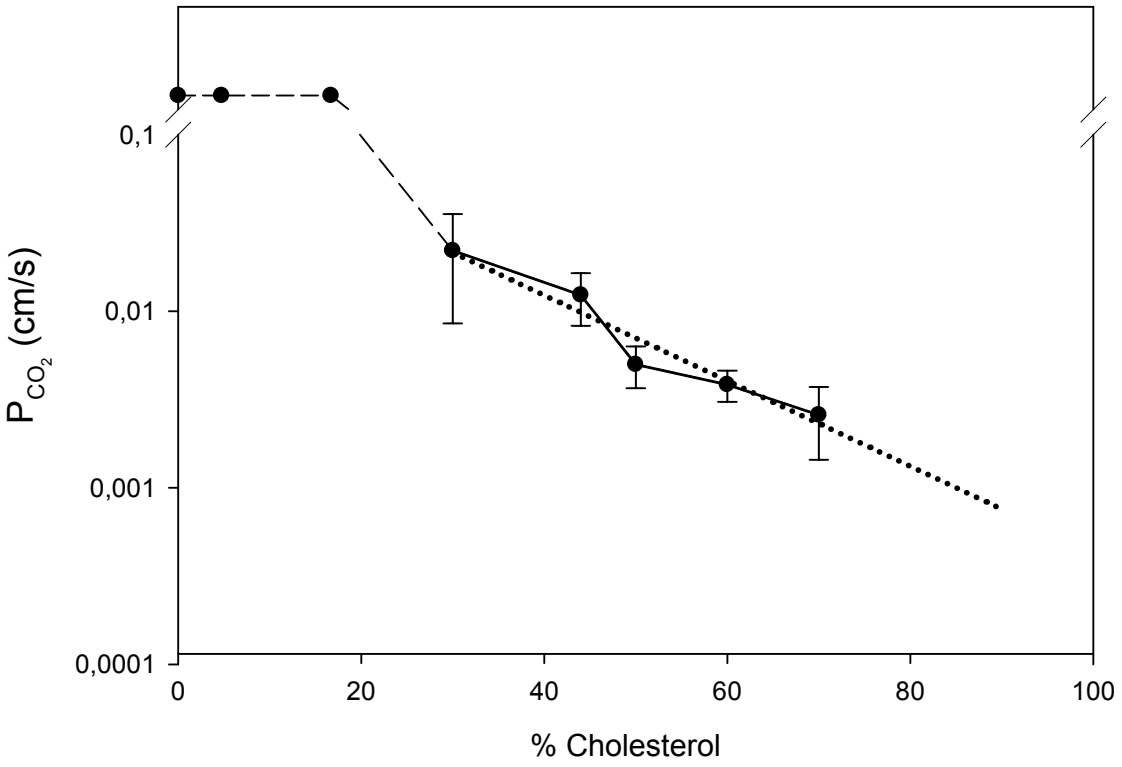
0,1
0,01
0,001
0,0001
P_{CO_2} (cm/s)
0
20
40
60
80
100
% Cholesterol

Fig. 1

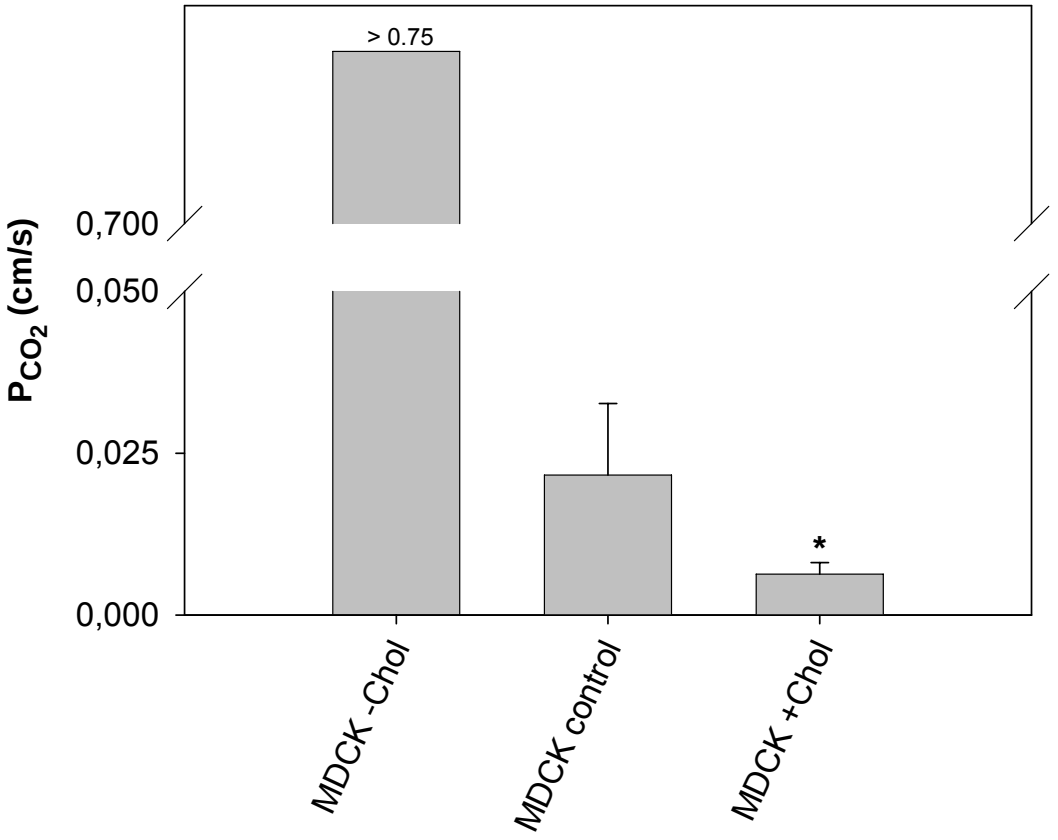
> 0.75
0,700
0,050
0,025
0,000
P_{CO_2} (cm/s)
*
MDCK -Chol
MDCK control
MDCK +Chol

Fig. 2

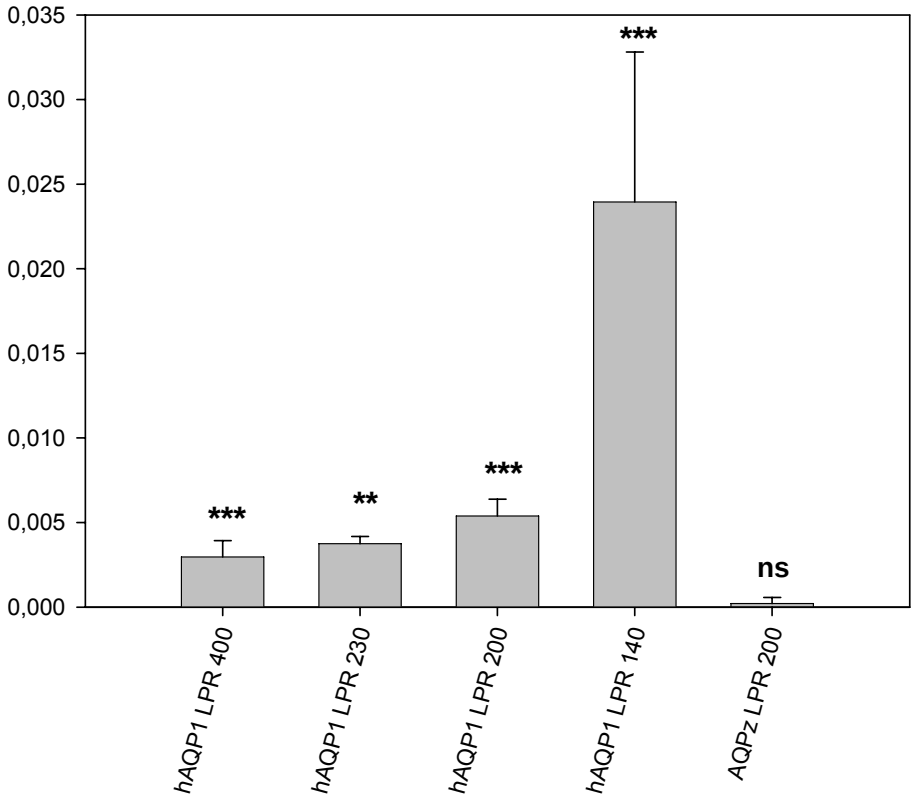
0,035
0,030
0,025
0,020
0,015
0,010
0,005
0,000
***
**
***
***
ns
hAQP1 LPR 400
hAQP1 LPR 230
hAQP1 LPR 200
hAQP1 LPR 140
AQPz LPR 200

Fig. 3a

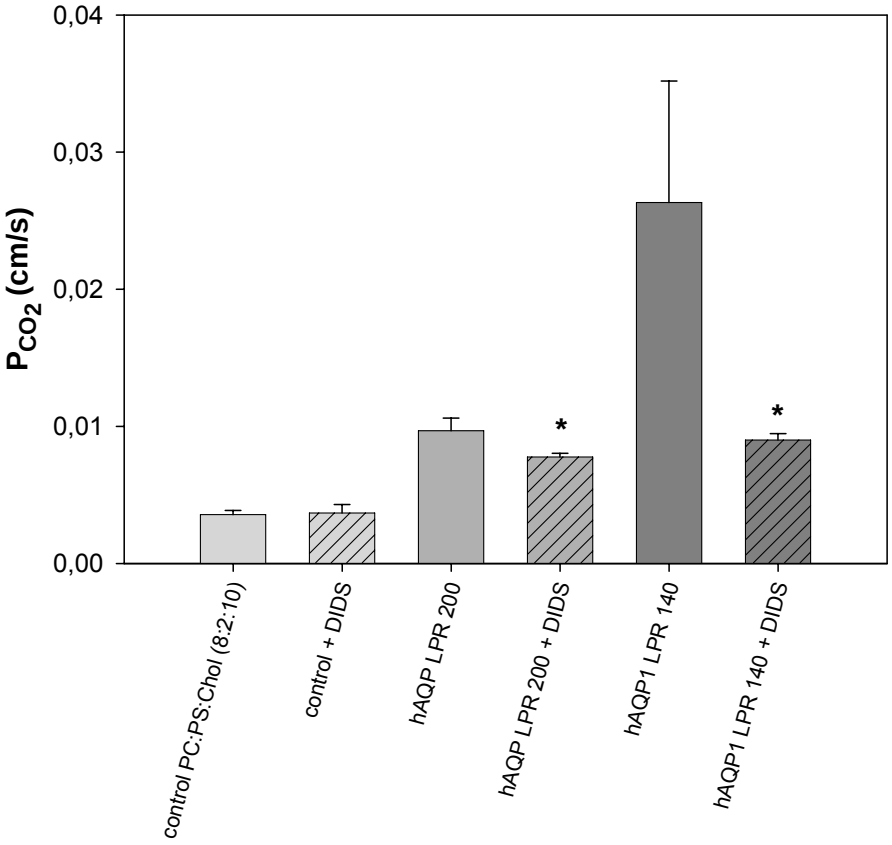
0,04
0,03
0,02
0,01
0,00
P_{CO_2} (cm/s)
*
*
control PC:PS:Chol (8:2:10)
control + DIDS
hAQP LPR 200
hAQP LPR 200 + DIDS
hAQP1 LPR 140
hAQP1 LPR 140 + DIDS

Fig. 3b

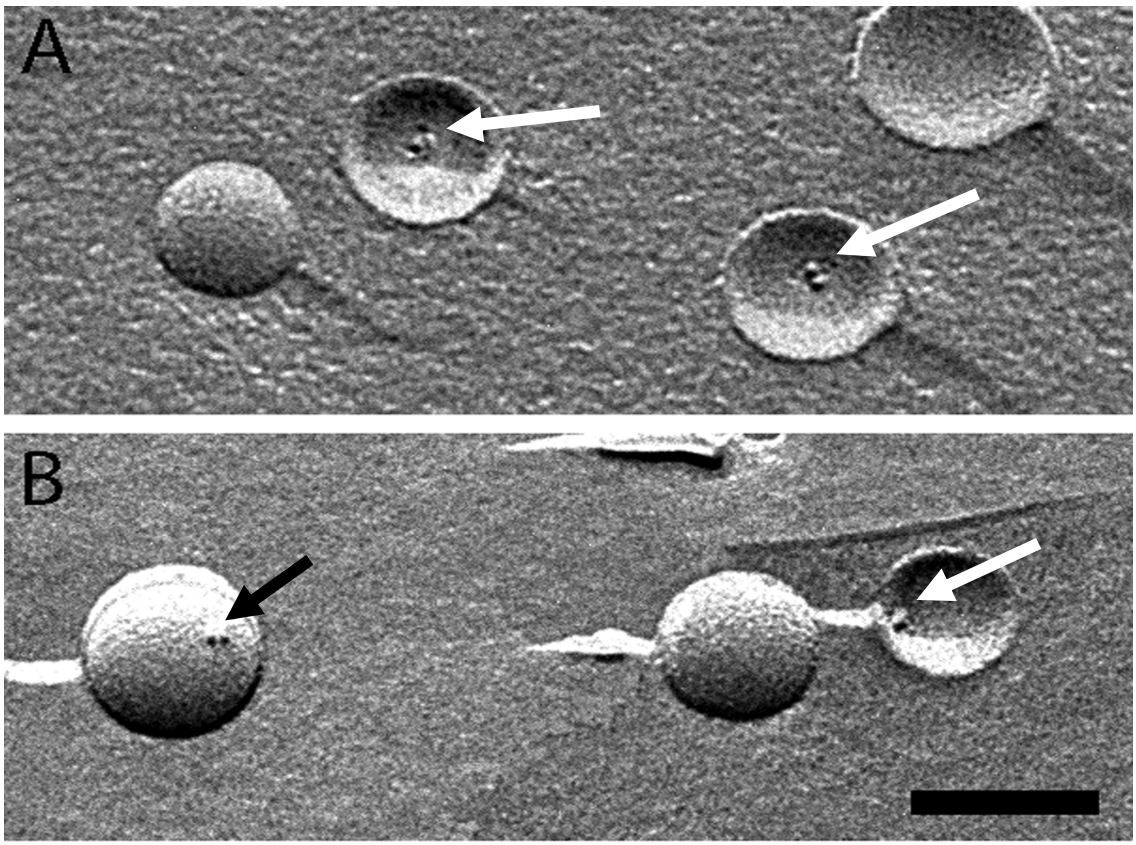
A
B

Fig. 3c

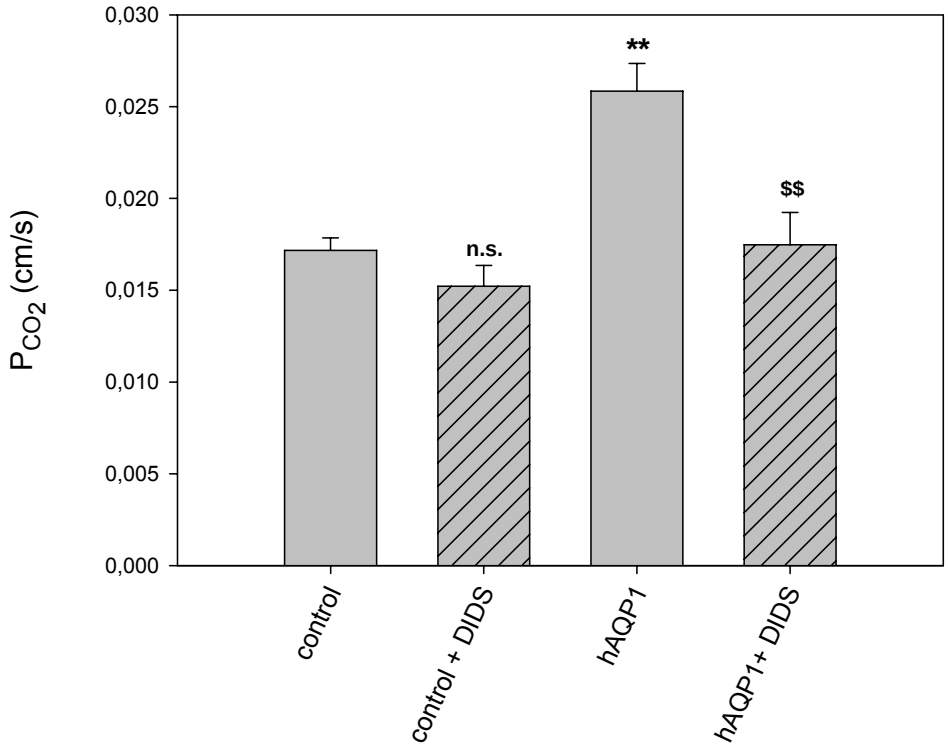
0,030
0,025
0,020
0,015
0,010
0,005
0,000
P_{CO_2} (cm/s)
**
n.s.
$$
control
control + DIDS
hAQP1
hAQP1+ DIDS

Fig. 4a

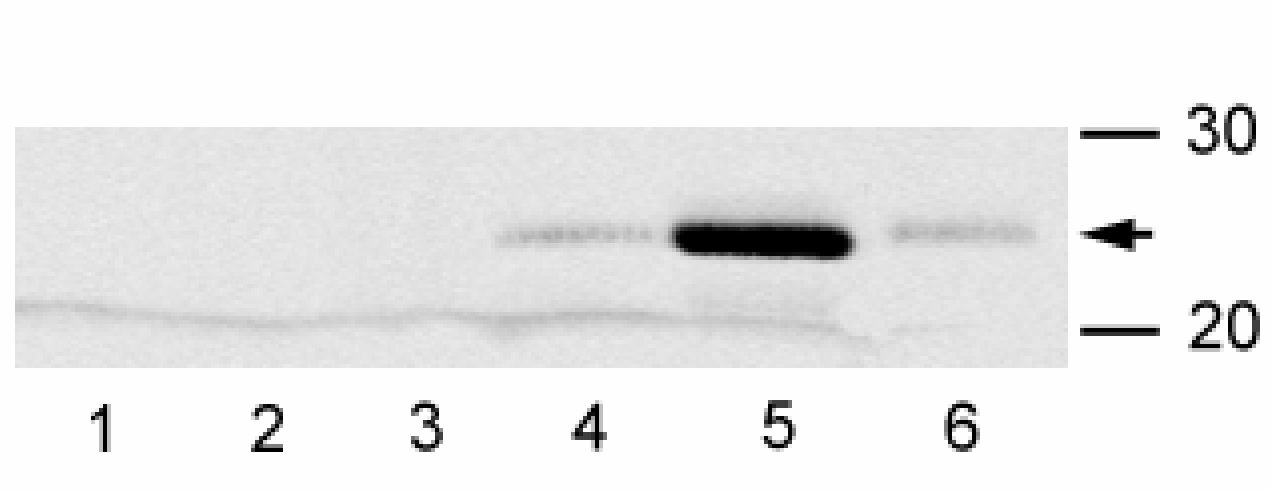

Fig. 4b

Manuskript 2

Activity and distribution of intracellular carbonic anhydrase II and their effects on the transport activity of anion exchanger AE1/SLC4A1

S. Al-Samir, S. Papadopoulos, W.S. Sly, J.P. Cartron, C.T. Supuran, S.L. Alper, G. Gros, V. Endeward

Vorbereitet für die Einreichung bei J. Biol. Chem.

Beitrag zu der Wissenschaftlichen Publikation „ **Activity and distribution of intracellular carbonic anhydrase II and their effects on the transport activity of anion exchanger AE1/SLC4A1**“ von Samer Al-Samir.

Experimentell habe ich Folgendes zu dieser Publikation beigetragen: Etablierung und Unterhaltung der Zellkultur der tsA201 Zellen sowie sämtliche Transfektionsexperimente mit diesen Zellen. Dazu gehörte auch die Konstruktion aller verwendeten Fusions-Proteine. Die Deletion des N-Terminus von CAII habe ich ebenfalls selber durchgeführt. Die Expression aller Konstrukte wurde von mir mit Western Blots kontrolliert. Die konfokale Mikroskopie, zusammen mit der Messung der Intensitätsprofile, habe ich selbständig durchgeführt. Die CO_2- und HCO_3^- -Permeabilitätsmessungen dieser Zellen habe ich ebenfalls durchgeführt. Ich habe den ersten Entwurf der Publikation geschrieben, an der Weiterverbesserung des Manuskripts mitgearbeitet und die meisten der Abbildungen entworfen.

Activity and distribution of intracellular carbonic anhydrase II and their effects on the transport activity of anion exchanger AE1/SLC4A1

S. Al-Samir[1], S. Papadopoulos[2], W.S. Sly[3], J.P. Cartron[4], C.T. Supuran[5], S.L. Alper[6], G. Gros[1],V. Endeward[1]

[1]Zentrum Physiologie, Vegetative Physiologie 4220, Medizinische Hochschule Hannover, 30625 Hannover, Germany; [2]Institut für Vegetative Physiologie, Universität Köln, Köln, Germany; [3]Dept. of Biochemistry and Molecular Biology, St. Louis University, St. Louis, USA; [4]l'Institut National de la Transfusion Sanguine, INSERM, Paris, France; [5]Faculty of Pharmacy, Dept. Chemistry, University of Florence, Florence, Italy; [6]Dept. Medicine, Harvard Medical School, Boston MA 02215, USA.

ABSTRACT

We have investigated the evidence for physical association of and direct functional interaction between carbonic anhydrase II (CAII) and the anion exchanger 1 (AE1) in the native human red cell and in tsA201 cells co-expressing heterologous fluorescent fusion proteins CyPet-CAII and YPet-AE1. In these doubly transfected tsA201 cells, YPet-AE1 is clearly associated with the cell membrane, whereas, CyPet-CAII is homogeneously distributed throughout the cell in a cytoplasmic pattern. FRET measurements fail to detect close proximity of YPet-AE1 and CyPet-CAII. Both the CA II and AE1 fusion proteins are fully functional in tsA201 cells as judged by CA activity and by cellular HCO_3^- permeability (P_{HCO3-}) sensitive to inhibition by DIDS. Expression of the non-catalytic CAII mutant V143Y leads to a drastic reduction of endogenous CAII and to a corresponding reduction of intracellular CA activity. Overexpression of an N-terminally truncated CAII lacking the proposed site of interaction with the C-terminal cytoplasmic tail of AE1 substantially increases intracellular CA activity, as does overexpression of wildtype CAII. These variously co-transfected tsA201 cells exhibit a simple positive relationship between cellular P_{HCO3-} and intracellular CA activity, consistent with changes in HCO_3^- transport that reflect either substrate supply to or removal from AE1 via altered intracellular CA activity, without requirement for a hypothesized CAII-AE1 metabolon involving physical interaction. A functional contribution of the hypothesized CAII-AE1 metabolon to erythroid AE1-mediated HCO_3^- transport was tested in normal red cells and red cells from CAII-deficient patients that retain substantial CA activity associated with the erythroid CAI protein lacking the proposed AE1-binding sequence. Erythroid P_{HCO3-} was indistinguishable in these two cell types, providing no support for the proposed functional importance of the physical interaction of CAII and AE1. A theoretical model predicts that a homogeneous cytoplasmic distribution of CA II is more favorable for cellular transport of HCO_3^- and CO_2 than is association of CA II with the cytoplasmic surface of the plasma membrane.

INTRODUCTION

The present study addresses the question of whether carbonic anhydrase II (CA II) in the human red cell is largely bound to the internal side of the plasma membrane, specifically to the short cytoplasmic C-terminal tail of the erythroid Cl^-/HCO_3^- exchanger 1 (AE1/SLC4A1). It further examines the hypothesis, originally proposed by Vince and Reithmeier (1998), that CAII binding to AE1 activates the latter such that the two proteins form a "metabolon" mediating bicarbonate transport across the red cell membrane.

It was postulated long ago that substantial CAII is bound to the interior of the red cell membrane (Enns, 1967). Subsequent investigations with red cell ghosts repeatedly washed before resealing led three groups to conclude that various wash procedures removed CAII almost completely from the red cell membrane. Rosenberg and Guidotti (1968) reported that red cell ghosts containing residual hemoglobin as < 0.4% of total protein also contained CAII at < 0.01% of the total protein. Tappan (1968) found that repeated washing decreased the CA activity of ghosts to < 0.03% of their original activity activity of the intact cells. Randall and Maren (1972), studying resealed, washed, human red cell ghosts that maintained full transport functions, found that residual hemoglobin and CA respectively constituted 1.1% and < 0.008% of total ghost protein. These studies together suggested the absence of high affinity association between CA II and the internal side of membrane.

However, Parkes and Coleman (1989) later observed that addition of human red cell ghost fragments increased human CAII activity by 3.5-fold. Kifor et al. (1993) then reported that addition of DIDS (presumed to bind mainly to AE1) altered the fluorescence of dansylsulfonamide bound to intraerythrocyte CA, consistent with direct interaction between AE1 and CAII. Vince and Reithmeier (1998) revived interest in the field with the following findings:

a) in (unwashed) red cell ghosts CAII immunofluorescence was mainly detected close to the internal side of the membrane (as also reported in intact erythrocytes by Campanella et al., 2005). Tomato lectin application to red cell ghosts caused clustering of both AE1 and CAII, although colocalization of AE1 and CA II in these clusters was not demonstrated;

b) coimmunoprecipitation of CAII and AE1, when probed with an antibody recognizing the N-terminus of AE1 (but not with an antibody recognizing the AE1 C-terminus);

c) a solid phase binding assay showing binding of intact, detergent-solubilized band 3 to immobilized CA II with Kd of 70 nM, and binding was inhibited by antibody against the AE1 C-terminus;
d) another solid-phase binding assay in which immobilized CAII interacted with a construct of glutathione S-transferase (GST) fused to the N-terminal end of the C-terminal (Ct) domain of AE1 presented in liquid phase. This ELISA assay revealed binding between CAII and the GST-AE1-Ct construct, and the assay was subsequently used to identify the CAII binding region within the AE1-Ct more precisely as the 4 residues 887DADD890 (Vince and Reithmeier, 2000). The authors pointed out that AE1 transporters of many other species show the same or very similar binding sequences, e.g. DGDD in mouse and rat and DADD in bovine RBC. The elements essential for binding were three, or at least two, negatively charged residues D within this group of four amino acids, always preceeded by an aliphatic residue. The GST-AE1-Ct ELISA assay was also used to demonstrate a binding site consisting of 6 positively charged histidine or lysine residues within the first 17 N-terminal residues of CAII, proposed to interact with the anionic residues in the AE1 C-terminal peptide mentioned above (Vince et al., 2000). CAI, which lacks all of these 6 residues, did not bind to AE1. A corollary of these studies derives from i) the fact that human red cells have ~10^6 copies each of AE1 and of CAII (the latter's estimated cytosolic concentration is ~ 20 μM if distributed throughout the cytoplasm), and ii) from the above-mentioned 70 nM Kd for binding of AE1 and CAII. These numbers predict an intra-erythrocyte equilibrium concentration of unbound (free cytosolic) CAII of only 1.2 μM, implying that 94% of RBC CAII is AE1-bound, and thus effectively membrane-bound. In contrast, Piermarini et al. (2007) reported no detectable in vitro binding interaction between the AE1-C-terminal peptide and CAII either by ELISA or by surface plasmon resonance assays.

While the results of Reithmeier and colleagues strongly suggest significant binding of CAII to AE1, whether the two proteins form a "metabolon" (i.e. whether CA II enhances the transport function of AE1) remained an open question. Such enhancement could occur through an allosteric effect of CAII binding on AE1, potentially independent of CAII enzymatic activity, or through the close proximity of carbonic anhydrase catalytic activity to the intracellular substrate transport site of AE1, allowing effectively instantaneous conversion of HCO_3^- to CO_2 after anion translocation, thus maintaining an optimal transmembrane HCO_3^- gradient. The latter mechanism could require either simple proximity of the AE1 transport site and CAII catalytic activity, or it could imply a more specific interaction between the AE1

transport site and the catalytic center of CAII to facilitate HCO_3^- translocation across permeability barrier within the AE1 polypeptide.
A first test of functional interaction between CAII and AE1 activity by Sterling et al. (2001, JBC) and Sterling et al. (2001b, JOP) overexpressed AE1 in HEK293 cells containing endogenous CAII. They found that a) the CA inhibitor acetazolamide inhibited extracellular Cl^- -induced Cl^-/HCO_3^- exchange by 50%, thus showing that CAII activity accelerates AE1 activity, b) AE1 with mutated C-terminal DADD (the proposed CAII binding site) exhibited a 90% reduced transport activity in HEK293 cells, a reduction attributed to reduced AE1 binding of CAII (but transport activities of these mutants were not tested in the absence of CAII), and c) HEK293 cells cotransfected with cDNAs encoding AE1 and the catalytically inactive CAII V143Y resulted in a 60% reduction of AE1 transport rates, interpreted as reflecting displacement of endogenous CAII of HEK293 cells from its AE1 binding site by the inactive heterologous mutant CAII. The implication of this interpretation is that CAII binding to AE1 is required to enhance AE1 transport activity.

The present study reinvestigates the metabolon hypothesis by probing the following questions that have not been examined to date:
i) Is fluorophore-labelled CAII in intact AE1-expressing cells indeed concentrated predominantly at the internal side of the plasma membrane, as postulated for RBC? We investigate this by expressing yellow fluorescent protein-labelled AE1 in tsA201 cells and studying the distribution of coexpressed cyan fluorescent protein-labelled CAII using confocal microscopy.
ii) Is CAII directly bound to AE1? We probe this by studying Förster resonance energy transfer (FRET) between the two fusion proteins.
iii) What is the effect of coexpressing the catalytically inactive CAII mutant V143Y on HCO_3^- transport by intact AE1-expressing cells, when intracellular CA activity is taken into account?
iv) What is the effect of expressing a truncated CAII whose N-terminal amino acids 1-24 have been deleted, so as to prevent AE1 binding to its CAII N-terminal binding site?
v) Is concentration of CA activity at the inner face of the plasma side membrane indeed better for maximal Cl^-/HCO_3^- exchange activity than a homogeneous cytoplasmic distribution of CA activity? We address this problem by applying a mathematical model simulating membrane transport in conjunction with intracellular diffusion and reaction processes of CO_2, HCO_3^- and H^+.

vi) Is HCO_3^- transport by AE1 different in CAII-deficient human red cells from that in normal human red cells? This is an interesting model in which to test the metabolon hypothesis, because CAII-deficient RBC still possess substantial CAI activity which, however, does not bind to AE1.

METHODS

Blood samples

Human red cells were taken from several members of our laboratory and used for mass spectrometric experiments on the same and the following day. Repeating the measurement 4 days after taking the blood made no difference in terms of mass spectrometric records. Two different CAII-deficient blood samples were taken from a member of a US family (CAII deficiency due to an ac145-148 GTTT del mutation in Exon 2) and from an Arabian patient (CAII deficiency due to a point mutation (G>A transition) at the exon2-intron2 junction). All red cells were washed three times in physiological saline before being used in the mass spectrometric experiments
and were controlled for hemolysis. Hematocrit and blood cell count were taken to determine mean corpuscular volumes. Informed consent was sought and given in accordance
with the Declaration of Helsinki. CAII-deficient blood samples were shipped chilled and red cells were used within 2–4 days after the samples were taken.

Cell culture

The tsA201 cell line was obtained from the European Collection of Cell Cultures. The cells were cultured in Dulbecco's Modified Eagle Medium (DMEM) supplemented with 2 mM L-Glutamine, 10% FBS and penicillin/streptomycin at 37°C in 5% CO_2. For confocal laser scanning microscopy the cells were seeded on 35 mm (9.6 cm²) glass bottom dishes (Matek, USA) with 2 ml culture medium and ~$8x10^4$ cells per ml culture medium. For mass spectrometric measurements the cells were seeded on 100 mm (78.5 cm^2) plastic dishes with 10 ml culture medium and ~$4.3x10^4$ cells per ml culture medium. For Western Blot analysis, cells were seeded in 80 cm² cell culture flask with 20 ml culture medium and $4.3x10^4$ cells per ml medium.

Transfections

Cells were transfected according to manufacturer's protocol with GeneJuice (Novagen). YPet-mAE1, YPet-hAE1, CAII-CyPet, CAII-V143Y-CyPet or truncated CAII-CyPet (truncation of the N-terminus of CAII) were transfected or co-transfected in different combinations of mAE1 and CAII. For confocal laser scanning microscopy, transfection was done 24 hours after seeding, for mass spectrometric measurements 48 hours after seeding.

Construction of CyPet- and YPet-tagged AE1 and CAII

The yellow and cyan fluorescent tags used in this study are fluorescent protein variants optimized for FRET and encoded by the vectors pECyPet-N1 and pEYPet-C1, kindly provided by Dr. Patrick S. Daugherty, University of California, Santa Barbara (Nguyen and Daugherty, 2005). For AE1 tagged N-terminally with YPet, an XhoI-SalI PCR product of the human AE1 and XhoI-EcoRI PCR product of murine AE1 were generated using Taq DNA Polymerase (New England Biolabs). The recognition sequences of the restriction endonucleases where added up- and downstream of the AE1 cDNA sequence using PCR primers. The resulting products were gel-purified and ligated 3' into the pEYPet-C1 vector cut with suitable endonucleases.

For the C-terminal tagging of the CAII-constructs with CyPet, a BglII-SalI PCR product of human CAII was generated as described above. The stop codon was replaced with the amino acid tryptophan. The PCR product was ligated into vector pECyPet-N1.

The truncated CAII was produced by PCR-mediated deletion of codons 1-24, encoding the reported binding site for the AE1 C-terminal sequence DADD (Vince et. al. 2000 Biochemistry). The PCR product was ligated into the host vector as described above.

The CAIIV143Y cDNA (encoding a mutant polypeptide with enzymatic activity 3000-fold lower than that of wild-type CAII; Fierke et al., 1991) kindly provided by Dr. Joe Casey, University of Alberta, was ligated into pECyPet-N1 as described above. To obtain an AE1 construct labelled at both, the N and the C terminus, the XhoI-EcoRI PCR product encoding the murine AE1 with the stop codon replaced by glycine was subcloned into a CyPet-YPet tandem protein expression vector, upon opening of the latter between the CyPet and YPet sequence via a XhoI/EcoRI double digest. This procedure produced CyPet-AE1-YPet, which we used as a membrane-associated, positive FRET control.

Confocal microscopy and measurements of Förster resonance energy transfer (FRET)

24, occasionally 48, hrs post-transfection, the culture dishes were mounted onto the stage of an inverse FV1000 confocal laser-scanning microscope (Olympus), and cells were observed under oil immersion using a 60x objective. CyPet and YPet were excited under low laser power (1 to 8 % setting) using a 440 nm blue diode and the 514 nm argon line, respectively, directed to the cells via a 458/514 nm dual dichroic mirror. CyPet and YPet emission intensities were photometrically detected using Olympus filters BA465-495 and BA535-565, respectively.

The experimental procedure to check for Förster resonance energy transfer (FRET) was as described in Papadopoulos *et al.* (2004). In brief, the intensity of CAII-CyPet emission (I_{Cy}) during excitation with the 458 nm argon line was measured photometrically before ($I_{Cy,Pre}$) and after ($I_{Cy,Post}$) complete bleaching of the potential FRET acceptor YPet-mAE1. Bleaching was conducted using the full laser power (100% setting) of the 514 nm argon line, a wavelength close to the excitation maximum of YPet, but with no excitation of CyPet. The entire cell was subjected to bleaching, but $I_{Cy,Post}$ and $I_{Cy,Pre}$ were determined exclusively for regions populated with the potential energy acceptor YPet-mAE1, i.e., at the cell membrane. In analyzing an acceptor bleaching experiment, the finding of $I_{Cy,Post} > I_{Cy,Pre}$ would indicate pre-bleach energy transfer from CAII-CyPet to YPet-mAE1. Since the latter phenomenon is measurable only when the two fluorophores are separated by < 8-10 nm, FRET in this case would confirm close proximity of CAII and mAE1, compatible with direct, physical interaction.

Western Blotting

Cells were harvested by scraping 3 days after seeding. Pooled cells from 10 flasks were washed once by dilution in 5 ml PBS and 10 min centrifugation at 2000 x g. The pellet was then diluted in 5 ml mannitol buffer (130 mM Mannitol, 50 mM Sucrose, 10 mM EGTA, 100 mm Tris, pH 7.4) and centrifuged 10 min at 1400 x g. The cell pellet was suspended 1:2 in mannitol buffer, and cells where lysed (Ultra Turrax, Janke&Kunkel) in three 1 sec bursts separated by 1 min cooldown. The final lysate was centrifuged 10 min at 10.000 x g, and the post-spin supernatant subsequently centrifuged 1 hr. at 100.000 g. The last supernatant was then used for SDS-Page. All centrifugation steps were performed at 4°C.
After termination of SDS-PAGE runs, gels were equilibrated in Blot buffer (containing 250 mM Tris, 1.92 M Glycine) for 20 min and semi-dry electro-transferred to nitrocellulose

membranes (BioRad Trans-Blot SD). Blots were washed with PBS-Tween (167 mM NaCl, 20.4 mM Na_2HPO_4, 1.7 mM H_2NaO_4P and 0.025 v/v % Tween 20) for 30 min and blocked for 45 min with 5% Dry Milk in PBS-Tween. After blocking, blots were washed 3 times for 10 min with PBS containing 0.025% Tween. Primary rabbit anti-CAII antibody (Acris Antibodies) was applied over night at 4°C, diluted 1:5000 in PBS -Tween.
Blots were then washed three times for 10 min in PBS-Tween and incubated with secondary antibody IRDye 680 LT (Li-Cor Biosciences), diluted 1:5000 in PBS-Tween containing 5% dry Milk, for 3.5 hours at room temperature. Binding was detected using the Li-Cor Odyssey Infrared Imaging System.

Mass spectrometric determination of bicarbonate permeability and cellular CA activity

This method was described in detail previously (Endeward and Gros, 2005; Endeward et al., 2006). Suspensions of human red cells (final hematocrit 0.03 %) or tsA201 cell (final cytocrit 0.3 %) were used in the mass spectrometric chamber at constant pH of 7.40 and temperature of 37°C. Briefly, in the presence of a solution of ^{18}O-labelled HCO_3^- the time course of the decay of $C^{18}O^{16}O$ in the suspension was followed via the special mass spectrometric inlet system described earlier. From these time courses, the permeabilities of the cells for HCO_3^-, P_{HCO3-}, and CO_2, P_{CO2}, were calculated as described (Endeward and Gros, 2005). In all red cell experiments, the extracellular CA inhibitor inhibitor 2,4,6-trimethyl-1-[(4-sulfamoylphenyl)ethyl]- pyridinium perchlorate (C14H17ClN2O6S) (Supuran, 2008), was present at $5 \cdot 10^{-5}$ M to ensure the absence of extracellular CA activity in the event of lowgrade hemolysis.
Evaluation of P_{HCO3-} from the time courses of $C^{18}O^{16}O$ requires knowledge of the intracellular CA activity (Endeward and Gros, 2005). This was obtained by lysing cell suspensions of defined hematocrit or cytocrit, followed by centrifugation at 100.000 g (1 hr), and determining the CA activity of the solutions by mass spectrometry. Conditions were 37°C, and, approximating intracellular conditions, pH 7.20 with final Cl^- concentrations of 60 mM for hemolysates and 10 mM for tsA cell lysates were adjusted.

Mathematical Model of HCO_3^- and CO_2 transport across cell membranes

The purpose of this mathematical model is to simulate the processes of CO_2 and HCO_3^- transfer across the cell membrane, together with the associated diffusion and reaction

processes in the intracellular space (see Fig. 1). The transfer of CO_2 or bicarbonate across the membrane is given by:

$$dm_{X,M}/dt = - Px \cdot A \cdot d[X], \quad (1)$$

where $dm_{X,M}$ is the amount of X (either CO_2 or HCO_3^-) transferred across the membrane per unit time, P_X is the membrane permeability of CO_2 or HCO_3^-, respectively, A is the membrane diffusion area (140 μm^2 for a human red cell; Documenta Geigy, 1960), d[X] is the concentration difference across the membrane for either of the two substrates. The rates of the CO_2 hydration-dehydration reaction in the intracellular compartment are described by:

$$d[CO_2]/dt = - k_u \cdot A_{CA} \cdot [CO_2] + (k_u \cdot A_{CA}/ K_1') \cdot [H^+] \cdot [HCO_3^-], \quad (2)$$

where k_u is the forward reaction rate constant of CO_2 hydration (0.15 s^{-1} at 37°C; c.f. Endeward and Gros, 2009), A_{CA} is the factor by which this reaction rate is accelerated due to carbonic anhydrase, $[CO_2]$, $[H^+]$ and $[HCO_3^-]$ are the concentrations of physically dissolved CO_2, of protons and bicarbonate, respectively, t is time, and K_1' is the first apparent dissociation constant of carbonic acid ($7.9 \cdot 10^{-7}$ M at 37°C). As indicated in Fig. 1 (upper part), in the standard case CA was assumed to be homogeneously distributed in the intracellular space, in special cases all intracellular CA was assumed to be concentrated in the immediate neighbourhood of the internal side of the membrane (Fig. 1, lower part). An equation analogous to eq. 2 is used to describe the change of HCO_3^- concentration per time, $d[HCO_3^-]/dt$. The intracellular diffusion processes of CO_2 and HCO_3^- are expressed by:

$$dm_X/dt = - Dx \cdot A \cdot d[X]/dx, \quad (3)$$

where dm_X/dt indicates the movement of substance per unit time between small volume elements of the intracellular space, D_X is the diffusion coefficient in the intracellular space, A is the diffusion area between the volume elements considered, and d[X]/dx is the concentration gradient of CO_2 or HCO_3^-, respectively. D_{CO2} was taken be $1.2 \cdot 10^{-5}$ cm^2s^{-1}, D_{HCO3-} $0.6 \cdot 10^{-5}$ cm^2s^{-1} (c.f. Endeward and Gros, 2009). A modified version of eq. 3 had to be used to describe intracellular diffusion of H^+, which, due to the extremely low intracellular concentrations and concentration gradients of free H^+, occurs almost entirely by hemoglobin-facilitated proton diffusion (Gros and Moll, 1972, 1974; Gros et al., 1976):

$$dm_{H+}/dt = - D_{Hb} \cdot BF \cdot A \cdot dpH/dx, \quad (4)$$

where dm_{H+}/dt is the total amount of protons transferred across the segment at the considered position x, D_{Hb} is the intraerythrocytic diffusion coefficient of hemoglobin ($6.4 \cdot 10^{-8}$ cm^2s^{-1} at 37°C; Moll, 1966), BF is the intraerythrocytic non-bicarbonate buffering power in moles H^+/L/ΔpH, mainly due to hemoglobin (63 mM/ΔpH), and dpH/dx is the intracellular pH

gradient. The minor contribution of the intraerythrocytic buffers of lower molecular weight (ATP, 2,3-BPG) is ignored in this treatment.

This system of equations is largely analogous to the one used previously to describe the exchange of $C^{18}O^{16}O$ between red cells and the extracellular space (Endeward and Gros, 2009), with the exception of proton transport, which did not have to be considered in the earlier model. Also, unlike the treatment there, the extracellular space was treated here as a well stirred compartment of infinite size, and unstirred layers around the cells were not considered. The example of a cell considered here was the human red blood cell, whose parameters were inserted into the equations (details see Endeward and Gros, 2009). The diffusion and reaction processes in the intracellular compartment were modelled by dividing the effective half-thickness of the erythrocyte of 0.8 μm (Forster, 1964) into 80 segments, as indicated in Fig. 1, and with these a finite difference method (as available in MATLAB 2008b) was used to numerically solve the equations.
The equations were solved in such a way as to obtain the amount of substance, i.e. CO_2 or HCO_3^-, taken up into the cell per unit membrane area (in units of moles/cm^2) as a function of time (as shown in Figs. 9,10 and 11). The fact that HCO_3^- transfer across the cell membrane approaches an intracellular HCO_3^- concentration that is not equal to but in Donnan equilibrium with the extracellular concentration was taken into account as described previously (Itada and Forster, 1977; Endeward and Gros, 2005). The condition of maintaining the Donnan distribution for HCO_3^- has also the consequence that CO_2 uptake (due to the ensuing intracellular CO_2 hydration reaction) is accompanied by a bicarbonate efflux (the Hamburger shift, as shown in Fig. 10d) and HCO_3^- uptake is accompanied by a CO_2 efflux (as seen in Figs. 10b and 11b).

RESULTS

Expression of Endogenous Carbonic Anhydrase II and of CA II Fusion Proteins in tsA201 Cells.

Fig. 2a illustrates expression of fusion protein CAII-CyPet in tsA cells, 24 h after transfection. The Western Blot shows in lane 3 the 30 kDa band of human red cell CAII, and in lane 1 the endogenous CAII of tsA201 cells with the same molecular weight, together with the expressed fusion protein CAII-CyPet at the expected mol. wt. of ~ 57 kDa.
Fig. 2b shows in lanes 1 and 2 endogenous CA II (30 kDa) and the catalytically inactive mutant CAII-V143-YPet (57 kDa) from tsA201 cells. Analogous polypeptide levels were observed in tsA201 cells expressing the truncated CAII-YPet fusion protein (not shown).

Localization and FRET Signal of YPet-AE1 and CA II-CyPet Coexpressed in tsA Cells.

Fig. 3a shows the subcellular localizations of CA II-CyPet (left) and murine YPet-mAE1 (right). It is apparent that the AE1 fusion protein is enriched at the plasma membrane of the tsA cell, with some minor association with intracellular vesicular structures, whereas the CA II fusion protein is homogeneously distributed throughout the cytoplasm, without evident enrichment at the plasma membrane. This is confirmed by the fluorescence intensity profiles of Fig. 3b that were recorded along the red lines shown in Fig. 3a. YPet-mAE1 exhibits low fluorescence intensity in the cytoplasm and marked intensity peaks associated with the plasma membranes. CA II-CyPet shows a high and rather homogeneous intensity across the cell cytoplasm region without enrichment of fluorescence intensity in the region of the plasmalemma. The same distribution pattern is seen for CAII-CyPet and human YPet-hAE1 in Fig. 4a. This suggests that the CAII fusion protein behaves as a typical cytosolic protein without detectable association with the membrane.

So as not to overlook subtle interactions between CAII and AE1, we checked for evidence of FRET. As described in Methods, the potential FRET acceptors YPet-mAE1 and YPet-hAE1 were bleached, after which the cells were examined for possible increase in FRET donor emission ($I_{Cy,\,post}$) over their prebleaching value $I_{Cy,\,pre}$. An increase in $I_{Cy,\,post}$, expressed in Fig. 4b as FRET ratio = $(I_{Cy,\,post} - I_{Cy,\,pre}) / I_{Cy,\,post}$, was never observed in cells co-expressing CAII-CyPet with either YPet-mAE1 or YPet-hAE1 (Fig. 4b). The absence of FRET is evidence against physical interaction of CAII fusion protein with AE1 fusion protein. In contrast, in tsA201 cells expressing the intramolecular FRET control construct CyPet-mAE1-Ypet, YPet bleaching elicited a significant increase in CyPet fluorescence intensity (Fig. 4b). The double-tagged mAE1 thus constitutes a positive FRET control, validating the negative results with the single-tagged CAII and AE1 fusion proteins.

Fig. 5 shows that both CAII constructs, that truncated at the N-terminus and the acatalytic CAII-V143Y, exhibited a cytosolic distribution identical to the WT CAII fusion protein shown in Fig. 3. Thus all tested WT and mutant CAII fusion proteins expressed here are homogeneously distributed in the cytoplasm and exhibit no enrichment at the plasma membrane.

Functional Effects of the Expression of YPet- mAE1 in tsA201 Cells.

Fig. 6 shows that the AE1 fusion protein is functional in tsA201 cells. Fig. 6a shows that the CA activity (acceleration factor of CO_2 hydration minus 1) of lysed tsA201 cells as measured by ^{18}O mass spectrometry is slighty over 600 in control as well as in AE1-expressing tsA cells (37°C). Fig. 6b presents ^{18}O mass spectrometry determinations of P_{HCO3-} in tsA201 cells. Control cells exhibit a P_{HCO3-} of ~ $2 \cdot 10^{-4}$ cm/s (37°C), and this value is not significantly altered in the presence of 10^{-5} M DIDS, indicating that AE1 is not responsible for the basal HCO_3^- permeability of tsA cells. Expression of the AE1 fusion protein almost doubles P_{HCO3-}, and DIDS restores this value to control level. We conclude that the AE1 fusion protein is functional when expressed in tsA cells, markedly increasing cellular HCO_3^- permeability.

Bicarbonate permeabilities of tsA201 cells expressing YPet-mAE1 together with various CAII-CyPet fusion proteins.

Fig. 7 shows P_{HCO3-} values obtained with fluorophore-labelled CAII, truncated CAII and the acatalytic CAII mutant, all co-expressed in tsA201 cells with AE1, and plotted vs. corresponding lysate CA activities measured as described above. Firstly, the figure shows that expression of tagged WT CAII as well as of tagged truncated CAII results in enhanced cytosolic CA activity, but expression of CAII-V143Y does not. Secondly, the data are well described by a linear regression line consistent with a dependence of P_{HCO3-} on intracellular CA activity. The second point from the left (▼) represents tsA201 cells expressing mAE1 together with endogenous CAII only (the "control" conditions of Fig. 6) with P_{HCO3-} of $3.8 \cdot 10^{-4}$ cm^2/s. The leftmost data point (▲) representing expression of acatalytic CAII (see Fig. 5b) with P_{HCO3-} of $3.6 \cdot 10^{-4}$ cm^2/s is slightly lower than the control value ($P<0.05$), and unexpectedly shows marked reduction in endogenous intracellular CA activity. The 3rd data point from the left (♦) represents tsA201 cells expressing the fusion protein with wildtype

CAII (see Fig. 3a). This leads to increased intracellular CA activity in parallel with statistically significantly increased HCO_3^- permeability ($5.6 \cdot 10^{-4}$ cm^2/s; $P<0.01$). The rightmost data point in Fig. 7 (●) reflects tsA201 cells expressing the fusion protein containing the CAII truncated at the N-terminus (see also Fig. 5a), which should prevent this protein from binding to the C-terminus of AE1. This truncated CAII increased intracellular CA activity almost 2-fold over control. At this highest CA activity , a slight further increase in P_{HCO3-} ($6 \cdot 10^{-4}$ cm^2/s) is observed ($P<0.05$ vs. control). In conclusion, in the cells coexpressing all tested types of CAII, the bicarbonate permeabilities follow a regression line of P_{HCO3} rising moderately with increasing intracellular CA activity. The correlation coefficient of the linear regression of the data points in Fig. 7 is r=0.90, and the slope of the regression line ($\Delta P_{HCO3-}/\Delta Ai = 2.6 \cdot 10^{-7}$ cm^2/s) is statistically significantly different from zero ($P<0.05$).

CA activity and P_{HCO3-} in Normal and CA II-deficient Human Red Blood Cells.

Here, we employ a different approach to test a functionally significant interaction between CAII and AE1, by examining red cells from two patients with CAII deficiency. Red cells in this disease lack all CA II activity, but maintain substantial erythroid CA activity due to the normal presence of CAI (Sly et al., 1983; Dodgson et al., 1988). While the intracellular CA activity of normal human red blood cells (RBC) at 37°C is 20,000 (Fig. 8a), in agreement with previous determinations (Endeward et al., 2008), the activity in RBC from both patients is around 5,000. Thus, erythroid CAI sustains 25% residual total erythroid CA activity, far in excess of that required for gas exchange at rest and with exercise (Dodgson et al., 1988). Fig. 8b shows that the HCO_3^- permeabilities of normal and CA II-deficient RBC are indistinguishable at 1.2 - 1.4 x 10^{-4} cm/s, in agreement with previously reported normal values (Endeward et al., 2006, 2008). We conclude that AE1 transport activity in human RBC is independent of the presence or complete absence of CAII activity. This complete lack of an effect of CA II on erythroid HCO_3^- transport may be compared to the small, albeit significant, effect of CA II expression in AE1-expressing tsA201 cells, which becomes apparent at a much lower level of absolute CA activity values of ~ 1,000.

Mathematical simulation of the effect of carbonic anhydrase on HCO_3^- uptake by red cells.

These calculations were performed for the conditions of the human RBC, but in principle apply qualitatively to any CA-containing cell. Fig. 9 portrays calculated time courses of bicarbonate uptake at different intracellular carbonic anhydrase activities. The time axis ends at 0.7 s, the capillary transit time in human lung and tissues. It is apparent that for the physiological intracellular CA activity of human RBCs of 20,000 (Fig. 8a), the process of erythroid bicarbonate uptake is complete within the capillary transit time. Even for a CA activity of ~ 5,000, as observed in CAII-deficient RBCs, the capillary transit time suffices to reach completion of bicarbonate uptake. However, below a CA activity of 1000 and extending to the complete absence of CA activity (= acceleration factor of CO_2 hydration of 1), further deceleration of HCO_3^- uptake progressively decreases the total HCO_3^- influx achieved within the capillary transit time. In this range of CA activities, erythroid HCO_3^- uptake depends dramatically on intracellular CA activity. Comparison of the initial rates of HCO_3^- uptake from curves in Fig. 9 with Ai = 1 and Ai = 500 reveals > 2-fold increase, whereas the initial rates from slopes with Ai = 5000 and Ai = 20,000 show only minimal Ai dependence. It is clear from Fig. 9 that AE1-mediated HCO_3^- fluxes or permeabilities cannot be appraised without knowledge of intracellular CA activity.

Mathematical Simulation of Membrane HCO_3^- and CO_2 Transport, with Intracellular CA Activity Either Homogeneously Distributed in the Cytoplasm or Associated with the Membrane.

Again, these calculations were performed assuming conditions of the human RBC. The aim was to determine whether it makes a difference for the process of HCO_3^- or CO_2 uptake by red cells if total intracellular CA activity is a) homogeneously distributed in the cytoplasm, as held by classical views, or b) is concentrated at the internal side of the membrane due to binding to membrane protein, as postulated for CA II by Vince and Reithmeier (1998). Fig. 10a shows the result for HCO_3^- uptake by RBC, when, starting from standard conditions of pCO_2 = 40 mmHg and extracellular pH (pH_e) of 7.40 at 37°C, the extracellular bicarbonate concentration $[HCO_3^-]_e$ is subjected to a step increase from 25 mM to 35 mM. It is apparent that total absence of CA in the cell (black curve) leads to a drastic slowing of the process of HCO_3^- uptake, which after a rapid initial influx becomes extremely slow because the reaction required to convert HCO_3^- in the cell to CO_2, thus maintaining a significant driving force for HCO_3^- across the cell membrane, is uncatalysed. After a capillary transit time of 0.7 s, HCO_3^- uptake is far from completion, as also shown in Fig. 9. If the normal intraerythrocytic CA activity of 20,000 is assumed to be homogeneously distributed in the cell interior (blue curve)

HCO_3^- uptake is considerably accelerated and reaches completion after about ½ s. This is similar for the case when all CA activity of the cell is concentrated in a layer of 0.01 μm thickness (1/80 of 0.8 μm) immediately adjacent to the internal side of the cell membrane (red curve). However, this latter condition does not lead to a faster HCO_3^- uptake compared to the homogeneously distributed CA activity, as might have been expected, but to a slightly slower one. In other words, it is somewhat more advantageous for HCO_3^- uptake to have the CA distributed all over the cell interior than to have it all very close to the membrane. Fig. 10b illustrates the process of CO_2 efflux associated with HCO_3^- uptake, reflecting the amount of CO_2 leaving the cell after it has been produced by dehydration of the HCO_3^- taken up. The behaviour of the CO_2 efflux is a mirror image of that of the HCO_3^- influx: an extreme retardation in the absence of CA, and a slightly faster kinetics for homogeneously distributed CA than for a membrane-associated CA.

A process of special physiological interest for the RBC is illustrated in Figs. 10c and d. It shows the kinetics of CO_2 influx as it occurs during passage of the RBC through tissue capillaries (Fig. 10c), along with the associated HCO_3^- efflux called Hamburger shift (Fig. 10d). Both figures show again the extreme limitation of the process in the absence of CA, and they show clearly that also for CO_2 uptake by RBC it is somewhat more advantageous to have the CA activity homogeneously distributed in the interior of the RBC. We conclude that in terms of the modeled kinetics of transfer of CO_2 and HCO_3^- across the cell membrane and the associated intracellular diffusion and reaction processes, it is of greater advantage to have the intraerythrocytic CA homogeneously distributed across the cytoplasm than to have it all concentrated at the internal side of the membrane.

Fig. 11 serves to illustrate the mechanism responsible for the difference between blue and red curves in Fig. 10. The curves represented by the open circles were calculated with the same assumption underlying the red curves, namely accumulation of all intraerythrocytic CA at the internal side of the membrane. However, the intracellular diffusion coefficient of hemoglobin was increased 100-fold above its actual value of $6.4 \cdot 10^{-8}$ cm^2 s^{-1}. This shows that the relatively slow diffusion of intraerythrocytic hemoglobin, and thus the relatively slow intraerythrocytic facilitated proton transport, are responsible for a retardation of CO_2 and HCO_3^- uptake when CA is concentrated at the internal side of the membrane rather than being, like hemoglobin, distributed homogeneously across the intracellular space (see discussion).

Discussion

Carbonic anhydrase supports membrane HCO_3^- transport most efficiently when it is homogeneously distributed in the cytoplasm. – Fig. 10 shows that a homogeneous presence of CA in the cytoplasm is predicted to be more favourable for uptake of HCO_3^- and CO_2 than restriction of intracellular CA to a 10 nm thick layer immediately adjacent to the membrane. Although the latter situation guarantees that any HCO_3^- or CO_2 transferred across the membrane has instantaneous access to an extremely high CA activity, it nonetheless slows down the uptake process. A model in which the CA is partly concentrated at the membrane and partly distributed in the cytoplasm yields uptake curves intermediate between the blue and red curves of Fig. 10, i.e. such a model is also inferior compared to the model with homogeneous intracellular CA distribution. This result admittedly appears counterintuitive. Indeed, the intuitive view that CA concentrated in the vicinity of the membrane should favor faster HCO_3^- transport has added to the great attractiveness of the metabolon concept. What is the reason for the contrary result? The answer is given in Fig. 11, which shows that 100-fold acceleration of intracellular hemoglobin diffusion causes the difference in uptake kinetics between the two models to disappear. Since hemoglobin is the major intraerythrocytic buffer, and its property of being a – mobile – buffer is its only function in the present model, this result leads to the following interpretation: when, for example, HCO_3^- has permeated the membrane and the catalysed dehydration reaction sets in, consuming protons to form CO_2, the reaction can only continue as far as sufficient amounts of protons are available at the site where the reaction takes place. The available protons, however, are bound to the major buffer hemoglobin, and the hemoglobin is homogeneously distributed across the intraerythrocytic space. Thus, delivery of protons from the cell interior towards the membrane region by hemoglobin-facilitated H^+ diffusion becomes rate-limiting, since free diffusion of cytosolic protons is negligible at the low intracellular H^+ concentration. The slow diffusion of hemoglobin inside the red cell is also slow compared to the rates of other components of the uptake process (Moll, 1966; Gros and Moll, 1974; Junge and McLaughlin, 1987). If hemoglobin diffusion were 100 times faster, this limitation would not exist. It should be noted that this problem is not restricted to red blood cells, but applies to all cells, because the total H^+ buffer capacity in most cells reaches 30-50% that of RBC, although the average buffer mobility is likely somewhat greater (Vaughan-Jones et al., 2002). We conclude that for all

cells, colocalization of the major buffers with carbonic anhydrase maximizes rates of HCO_3^- transport. This situation applies when both are distributed homogeneously in the cytoplasm. This requires HCO_3^- (in the case of AE1-mediated HCO_3^- uptake, with HCO_3^- diffusion tightly coupled to oppositely directed diffusion of Cl^-) or CO_2 (in the case of CO_2 uptake) to diffuse to the locations of buffer and CA. Thess diffusion processes are much faster than facilitated proton transport because both HCO_3^- and CO_2 have rather high intracellular diffusivities (see Methods). The following illustrative example assumes identical concentration gradients of HCO_3^- and buffered protons. These intracellular concentration gradients must be identical due to the 1:1 stoichiometry of the reaction of H^+ and HCO_3^-. However, the gradients have opposite signs because, in the given example, we look either at the diffusion of HCO_3^- from the membrane into the cell interior (CA homogeneously distributed in the cytoplasm), or, alternatively, at the diffusional transport of protons from the cell interior towards the membrane (CA concentrated at the internal side of the membrane). As a note on the side, in both cases electroneutrality of these intracellular ion fluxes will be maintained by the intracellular Cl^- fluxes required to maintain the Hamburger shift. With an arbitrarily chosen concentration difference of 5 mM for both HCO_3^- and bound protons (the free H^+ being negligible), the products of diffusion coefficients and concentration gradients then are

for H^+: $D_{Hb} \cdot BF \cdot \Delta pH = -6.4 \cdot 10^{-8}\ cm^2 s^{-1} \cdot 5\ mM = -3.2 \cdot 10^{-7}\ cm^2\ mM\ s^{-1}$

for HCO_3^-: $D_{HCO3-} \cdot \Delta[HCO_3^-] = 0.6 \cdot 10^{-5}\ cm^2 s^{-1} \cdot 5\ mM = 3 \cdot 10^{-5}\ cm^2\ mM\ s^{-1}$.

HCO_3^- diffusion inside cells – and similarly CO_2 diffusion – thus is two orders of magnitude faster than proton transport. This fact makes it more efficient to put the carbonic anhydrase to where the buffer is.

We note that these results have no direct bearing on the existence or non-existence of an AE1-CA II metabolon. Such a metabolon could in principle accelerate substantially the HCO_3^- transport rate, by an allosteric effect or by facilitation of HCO_3^- entry into or release from AE1 via a closely attached CAII, potentially overriding the relatively small negative effects of a CA II localization directly at the membrane as presented above.

No colocalization with AE1 and no FRET signal detectable in CA II-expressing tsA201 cells. - No subcellular localization studies of intact non-erythroid cells co-expressing AE1 and CAII have been reported to date. In Figs. 3 – 5 we present clear evidence that the fluorescent fusion proteins wildtype human CAII, N-terminally truncated CAII and the acatalytic V143Y CAII are all distributed homogeneously across the cytoplasm of transfected tsA201 cells. Qualitatively as well as quantitatively, the CAII fluorescence intensities show

no accumulation of either CA II variant in the vicinity of the membrane. In contrast, fluorescent human and murine AE1 fusion proteins clearly colocalize with the cell surface membranes, (with a small fraction of AE1 associated with intracellular vesicular structures). This clear result is confirmed by the absence of a FRET signal arising from coexpressed CyPet-labelled CAII and YPet-labelled human or murine AE1, whereas a doubly labelled AE1 provides a strong positive FRET signal. Thus, the present morphological studies show no evidence for association between CAII and AE1 any closer than 8-10 nm. We conclude that these two heterologous proteins do not form a physical complex at the plasma membrane of transfected tsA201 cells. Vince and Reithmeier (1998) investigated red cell ghosts washed only once, i.e. mildly in comparison to earlier studies (Tappan, 1968; Rosenberg and Guidotti, 1968; Randall and Maren, 1972). Immunofluorescent imating of smears of these pink ghosts revealed both CA II and AE1 homogeneously distributed across the ghosts. Upon treatment with tomato lectin to promote clustering of AE1, they observed clustering of both AE1 and CA II. Since the authors did not costain with antibodies to both AE1 and CAII, the colocalization of the two proteins in the clusters was not definitively shown. On the other hand, Campanella et al (2005) have shown an enrichment of CA II at the membrane in red cells after fixation and immunohistochemical localization.

No evidence for a functional metabolon of CA II and AE1 in tsA201 cells. – Fig. 9 shows clearly that calculated HCO_3^- uptake rate by cells, as when induced by an extracellular step change in HCO_3^- or Cl^- concentration and observed by an intracellular pH dye, depends very strongly on intracellular CA activity. This dependency is most pronounced in the CA activity range between 0 and ~1000, exactly the range of intracellular CA activity present in cell lines such as HEK293, tsA201, or MDCK cells. Therefore, valid comparisons of bicarbonate fluxes between cells in which various CA II constructs are expressed, can only be made, if the intracellular CA activity is carefully controlled. These controls have often been missing in the literature reporting such flux measurements.

The present method of measuring HCO_3^- permeability differs from this classical type of experimental approach. We estimate P_{HCO3-} by observing the exchange of ^{18}O between CO_2, HCO_3^- and H_2O under conditions of perfect chemical – but not isotopic – equilibrium (Endeward and Gros, 2005; Endeward et al., 2006). The moderate dependency of P_{HCO3-} on Ai that we see in Fig. 7, is due to the fact that the calculation of P_{HCO3-} from ^{18}O exchange measurements assumes perfect stirring of the intracellular space (Endeward et al., 2005). As

we have shown previously (Endeward and Gros, 2009), this is of course not realistic and the lack of intracellular mixing causes a delay in the cellular uptake of the substance considered, due to a build-up of the substance transferred into the cell at the internal side of the membrane. For CO_2 and bicarbonate, this delay is diminished with increasing intracellular CA activity, which promotes interconversion between CO_2 and HCO_3^-, thus reducing the build-up of CO_2 or bicarbonate at the membrane and accelerating the respective fluxes. As a consequence, slightly increased bicarbonate fluxes and slightly increased P_{HCO3-} are expected to parallel increasing Ai, as evident between CA activities of 500 and 1500 in Fig. 7. Between CA activities of 5000 and 20,000, such an effect is no longer visible (Fig. 8), consistent with prediction (Fig. 9).

Considering the effects of the three types of CA II constructs expressed in tsA201 cells, the following conclusions can be drawn from Fig. 7:

1) Expression of heterologous wild-type CAII fusion protein (♦) increases Ai over that in the mere presence of endogenous CAII (▼), and in parallel causes a moderate increase in P_{HCO3-}. This could potentially be compatible with increased concentration of an AE1-CAII metabolon. However, in view of the general dependence of P_{HCO3-} on Ai, such an explanation would not be conclusive. The fact that (in the present study) expression of wild-type CAII has a noticeable effect on P_{HCO3-}, is at variance with the report by Sterling et al. (2001), who found no effect of CAII expression in HEK293 cells, which they interpreted to indicate that the endogenous CAII activity of HEK293 cells is sufficient for a full metabolon effect. The cause of this discrepancy is not clear, but does not affect the current finding that P_{HCO3-} is directly proportional to Ai (Fig. 7).

2) Expressing the (almost) acatalytic CA II mutant V143Y decreases endogenous CA activity from ~800 to ~480. This pronounced effect causes a reduction in P_{HCO3}-, which follows the general dependency of P_{HCO3-} on Ai seen in Fig. 7. The metabolon hypothesis predicts that the V143Y mutant displaces some of the catalytically active native CA II from its binding site at AE1 to reduce transport activity. Indeed, Sterling et al. (2001a, 2001b) observed that expression of CAII V143Y reduced bicarbonate transport rate up to 60%. Similarly, Sowah and Casey (2011) observed substantial reduction of HCO_3^- transport activity of an AE1+CAII fusion protein expressed in HEK293 cells with co-expression in the same cell of increasing levels of CAII-V143Y in the same cell. Comparing the present expression of CAII-V143Y (Fig. 2a) with the immunoblots of Sterling et al. (2001a), it appears likely that the expression of the mutant protein was stronger in some of their experiments than in the present ones. The

maximum amount of cDNA used by Sterling et al (2001a) per culture dish area was about twice as much as the amount of cDNA routinely used in this study. In addition, the calcium phosphate method used by these authors may have produced higher transfection rates than the method used here. On the other hand, even with the present modest transfection efficiencies of 30-40%, expression of V143Y-CAII causes a drastic reduction of average intracellular CA activity from 800 to 480. This shows that the expression of this mutant is associated with a very marked reduction of endogenous CAII activity in the transfected cells. If the same occurred in Sterling's experiments, such a reduction of CA activity in their transfected cells might explain the observed 60% reduction in Cl^-/HCO_3^- exchange activity. The mechanism by which AE1 activity was reduced in the experiments of Sterling et al. (2001a) might then represent marked reduction in intracellular CA activity rather than the proposed displacement of endogenous CAII from its AE1 binding site by the V143Y mutant. Thus, the influential result of Sterling et al. (2001a) can be explained by a mechanism that does not require the existence of a functionally important AE1-CAII metabolon.

3) Another striking finding illustrated in Fig. 7 in terms of the metabolon hypothesis is the expression of truncated CAII, which lacks the proposed binding site of CAII to AE1. This expression leads to an increase in Ai from 800 to 1500, attesting to the intact catalytic activity of this mutant, and in parallel increasing P_{HCO3-} from 3.8 to $6 \cdot 10^{-4}$ cm/s ($P<0.05$). The in vitro assays of Vince et al. (2000) showed that the truncated CAII does not bind to AE1. Unfortunately, measurements of the effect of expression of truncated CAII on bicarbonate transport have not previously been reported. The metabolon concept predicts most simply that expression of the truncated CAII would not compete with endogenous CAII for the AE1 binding site, and thus would not alter AE1 transport activity. Because likely the expression of endogenous CA II is somewhat reduced by the expression of the truncated form, rather a decrease in AE1 activity would be expected. Instead, we observe a significant increase in P_{HCO3-}, again consistent with the direct relationship between P_{HCO3-} and intracellular CA activity.

Sterling et al. (2001) also reported that AE1 mutants in which the C-terminal binding motif for CA II was changed or deleted exhibited a 90% reduction of transport activity when expressed in HEK293 cells. The authors did not confirm preservation of intrinsic transport activity of these mutants in the absence of CAII, so these experiments appear not entirely conclusive.

HCO_3^- permeability of CAII-deficient red cells is identical to that of normal red cells. – The CAII-deficient red blood cells from two different patients were free of CAII activity as reported in the original description of this syndrome (Sly et al., 1983) and in a later review (Shah et al., 2004). However, as reported previously (Dodgson et al., 1988) and shown in Fig. 6a, the substantial residual CAI activity of these cells that is more than sufficient for the requirements of capillary CO_2 exchange in lung and tissues (Swenson and Maren, 1978). It can ths be expected that the processes of HCO_3^- and CO_2 uptake by CAII-deficient red cells is minimally impaired compared to those of normal RBC. This is demonstrated in Fig. 9, which applies the mathematical model described above to illustrate the effect of different cytoplasmic CA activities on the kinetics of HCO_3^- uptake. It is apparent that varying intracellular CA activities between 5,000 (as in CAII-deficient RBC) and 20,000 (as in normal RBC) is of minimal consequence to HCO_3^- uptake kinetics.

Thus, the CAII-deficient human red cell appears to be an ideal model in which to study the question of whether CAII affects HCO_3^- permeation across the cell membrane: it retains substantial CA activity from its residual CA1, but lacks the ability of CA2 to bind to AE1 (Vince and Reithmeier, 1998). As seen in Fig. 8b, the calculated bicarbonate permeabilities for normal and CAII-deficient RBC are indistinguishable. These values of P_{HCO3-} calculated from the mass spectrometric records of course use the correct respective intracellular CA activities as described previously (Endeward and Gros, 2005; Endeward et al., 2008). Fig. 8b shows that absence of CAII does not affect bicarbonate permeation, and thus CA II in human red cells has no functional effect on bicarbonate transport by AE1. HCO_3^- uptake would slow down considerably if intraerythrocytic CA activity were to decrease below about 1,000, as indicated in Fig. 9, but this is a general effect of the speed of the intracellular hydration-dehydration reaction, and reflects no specific effect of CAII on AE1.

Conclusion. – The present study investigates the AE1-CAII metabolon hypothesis by a variety of approaches. First, we study by an elaborate theoretical model which level of intracellular CA activity is required to abolish limitation of the rate of uptake or release of HCO_3^- by cells by the intracellular speed of hydration-dehydration. This CA activity is roughly between 1000 and 5000. Since many cell lines have CA activities below 1000, it is to be expected that in AE1-expressing cells the speed of HCO_3^- transport is often limited by their intracellular CA activity. This is also the case in the results reported here, which show a moderate increase in P_{HCO3-} of tsA201 cells with intracellular CA activity increasing from 500

to 1500. We find that expression of the acatalytic CAII mutant V143Y reduces P_{HCO3-}, that additional expression of wildtype CAII increases P_{HCO3-}, and that expression of an N-terminally truncated CA II lacking the proposed AE1 binding region further increases P_{HCO3-}. All these changes in P_{HCO3-} can be attributed to corresponding changes in intracellular CA activity. Thus, none of these experiments suggests any specific interaction of AE1 and CAII as proposed in the metabolon hypothesis. These data are strongly supported by the fact that CAII-deficient human red blood cells exhibit a bicarbonate permeability identical to that of normal human red cells. The CAII-deficient red cells have sufficiently high intracellular CA activity (due to residual CAI that lacks an AE1 binding motif) to ensure a HCO_3^- transport rate not limited by the speed of the CO_2 hydration-dehydration reaction. Thus, the present results offer no evidence of functional molecular interaction of CA II and AE1. Studies expressing YPet and CyPet-labelled human CA II and human and murine AE1 in tsA201 cells show no colocalization of CA II with AE1 at the cell membrane. This result is further supported by the absence of a FRET signal, indicating that CA II and AE1 in the cell are further apart than 8-10 μm, i.e. they do not form a complex. As a further interesting piece of evidence, the theoretical model presented here shows that is more effective for transmembrane CO_2 as well as HCO_3^- transport to have the cellular carbonic anhydrase homogeneously distributed across the cytoplasm, for the major reason that the cellular buffers are also distributed all over the cell interior, thereby ensuring that H^+ produced or consumed by the CA-mediated reactions have immediate access to these buffers.
In conclusion, the actual and also the most favourable localization of CA II within cells in terms of AE1 transport activity appears to be a homogeneous distribution all over the cell interior.

Other HCO_3^- transporters than AE1 have been reported to possess the binding motif suggested to bind to CA II and to form a metabolon with CA II, similar to that with AE1: the sodium bicarbonate cotransporters NBC1 and NBC3 and the human putative anion transport 1, SLC26A6/PAT-1 (Alvarez et al., 2003; Gross et al., 2002; Loiselle et al., 2004; Alvarez et al., 2003). Our data do not allow us to draw any inferences on these proposed metabola. It should be noted, however, that recently Schueler et al. (2011) have reported that CA I, which lacks the binding region proposed to mediate the binding between all these transporters and CA II, clearly increases the transport activity of NBCe1. These authors show that the major determinant of NBCe1 transport activity appears to be the level of intracellular carbonic anhydrase catalytic activity, independent of the CA isoform responsible for this activity. This

conclusion is entirely in line with the main conclusion of the present study on AE1 transport properties.

References

1. Vince, J.W., Reithmeier R.A. (1998) Carbonic anhydrase II binds to the carboxyl terminus of human band 3, the erythrocyte C1-/HCO3- exchanger. *J. Biol. Chem.* **273**, 28430-28437

2. Enns, T. (1967) Gas transport and the red cell. *Fed. Proc*. **26**, 1802-1804

3. Rosenberg, S.A., Guidotti, G. (1968) The protein of human erythrocyte membranes. I. Preparation, solubilization, and partial characterization. *J. Biol. Chem.* 243, 1985-1992.

4. Tappan, D.V. (1968) Carbonic anhydrase activity of erythrocyte ghosts. *Experientia* **24**, 127

5. Randall, R.F., Maren, T.H. (1972) Absence of carbonic anhydrase in red cell membranes. *Biochim. Biophys. Acta.* **268**, 730-732

6. Parkes, J.L., Coleman, P.S. (1989) Enhancement of carbonic anhydrase activity by erythrocyte membranes. *Arch. Biochem. Biophys.* **275**, 459-468.

7. Kifor, G., Toon, M.R., Janoshazi, A., Solomon, A.K. (1993) Interaction between red cell membrane band 3 and cytosolic carbonic anhydrase. *J. Membr. Biol.* **134**, 169-179.

8. Campanella, M.E., Chu, H., Low, P.S. (2005) Assembly and regulation of a glycolytic enzyme complex on the human erythrocyte membrane. *Proc. Natl. Acad. Sci.* **102**, 2402-2407.

9. Vince, J.W., Reithmeier, R.A. (2000) Identification of the carbonic anhydrase II binding site in the Cl(-)/HCO(3)(-) anion exchanger AE1. *Biochemistry.* **39**, 5527-5533.

10. Vince, J.W., Carlsson, U., Reithmeier, R.A. (2000) Localization of the Cl-/HCO3- anion exchanger binding site to the amino-terminal region of carbonic anhydrase II. *Biochemistry.* **39**, 13344-13349

11. Piermarini, P.M., Kim, E.Y., Boron, W.F. (2007) Evidence against a direct interaction between intracellular carbonic anhydrase II and pure C-terminal domains of SLC4 bicarbonate transporters. *J. Biol. Chem.* **282**, 1409-1421

12. Sterling, D., Reithmeier, R.A., Casey, J.R. (2001) A transport metabolon. Functional interaction of carbonic anhydrase II and chloride/bicarbonate exchangers. *J. Biol. Chem.* **276**, 47886-47894

13. Sterling, D., Reithmeier, R.A., Casey, J.R. (2001) Carbonic anhydrase: in the driver's seat for bicarbonate transport. *J. Pancreas.* **2**, 165-170

14. Nguyen, A.W., Daugherty, P.S. (2005) Evolutionary optimization of fluorescent proteins for intracellular FRET. *Nat. Biotechnol.* **23**, 355-360

15. Fierke, C.A., Calderone, T.L., Krebs, J.F. (1991) Functional consequences of engineering the hydrophobic pocket of carbonic anhydrase II. *Biochemistry.* **30**, 11054-11063

16. Papadopoulos, S., Leuranguer, V., Bannister, R.A., Beam, K.G. (2004) Mapping sites of potential proximity between the dihydropyridine receptor and RyR1 in muscle using a cyan fluorescent protein-yellow fluorescent protein tandem as a fluorescence resonance energy transfer probe. *J. Biol. Chem.* **279**, 44046-44056

17. Endeward, V., Gros, G. (2005) Low carbon dioxide permeability of the apical epithelial membrane of guinea-pig colon. *J. Physiol.* **567**, 253-265

18. Endeward, V., Cartron, J.P., Ripoche, P., Gros, G. (2006) Red cell membrane CO2 permeability in normal human blood and in blood deficient in various blood groups, and effect of DIDS. *Transfus. Clin. Biol.* **13**, 123-127

19. Supuran, C.T. (2008) Carbonic anhydrases: novel therapeutic applications for inhibitors and activators. *Nature Rev. Drug Discov.* **7**, 168-181

20. Geigy, J.R. (1960) *Ducumenta Geigy Wissenschaftliche Tabellen*, 6th Ed., Geigy, Basel

21. Endeward, V., Gros, G. (2009) Extra- and intracellular unstirred layer effects in measurements of CO2 diffusion across membranes--a novel approach applied to the mass spectrometric 18O technique for red blood cells. *J. Physiol.* **587**, 1153-1167

22. Gros, G., Moll, W. (1972) The facilitated diffusion of CO2 in hemoglobin solutions and phosphate solutions. *Oxygen Affinity of Hemoglobin and Red Cell Acid Base Status* Academic Press, Copenhagen.

23. Gros, G., Moll, W. (1974) Facilitated diffusion of CO2 across albumin solutions. *J. Gen. Physiol.* **64**, 356-371.

24. Gros, G., Moll, W., Hoppe, H., Gros, H. (1976) Proton transport by phosphate diffusion--a mechanism of facilitated CO2 transfer. *J. Gen. Physiol.* **67**, 773-790

25. Moll, W. (1966) The diffusion coefficient of haemoglobin. *Respir. Physiol.* **1**, 357-365.

26. Forster, R.E. (1964) Rate of gas uptake by red cells. *Handbook of Physiology*, The American Physiological Society, Washington, DC

27. Itada, N., Forster, R.E. (1977) Carbonic anhydrase activity in intact red blood cells measured with 18O exchange. *J. Biol. Chem.* **252**, 3881-3890

28. Sly, W.S., Hewett-Emmett, D., Whyte, M.P., Yu, Y.S., Tashian, R.E. (1983) Carbonic anhydrase II deficiency identified as the primary defect in the autosomal recessive syndrome of osteopetrosis with renal tubular acidosis and cerebral calcification. *Proc. Natl. Acad. Sci.* **80**, 2752-2756

29. Dodgson, S.J., Forster, R.E., Sly, W.S., Tashian, R.E. (1988) Carbonic anhydrase activity of intact carbonic anhydrase II-deficient human erythrocytes. *J. Appl. Physiol.* **65**, 1472-1480

30. Endeward, V., Cartron, J.P., Ripoche, P., Gros, G. (2008) RhAG protein of the Rhesus complex is a CO2 channel in the human red cell membrane. *FASEB J.* **22**, 64-73

31. Junge, W., McLaughlin, S. (1987) The role of fixed and mobile buffers in the kinetics of proton movement. *Biochim. Biophys. Acta.* **890**, 1-5

32. Vaughan-Jones, R.D., Peercy, B.E., Keener, J.P., Spitzer, K.W. (2002) Intrinsic H(+) ion mobility in the rabbit ventricular myocyte. *J. Physiol.* **541**, 139-158

33. Sowah, D., Casey, J.R. (2011) An intramolecular transport metabolon: fusion of carbonic anhydrase II to the COOH terminus of the Cl(-)/HCO(3)(-)exchanger, AE1. *Am. J. Physiol. Cell Physiol.* **301**, 336-346

34. Shah, G.N., Bonapace, G., Hu, P.Y., Strisciuglio, P., Sly, W.S. (2004) Carbonic anhydrase II deficiency syndrome (osteopetrosis with renal tubular acidosis and brain calcification): novel mutations in CA2 identified by direct sequencing expand the opportunity for genotype-phenotype correlation. *Hum. Mutat.* **24**, 272

35. Swenson, E.R., Maren, T.H. (1978) A quantitative analysis of CO2 transport at rest and during maximal exercise. *Respir. Physiol.* **35**, 129-159.

36. Alvarez, B.V., Loiselle, F.B., Supuran, C.T., Schwartz, G.J., Casey, J.R. (2003) Direct extracellular interaction between carbonic anhydrase IV and the human NBC1 sodium/bicarbonate co-transporter. *Biochemistry.* **28**, 12321-12329

37. Gross, E., Pushkin, A., Abuladze, N., Fedotoff, O., Kurtz, I. (2002) Regulation of the sodium bicarbonate cotransporter kNBC1 function: role of Asp986, Asp988 and kNBC1-carbonic anhydrase II binding. *J. Physiol.* **544**, 679–685

38. Loiselle, F.B., Morgan, P.E., Alvarez, B.V., Casey, J.R. (2004) Regulation of the human NBC3 Na+/HCO3- cotransporter by carbonic anhydrase II and PKA. *Am. J. Physiol. Cell Physiol.* **286**, 1423-1433

39. Schueler, C., Becker, H.M., McKenna, R., Deitmer, J.W. (2011)
Transport activity of the sodium bicarbonate cotransporter NBCe1 is enhanced by different isoforms of carbonic anhydrase. *PLoS One*. **6**, 27167

Legends to Figures

Fig. 1. Scheme explaining the theoretical model used to simulate HCO_3^- and CO_2 transport across a cell membrane. The calculations were performed for the parameters of a human red cell. The extracellular compartment was considered to be well-stirred. The intracellular compartment was divided into 800 segments per red cell half-thickness, and a finite difference method was used to solve the system of differential equations describing diffusion of CO_2 and HCO_3^- as well as buffer-facilitated H^+ diffusion. In conjunction with these diffusion processes the simultaneous reactions $CO_2 + H_2O \leftrightarrow HCO_3^- + H^+$ and $H^+ + Hb \leftrightarrow HbH^+$ were considered. The results of the calculations are shown in Figs. 9-11. In the upper scheme a cytoplasmic carbonic anhydrase activity of 20,000 (activity defined as acceleration factor of CO_2 hydration minus 1) was assumed to be present everywhere inside the cell. To study the effect of complete binding of all intraerythrocytic CA at the internal side of the membrane (lower scheme of Fig. 1), the total amount of CA present in the red cell was assumed to be accumulated in the last segment immediately adjacent to the cell membrane (segment thickness 0.01 μm, CA activity in this segment, 800 x 20,000).

Fig. 2. Western Blots showing expression of fluorescent CAII fusion proteins in tsA201 cells. a) Lane 1: upper band is WT-CAII-CyPet, lower band is endogenous CAII of tsA201 cells. Loaded lysate derived from ~1 x 10^5 cells; Lane 3: CAII of human red cell lysate. b) Lane 1: upper band is non-catalytic mutant CAII-V143Y-CyPet, and lower band is endogenous CAII of tsA201 cells. Loaded lysate derived from ~1.4 x 10^6 cells; Lane 2: CAII from human red cell lysate.

Fig. 3. a) Confocal microscopic images of a tsA291 cell co-transfected with human CAII-CyPet and murine YPet-AE1 fusion proteins. CyPet was linked to the C-terminus of CAII, and YPet was linked to the N-terminus of mAE1. B) Fluorescence emission intensity profiles at wavelengths appropriate for CyPet and for YPet as recorded along the red lines in panels a.

Fig. 4. a) Confocal microscopic images of a tsA201 cell cotransfected with hCA II-CyPet (above) and with YPet-hAE1 (below) show the same distribution pattern as mAE1-transfected cells in Fig. 3a . b) Results of FRET experiments with tsA cells cotransfected with hCA II-CyPet and YPet-hAE1 (left), with hCA II-CyPet and YPet-mAE1 (center) and a

FRET control in cells transfected with YPet-mAE1-CyPet (right). This latter construct ensures proximity of the two dyes, reflected in its significantly positive FRET signal. *, $p <$ 0.0X xxxx.

Fig. 5. a) Confocal microscopic images of tsA201 cells co-transfected with N-terminally truncated CA II-CyPet (left) and YPet-mAE1 (right). Intracellular distribution patterns are identical to those in Figs. 3 and 4. b) tsA201 cells co-transfected with non-catalytic CAII mutant CAII-V143Y-CyPet (left) and YPet-mAE1 (right). Distribution patterns are identical to those in Fig. 5 a.

Fig. 6. a) Intracellular CA activities measured in lysates of untreated tsA201 cells (control) and tsA201 cells transfected with YPet-mAE1 (AE1), using the mass spectrometric ^{18}O technique. b). Cellular P_{HCO3}- measured in untreated tsA201 cells (control) and tsA201 cells expressing YPet-mAE1 (AE1), in the absence and presence of DIDS (10^{-5} M), a strong inhibitor of AE1 transport function. DIDS showed no effect on P_{HCO3-} of control cells, but inhibited the AE1-associated increase in P_{HCO3}-. Ns, $p > 0.05$; *, $p < 0.05$ xxxx; §, $p <$ 0.0X xxxx.

Fig. 7. Bicarbonate permeability of tsA201 cells as a function of intracellular CA activity, Ai.
▼ represents tsA201 cells transfected with YPet-mAE1.
▲ represents tsA201 cells co-transfected with CAII-V143Y-CyPet and YPet-mAE1.
♦ represents co-transfection with WT CAII-CyPet and YPet-AE1,
● represents co-transfection with N-terminally truncated CA II-CyPet and YPet-mAE1.
Observed variations of P_{HCO3-} are proportional to measured intracellular CA activity.

Fig. 8. Intraerythrocytic CA activity and bicarbonate permeability of normal (control) and CA II-deficient human red blood cells (the latter from two individuals #1 and #2). a) While normal human red cells exhibit a CA activity of 20.000, CA II-deficient have an activity of ~ 5.000 due to the remaining CA I in these cells. b) P_{HCO3-} is identical no matter whether CA II is present or completely absent.

Fig. 9. Time course of bicarbonate influx (expressed as mol HCO_3^- / membrane surface area in cm^2) for various intraerythrocytic CA activities, calculated with model illustrated in Fig. 1

(upper scheme). The numbers on the curves give the acceleration factors of CO_2 hydration. Therefore, 1 indicates the absence of CA activity, 20.000 an activity of (20.000 – 1). The dependence of HCO_3^-influx on CA activity is most pronounced between 1 and 1000, and becomes minor between 5.000 and 20.000. The figure also indicates that the process is complete within the capillary transit time of 0.7 sec, when the actual intraerythrocytic CA activity of 20.000 is present.

Fig. 10. Significance of the subcellular localization of CA for uptake and release of HCO_3^- and CO_2 in human red cells. Blue curves: calculated for a homogeneous intracellualr distribution of CA in the cytoplasm of red cells (upper scheme in Fig. 1). Red curves: calculated for an accumulation of all the CA of the red cell in a thin (0.01 μm) layer immediately adjacent to the internal side of the red cell membrane (lower scheme in Fig. 1). Black curves: complete absence of CA activity inside red cell. a) HCO_3^- influx after a step change in extracellular HCO_3^- from 25 to 35 mM, b) the efflux of CO_2 following the influx of bicarbonate shown in Fig. 1a, c) CO_2 influx after a step change in extracellular pCO_2 from 40 to 46 mmHg, d) efflux of HCO_3^- following the influx of CO_2 shown in Fig. 10 c (Hamburger shift). All four situations analysed show: 1) CO2 as well as HCO3- exchanges are very far from completion after 0.7 sec when CA is completely absent; 2) all fluxes in either direction occur somewhat faster when CA is distributed homogeneously across the cytoplasm than when it is accumulated at the membrane. Thus, in the absence of a CA II-AE1 metabolon, a homogeneous distribution of CA activity in the cytoplasm represents the situation most favourable for the exchange of HCO_3^- as well as CO_2.

Fig. 11. Effect of hemoglobin diffusivity on the kinetics of HCO_3^- and CO_2 exchange. Blue and red curves are identical to those of Fig. 10 a and b. The curves with the open circles are calculated for the accumulation of all red cell CA at the cytoplasmic side of the membrane, like in the red curve, with the exception that the diffusivity of hemoglobin was set to 100-fold of its true value. This makes both types of CA distribution equivalent in terms of HCO_3^-/CO_2 exchange, indicating that intraerythrocytic Hb-facilitated proton transport causes the limitation of the process when CA is associated with the membrane. It appears logical then that CA exhibits an intracellular distribution identical to that of the main buffer hemoglobin, as this provides for immediate buffering of the H^+ produced by CA.

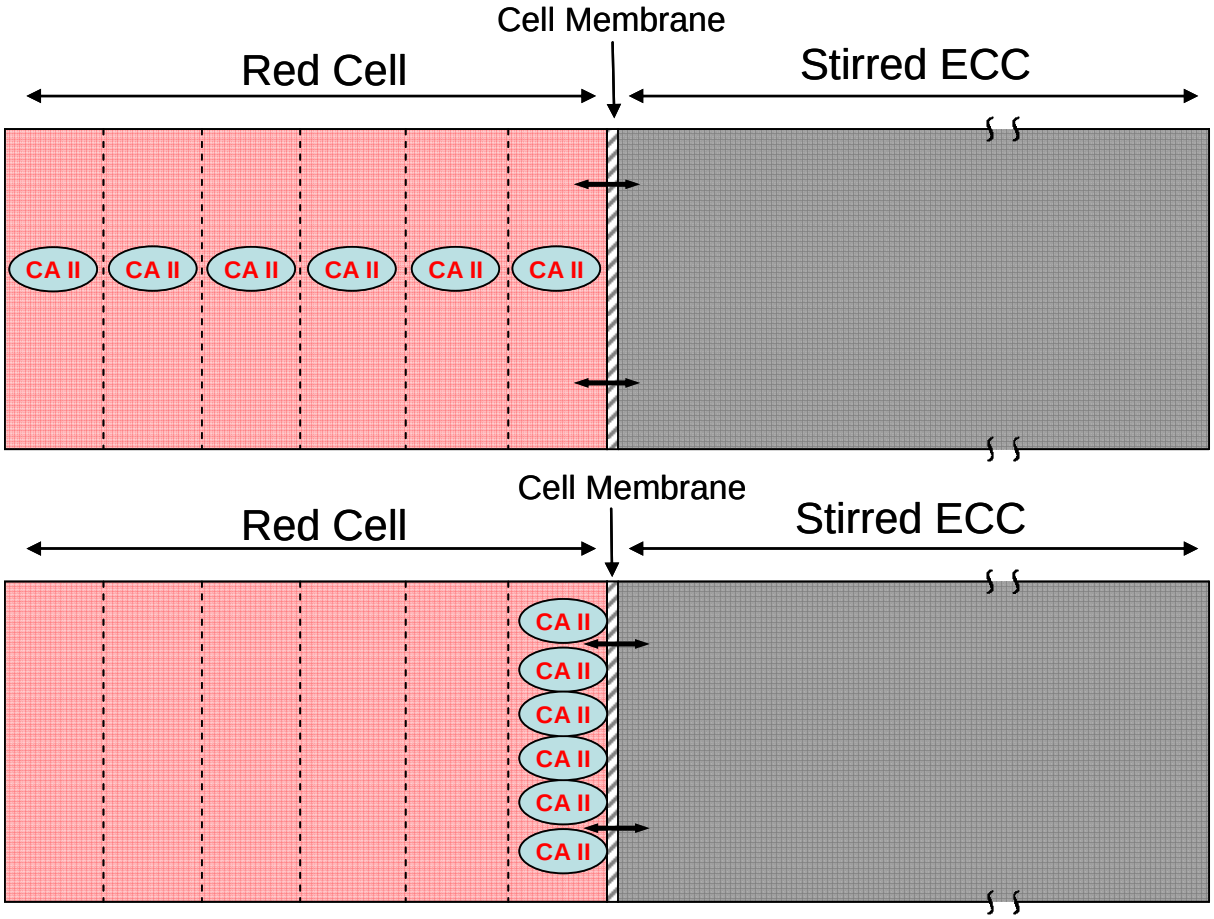
Cell Membrane
Red Cell
Stirred ECC
CA II
CA II
CA II
CA II
CA II
CA II
Cell Membrane
Red Cell
Stirred ECC
CA II
CA II
CA II
CA II
CA II
CA II

Fig. 1

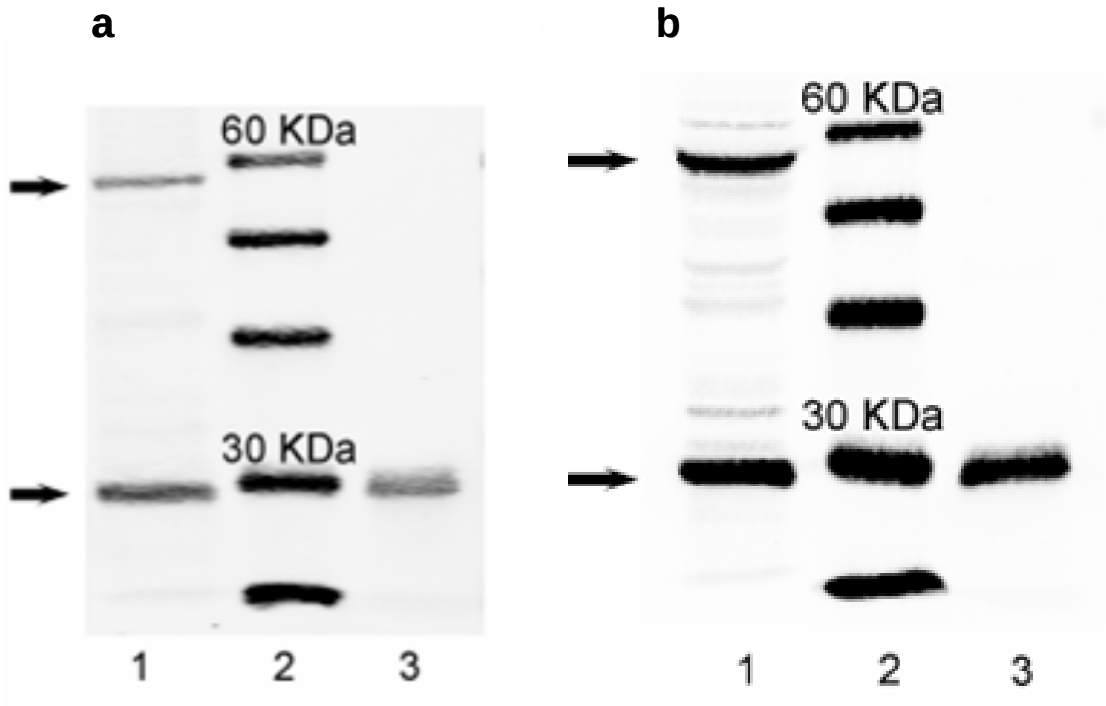
a
60 KDa
30 KDa
1
2
3
b
60 KDa
30 KDa
1
2
3

Fig. 2

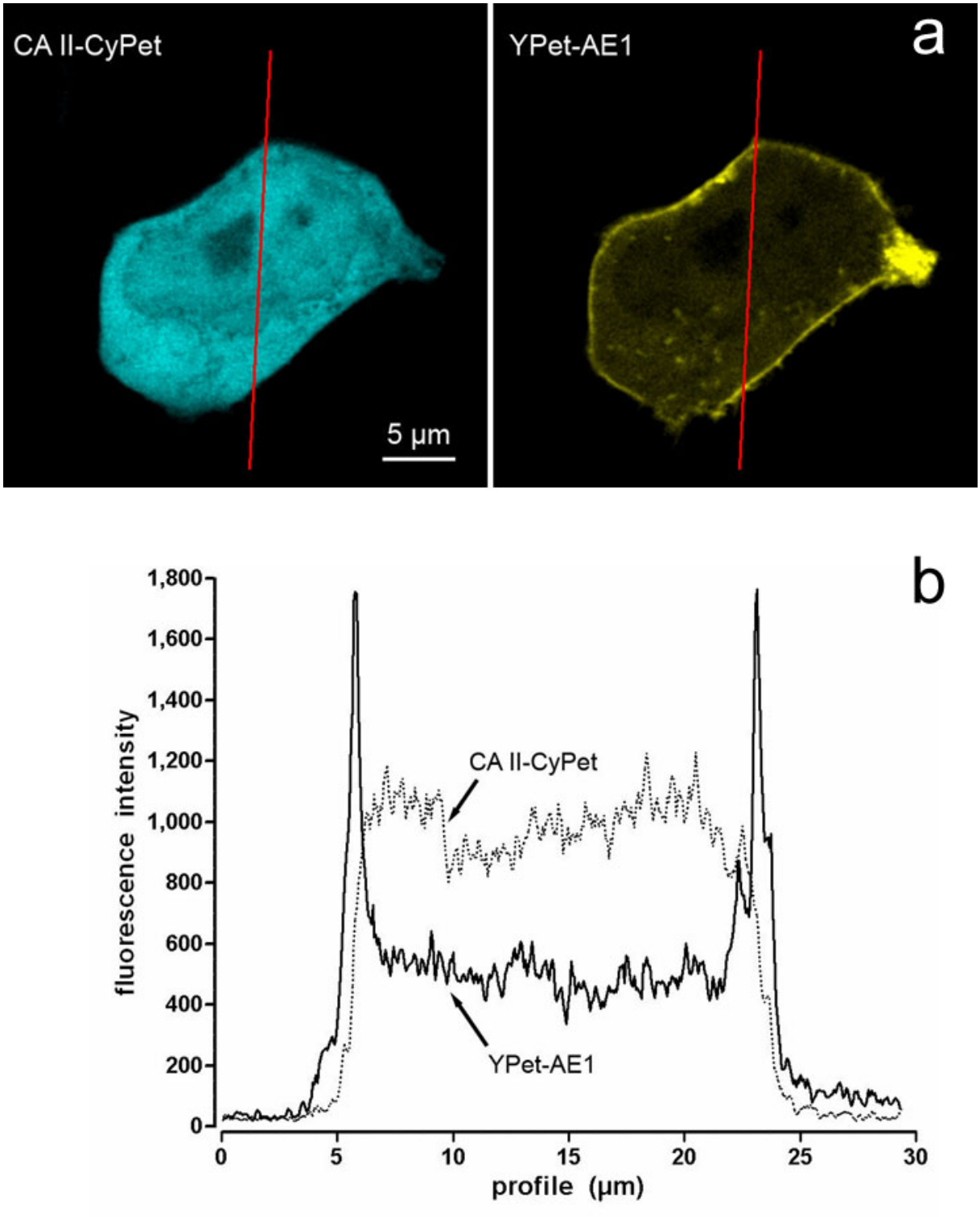
CA II-CyPet
5 µm
YPet-AE1
a
b
fluorescence intensity
1,800
1,600
1,400
1,200
1,000
800
600
400
200
0
CA II-CyPet
YPet-AE1
0
5
10
15
20
25
30
profile (µm)

Fig. 3

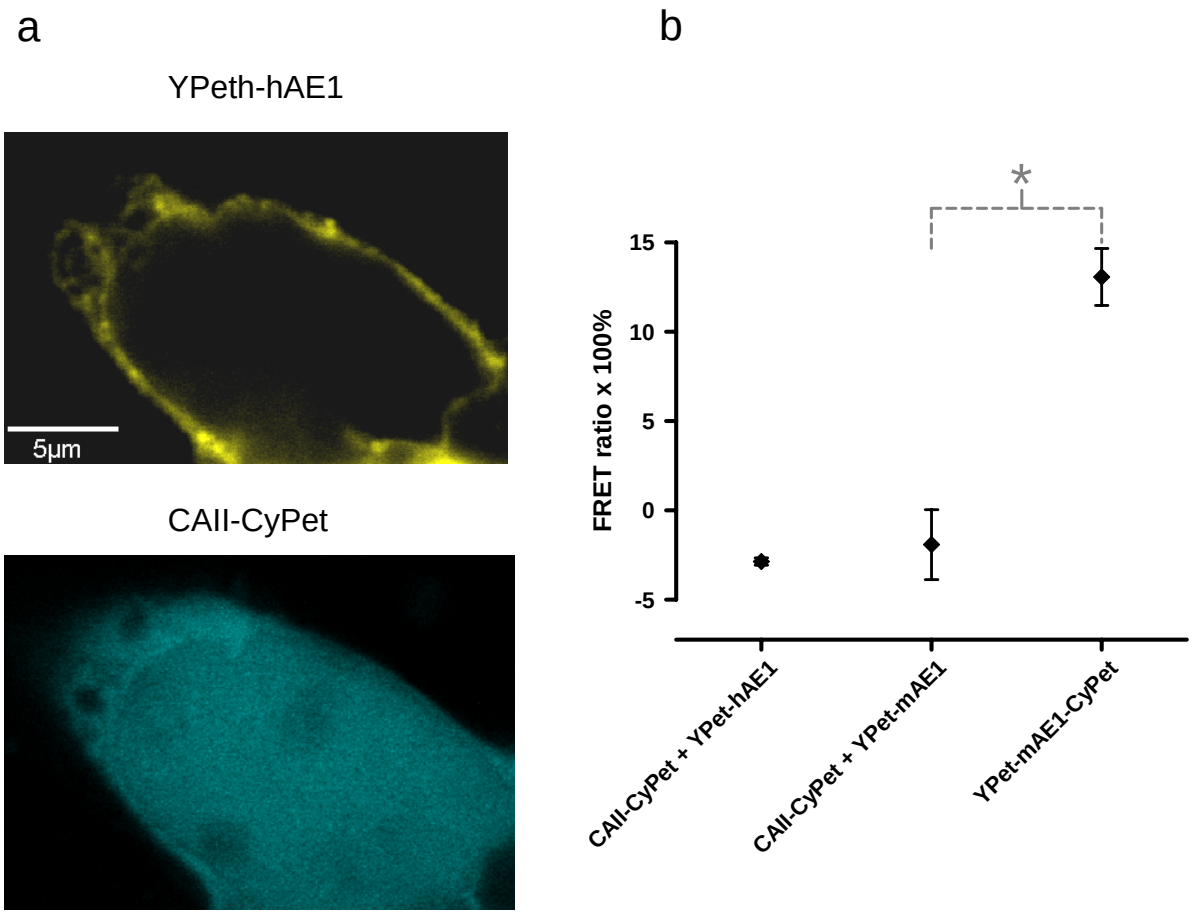
a
YPeth-hAE1
5µm
CAII-CyPet
b
FRET ratio x 100%
15
10
5
0
-5
*
CAII-CyPet + YPet-hAE1
CAII-CyPet + YPet-mAE1
YPet-mAE1-CyPet

Fig. 4

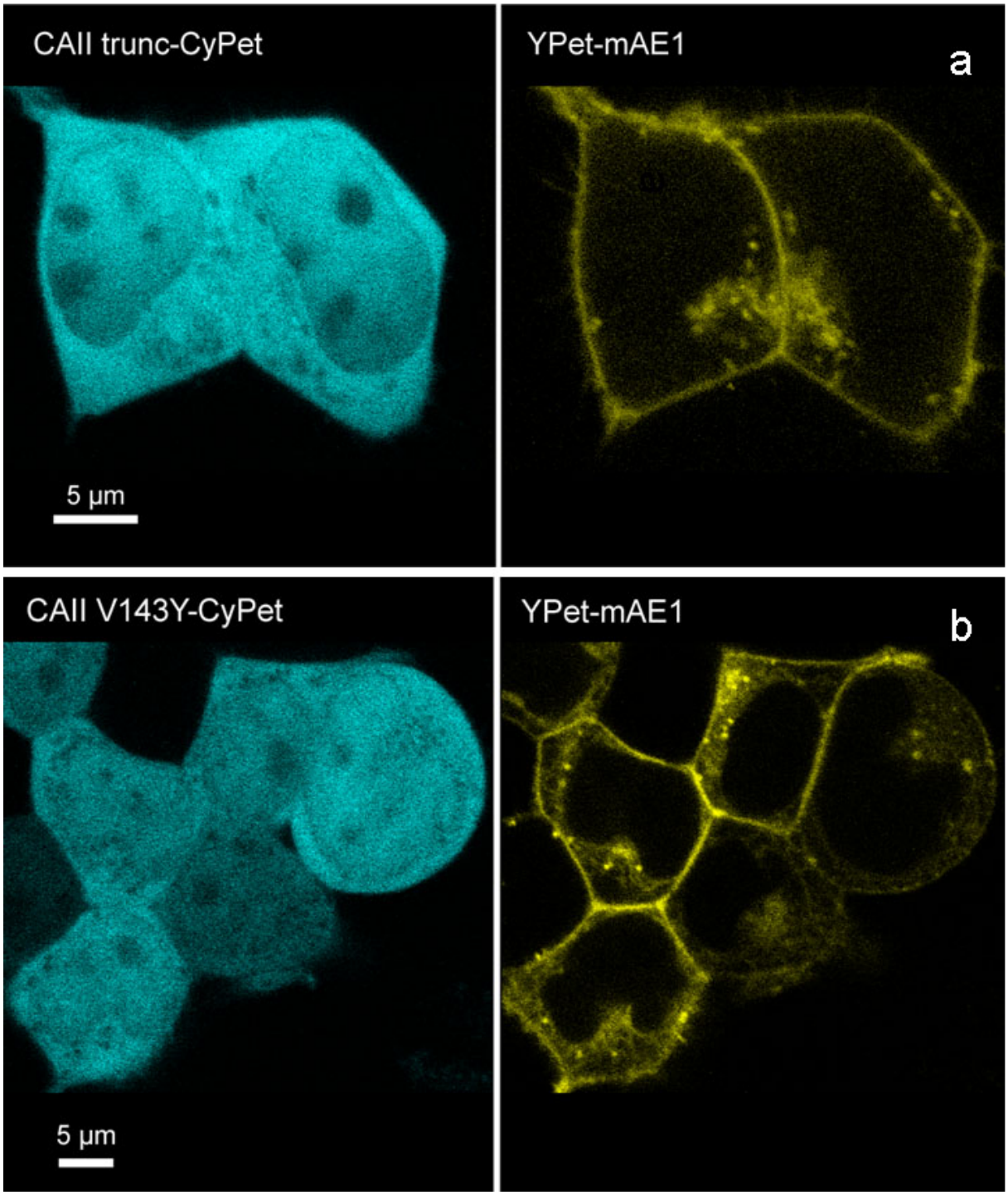
CAII trunc-CyPet
YPet-mAE1
a
5 µm
CAII V143Y-CyPet
YPet-mAE1
b
5 µm

Fig. 5

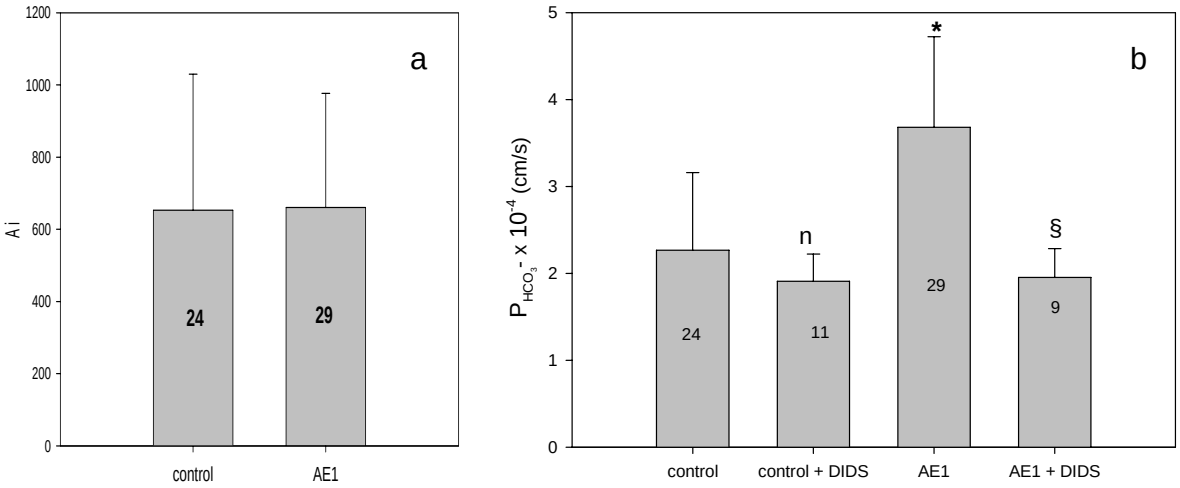
a
b
A i
$P_{HCO_3^-}$ x 10^{-4} (cm/s)
1200
1000
800
600
400
200
0
5
4
3
2
1
0
24
29
11
9
*
n
§
control
AE1
control + DIDS
AE1 + DIDS

Fig. 6

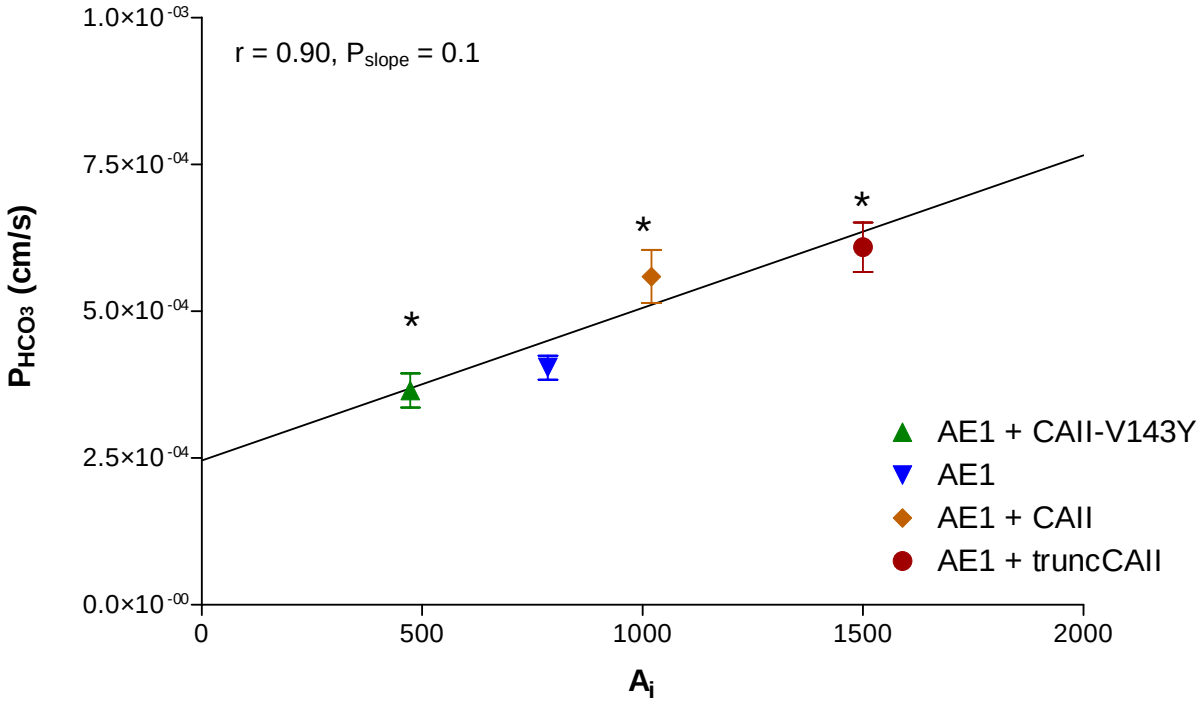
r = 0.90, P_{slope} = 0.1
P_{HCO3} (cm/s)
A_i
1.0×10-03
7.5×10-04
5.0×10-04
2.5×10-04
0.0×10-00
0
500
1000
1500
2000
*
AE1 + CAII-V143Y
AE1
AE1 + CAII
AE1 + truncCAII

Fig. 7

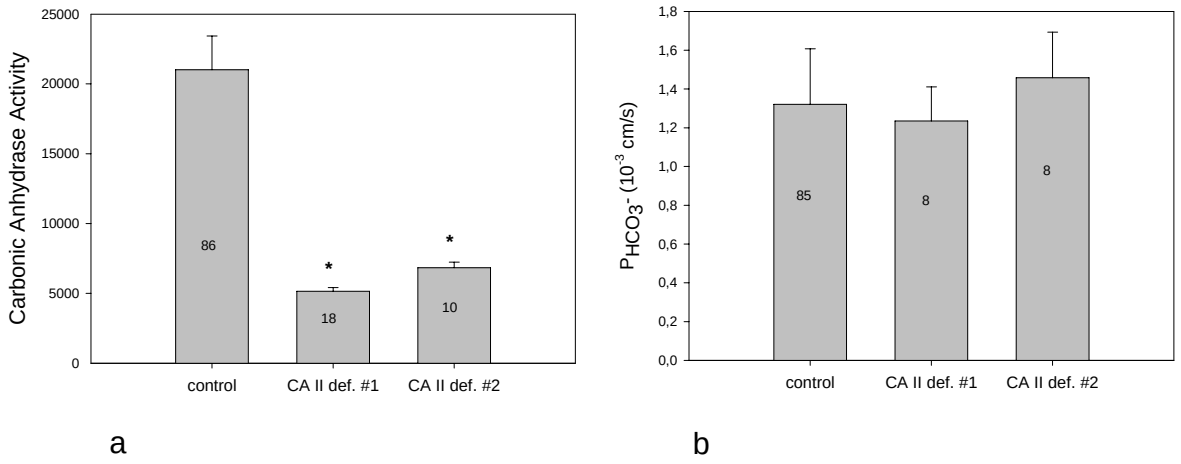
Carbonic Anhydrase Activity
25000
20000
15000
10000
5000
0
86
18
10
*
*
control
CA II def. #1
CA II def. #2
a
$P_{HCO_3^-}$ (10^{-3} cm/s)
1,8
1,6
1,4
1,2
1,0
0,8
0,6
0,4
0,2
0,0
85
8
8
control
CA II def. #1
CA II def. #2
b

Fig. 8

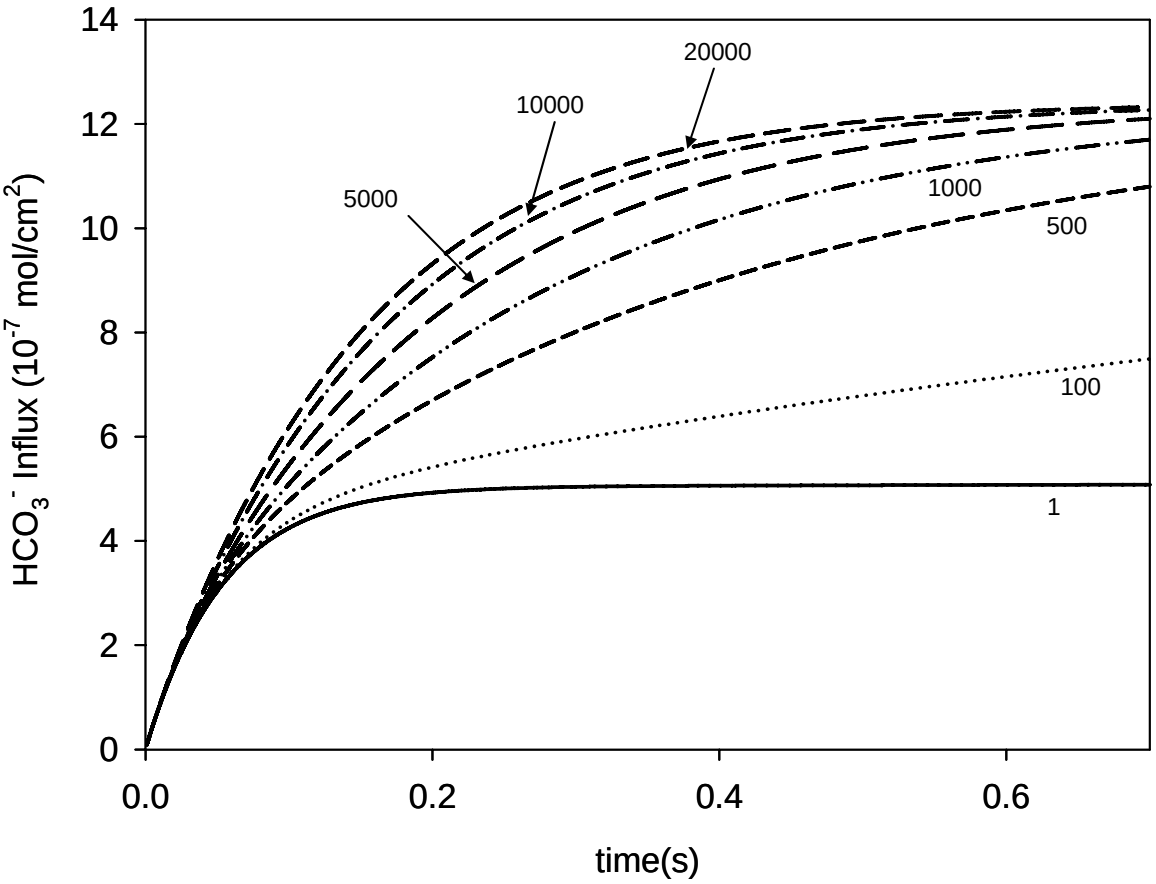
HCO_3^- Influx (10^{-7} mol/cm^2)
14
12
10
8
6
4
2
0
0.0
0.2
0.4
0.6
time(s)
20000
10000
5000
1000
500
100
1

Fig. 9

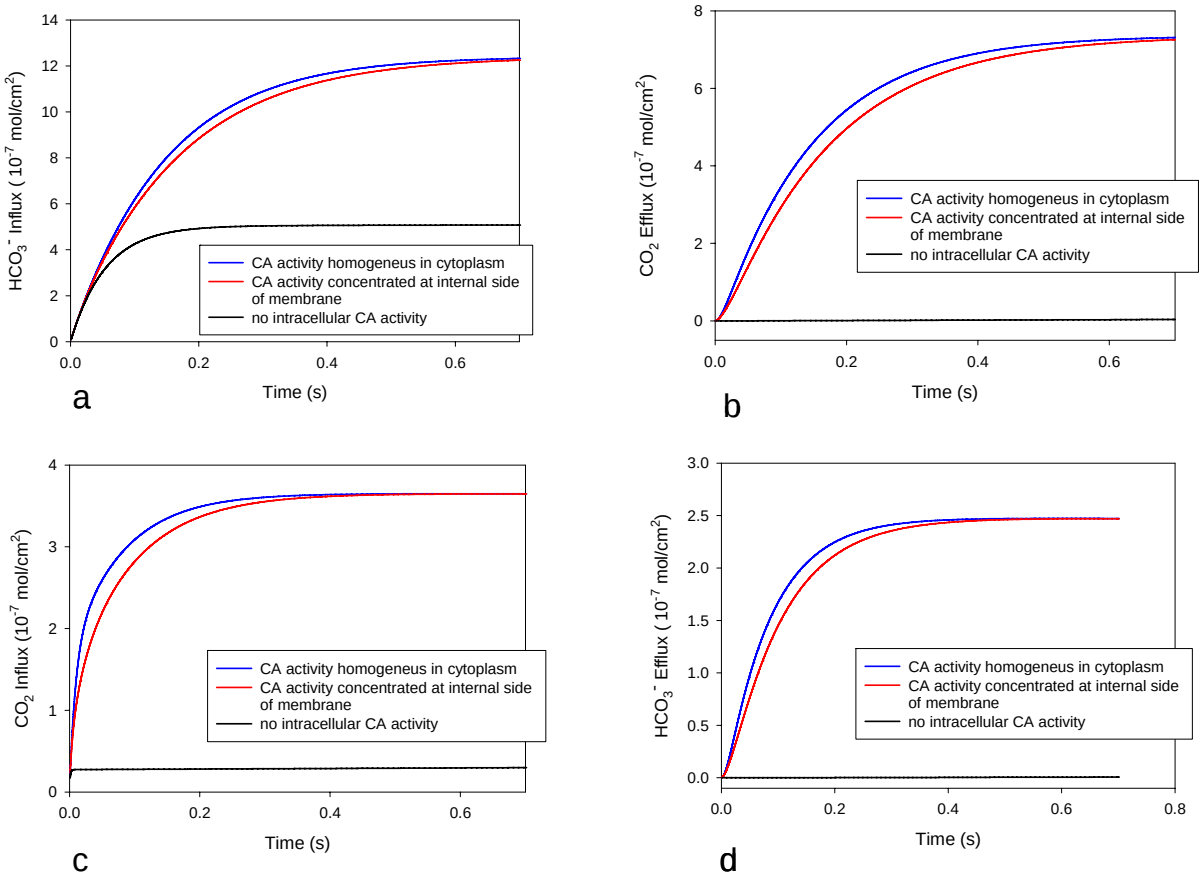
HCO3- Influx (10-7 mol/cm2)
CO2 Efflux (10-7 mol/cm2)
CO2 Influx (10-7 mol/cm2)
HCO3- Efflux (10-7 mol/cm2)
Time (s)
CA activity homogeneus in cytoplasm
CA activity concentrated at internal side of membrane
no intracellular CA activity
a
b
c
d

Fig. 10

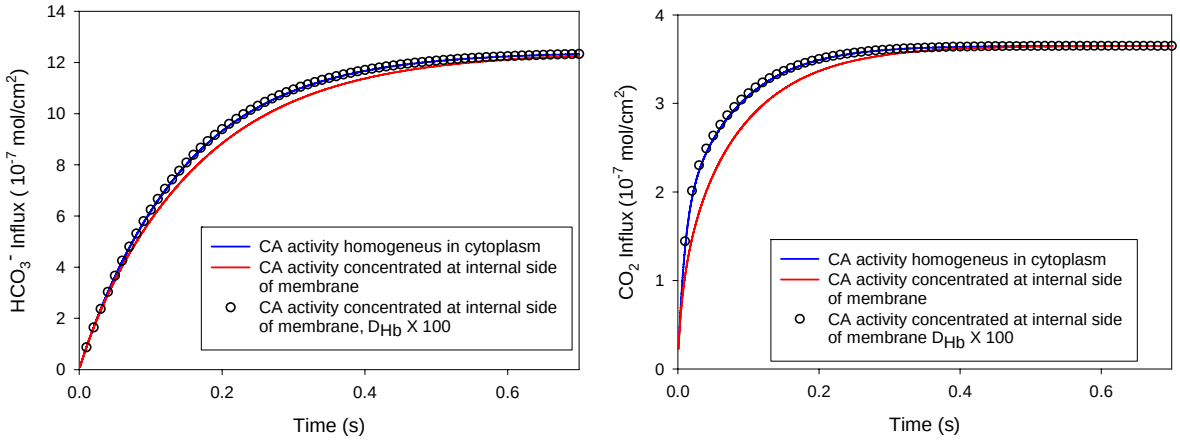
HCO3- Influx (10-7 mol/cm2)
CO2 Influx (10-7 mol/cm2)
Time (s)
CA activity homogeneus in cytoplasm
CA activity concentrated at internal side of membrane
CA activity concentrated at internal side of membrane, DHb X 100
CA activity concentrated at internal side of membrane DHb X 100

Fig. 11

Lebenslauf

Name: Samer Al-Samir

Anschrift: Oderstrasse 20 31535 Neustadt a. Rbge.

Geburtsdatum: 10.06.1981 Hannover

Wissenschaftliche Arbeit

Seit 01.04.2008	Wissenschaftlicher Mitarbeiter an der MHH Abteilung Vegetative Physiologie

Hochschulausbildung / Studium

01.10.2001 Bis 31.03.2008	*Abschluss:* Diplom Biologe Studium der Biologie an der Leibniz Universität Hannover *Schwerpunkte:* Zoologie, Molekularbiologie, Immunologie

Wehr- oder Zivildienst

04.10.2000 bis 31.08.2001	Zivildienst geleistet am Krankenhaus Heidehaus des Klinikums Hannover

Schulbildung

28.08.1997 bis 03.07.2000	*Abschluss*: Allgemeine Hochschulreife Oberstufe der Integrierten Gesamtschule Garbsen
01.08.1991 bis 16.07.1997	*Abschluss:* Erweiterter Realschulabschluss Unterstufe der Integrierten Gesamtschule Garbsen
August 1987 bis 03.07.1991	Besuch der Grundschule Schloß Ricklingen

Danksagung

Ich danke Prof. Dr. Gerolf Gros dafür, dass ich in seinem Institut für Vegetative Physiologie meinen Einstieg in die Wissenschaft gefunden habe, sowie der Möglichkeit meine Doktorarbeit unter sehr guter Betreuung in seinem Labor durchzuführen. Ich danke auch Dr. Volker Endeward für seine tatkräftige Unterstützung und Anleitung in den Projekten, die ich mit ihm zusammen im Laufe der Jahre dabei durchgeführt habe. Des Weiteren danke ich Herrn Werner Zingel für die Unterstützung bei diversen praktischen Problemen im Labor. Weiterer Dank geht an Prof. Dr. Simon Papadopoulos für seine Unterstützung am konfokalen Mikroskop und guten Tipps für die Filterauswahl. Auch möchte ich Dr. Alexander Polster danken, der mir während meiner Diplomarbeit die Anfänge in der molekularbiologischen Herangehensweise beigebracht hatte. Besonderen Dank geht an meine Mutter, die mir geholfen hat mobil zu bleiben wenn es wieder Probleme mit meinen Wagen gab. Ich danke auch meiner Schwester Jasmin Al-Samir, die mir beim Drucken dieser Arbeit geholfen hat. Zudem möchte ich allen an den Publikationen beteiligten Mitautoren für ihre tatkräftige Unterstützung danken.